

STREAK CAMERA ANALYSIS OF DYNAMIC CHARACTERISTICS
OF CURRENT MODULATED DIODE LASER ARRAYS

Kathleen A. Hartnett
A.B., Bowdoin College, 1983

A thesis submitted to the faculty
of the Oregon Graduate Center
in partial fulfillment of the
requirements for the degree
Master of Science
in
Applied Physics

March, 1988

The thesis "Streak Camera Analysis of Dynamic Characteristics of Current Modulated Diode Laser Arrays" by Kathleen A. Hartnett has been examined and approved by the following Examination Committee:

Richard A. Elliott
Professor
Thesis Research Advisor

Richard K. DeFrez
Adjunct Assistant Professor

J. Fred Holmes
Professor

Jean Delord
Professor, Reed College

Table of Contents

LIST OF FIGURES	iv
ABSTRACT	vii
1. INTRODUCTION	1
2. DEVELOPMENT OF PHASE-LOCKED ARRAYS OF SEMICONDUCTOR DIODE LASERS	5
3. OPERATIONAL CHARACTERISTICS OF PHASED ARRAY LASERS	14
4. DYNAMIC RESPONSE OF SEMICONDUCTOR DIODE LASERS	26
5. EXPERIMENTAL STUDIES	30
6. RESULTS	50
7. CONCLUSIONS	96
REFERENCES	98
APPENDIX A	102
APPENDIX B	105
APPENDIX C	110
APPENDIX D	122
BIOGRAPHICAL NOTE	125

List of Figures

2.1 Fundamental array types.	12
3.1 Array far-field pattern from simple diffraction theory.	17
3.2 Normalized amplitudes of the allowed modes.	22
3.3 Normalized far-field pattern for the allowed modes.	24
4.1 Time dependence of photon density and injected carrier concentration during switch-on.	29
5.1 Schematic diagram of the streak camera video frame-grab system.	32
5.2 Spatial variation of the intensity across the array.	37
6.1 Time evolution of the near-field pattern for Xerox laser 3-C-2.	52
6.2 Intensity profile for frame 5.	54
6.3 Average intensity of the array for frame 5.	55
6.4 Intensity profile for emitters 4 and 5.	56
6.5 Average intensity profile.	57
6.6 Time evolution of the near-field pattern for SDL laser C500 at $1.5I_{th}$ (beginning & end of pulse).	59
6.7 Time evolution of the near-field pattern for SDL laser C500 at $2.0I_{th}$ (beginning of pulse).	60
6.8 Three dimensional plot of the intensity surface for the near-field pattern of Figure 6.7a.	62

6.9 An expanded view of the first third of the intensity surface of Figure 6.8.	63
6.10 An expanded view of the middle third of the intensity surface of Figure 6.8.	64
6.11 An expanded view of the last third of the intensity surface of Figure 6.8.	65
6.12 Average intensity of the array at the beginning of the pulse.	67
6.13 Intensity profile for frames 5 and 6.	68
6.14 Intensity profile for frame 10 and the average profile.	69
6.15 Time evolution of the near-field pattern for SDL laser C500 at $2.0I_{th}$ (middle of pulse).	70
6.16 Three dimensional plot of the intensity surface for the near-field pattern of Figure 6.15.	72
6.17 An expanded view of the first third of the intensity surface of Figure 6.16.	73
6.18 Average intensity of the array at the middle of the pulse.	74
6.19 Intensity profile for frames 4 and 5.	75
6.20 Intensity profile for frame 10 and the average profile.	76
6.21 Time evolution of the near-field pattern for SDL laser C500 at $2.0I_{th}$ (end of pulse).	78
6.22 Three dimensional plot of the intensity surface for the near-field pattern of Figure 6.21.	79

6.23 An expanded view of the first third of the intensity surface of Figure 6.22.	80
6.24 Average intensity of the array at the end of the pulse.	81
6.25 Intensity profile for frames 4 and 5.	82
6.26 Intensity profile for frame 10 and the average profile.	83
6.27 Fourier transform of the near-field intensity for SDL laser C500 at $2.0I_{th}$ (beginning of pulse).	85
6.28 Fourier transform of the near-field intensity for SDL laser C500 at $2.0I_{th}$ (middle of pulse).	86
6.29 Fourier transform of the near-field intensity for SDL laser C500 at $2.0I_{th}$ (end of pulse).	87
6.30 Cross correlation between the fifth emitter and the others for SDL laser C500 at $2.0I_{th}$ (beginning, middle, and end of pulse).	89
6.31 Time evolution of the near-field pattern for a Y-guide at $1.5I_{th}$	91
6.32 Three dimensional plot of the intensity surface for the near-field pattern of Figure 6.31.	92
6.33 An expanded view of the first third of the intensity surface of Figure 6.32.	93
6.34 Time evolution of the far-field pattern for a Y-guide at $1.5I_{th}$	95

ABSTRACT

STREAK CAMERA ANALYSIS OF DYNAMIC CHARACTERISTICS OF CURRENT MODULATED DIODE LASER ARRAYS

Kathleen A. Hartnett, M.S.

Oregon Graduate Center, 1988

Supervising Professor: Richard A. Elliott

Phase-locked arrays of diode lasers emit high optical power in a spatially coherent beam. Emission can be controlled through modulation of the drive current enabling these phased array devices to produce short, high power optical pulses. The combination of these characteristics makes them directly applicable to high data rate communication systems. The temporal stability of phased arrays under pulsed operation is especially important when considering applications such as optical communication systems; however, the dynamic characteristics of these arrays are not yet well understood.

A streak camera video frame-grab system was developed to analyze the dynamic characteristics of the radiation emitted by current modulated diode laser arrays. The use of a streak camera is a significant departure from the more traditional observation of the emission with a photodiode since the streak camera permits measurements to be made on a single pulse with a time resolution of a few picoseconds. In addition,

the streak camera provides a three-dimensional record of intensity versus space and time which makes possible the simultaneous observation of the evolution of the intensity profile for each of the individual emitters in the array or particular spatial features of the far field. Software needed to analyze and display the intensity data has been developed. Using this software discrete fourier transforms and cross correlations of the near-field intensity of the emitters in the array, noise spectra, and halftone and graphical representations of the near- and far-field patterns' evolution may be obtained.

1. INTRODUCTION

Monolithic phase-locked arrays of semiconductor diode lasers have excited much recent interest because they can produce several watts of CW optical power in a spatially coherent beam¹. This makes these lasers potentially useful for high data rate communication either via optical fiber or for satellite-to-satellite systems, as well as for optical recording at high data rates, high speed printing, and many other applications. However, such phase-locked arrays tend to emit a multiple-lobed far-field radiation pattern²⁻⁵, which severely limits their usefulness. A further problem with these arrays is the strong noise spikes in the emission of the individual emitters and the somewhat less severe fluctuations in the intensity emitted by the entire array noted by Elliott, DeFreez, et al^{6,7}.

Multiple-lobed far-field patterns result when individual array elements operate 180° out-of-phase^{8,9} or, in the case of gain-guided arrays, when there is wavefront curvature in the near-field of in-phase array elements^{2,6}. In any case the near-field radiation pattern must be in-phase in order to have a single lobe in the far-field. Several different approaches have been taken in array design to promote in-phase emitter operation and thus a single-lobed far-field pattern. These include varying the spacing¹⁰ and the width of the emitters¹¹⁻¹³, introducing optical loss between emitters¹⁴, increasing inter-stripe gain¹⁵⁻¹⁹, and, most recently, using Y-shaped index guides for the array elements²⁰. Also, a cleaved-coupled-cavity phase-locked array

operating in a tunable single-longitudinal mode and single-lobed far-field pattern has been demonstrated²¹.

One of the primary applications of phased array lasers is in high data rate communication systems. Such systems require either rapid current modulation or fast pulse operation. In a recent review paper²² on phase locked arrays, Botez and Ackley stated, after noting the streak camera study of the transient behavior of ten-element gain-guided arrays cited above^{6,7}, that "there is only a limited amount of data available on the behavior of phase-locked arrays under high-speed modulation ... and the stability of array operation under transient conditions needs further investigation". To date there have been only a few reports of experimental work investigating the dynamics of phased array devices and only one of these has been concerned with arrays exhibiting single-lobed far-field patterns²³. The only other work in this area published subsequently is that of Forrest and Abshire²⁴ who studied the evolution of the far-field patterns of gain-guided arrays under fast pulsed conditions using a synchronous scanning technique.

The streak camera allows observation of the dynamics of the near-fields of individual emitters in the array, of the far-fields, and also real-time single pulse measurements with a time resolution of a few picoseconds²⁵. Previously, only a pair of adjacent emitters were able to be viewed simultaneously preventing a single pulse global view of the array. The addition of video frame grabbing capability to the streak camera has made it possible to record the time evolution of the emission from all the individual emitters simultaneously.

This thesis describes the development and use of the streak camera video frame-grab system and the software written for statistical analysis and graphic display. The organization of the thesis is as follows. Chapter 2 describes the

development of phase-locked arrays of diode lasers. In Section 2.1, the development of high power diode lasers is discussed. A variety of techniques for increasing the power output of diode lasers are presented. The fundamental array types are described in Section 2.2.

The operational characteristics of these phased array lasers is discussed in Chapter 3. Section 3.1 gives an explanation of far-field behavior in terms of simple diffraction theory. Coupled-mode analysis is detailed in Section 3.2.

Chapter 4 gives an overview of the transient response of diode lasers to a modulated drive current. A simple physical model is presented to give a basic understanding of the complex interactions taking place as the laser is modulated. A more rigorous analysis is beyond the scope of this thesis.

Chapter 5 outlines the experimental studies. Section 5.1 provides an overview of the experiment. Details on the method of data acquisition are given in Section 5.2. The process of extraction of the data from the analog video signal is described in Section 5.3. The last few sections provide information on the software developed, by the author, specifically to handle the data transfer and, to perform both the statistical analysis and the graphic presentation of the intensity data. Section 5.4 deals with data transfer and the creation of the array files used in the analysis. The statistical analysis software is discussed in Section 5.5. Software for graphic presentation of both the intensity data and the results is described in Section 5.6.

Results are presented in Chapter 6. The near-field optical response is given in the first section for two of the lasers studied. In Section 6.2 a representative sampling of the discrete Fourier transform and correlation results are provided. The last section includes the near- and far-field optical response of a Y-guide array.

In the final chapter, Chapter 7, concluding remarks are made. Results are discussed and comparisons are made with those of previous studies. Suggestions for further work are also given.

2. DEVELOPMENT OF PHASE-LOCKED ARRAYS OF SEMICONDUCTOR DIODE LASERS

When semiconductor lasers first became available their applications were limited, by the existing technology, to those requiring relatively low optical power. Semiconductor lasers were readily integrated into fiber-optic communication systems where a single stable beam of 3 to 5 mW is required. The emission from semiconductor lasers is inherently easy to modulate by direct modulation of the input drive current. This feature makes semiconductor lasers especially attractive for use in optical fiber communications and optical (digital) memories such as: audio disks, video disks, and read-write memory (magneto-optic) where a modulated source is desired. As process technology evolved, the potential applications for these semiconductor lasers expanded to include: spectroscopy, optical pumping of lasers, and, line of sight communication. As many of these applications require higher optical power than the earlier lasers could emit (only a few mW), the direction of the research effort was toward developing high power, single-mode semiconductor lasers that would emit a well-defined narrow beam.

2.1 Development of High Power Diode Lasers

The limiting factor in development AlGaAs high power diode lasers is degradation of the diode's mirror facet which causes either a reduction in the performance or

a complete failure of the device. At optical-power densities greater than 6 to 9 $\text{mW}/\mu\text{m}^2$ of emitting area an AlGaAs laser suffers from gradual degradation of its facets caused by a chemical reaction initiated by the high internal power density²⁶. A photochemical reaction occurs at the mirror facets which causes an amorphous oxide to form, darkening the mirror. The diode's performance degrades as the partially reflecting mirror facet darkens. At even higher optical-power densities (20 to 25 $\text{mW}/\mu\text{m}^2$) the normally occurring absorption process at the diode-air interface is greatly increased and this in turn causes a thermal runaway process which heats the mirror facet to the melting point and thus catastrophically damages the laser. There are several techniques that may be used to increase the output-power limits stemming from the gradual or catastrophic degradation of the diode's mirror facets--

1. increasing the area of the lasing spot (perpendicular and parallel to the p-n junction) thus spreading the emitted light over a broader area of the facet allowing the diode to operate at higher powers before the facet suffers from damage. A discussion of this technique may be found in an article by Botez²⁶ and will not be covered here in any further detail.
2. increasing the ratio of emitted power to internal power by using antireflection coating on the output mirror facet thus increasing the energy output for a given internal power.
3. creating regions near the diode's mirror facets that are nonabsorbing thereby increasing the threshold at which degradation of the facet occurs.

2.1.1 Increasing the ratio of emitted to internal power with antireflection coatings

The ratio of emitted power to internal power may be modified by changing the reflectivity of the mirror facets, the cleaved surfaces of the laser diode. Higher output powers, for a given internal power, may be obtained by reducing the reflectivity of the output facet. An antireflection coating applied to the front mirror facet which reduces the reflectivity from about 30 percent to less than 5 percent yields an increase in light output roughly twice that of an uncoated device operating at the same internal lasing power. Since it is the internal power level that determines whether the mirror facet suffers degradation, antireflection coatings provide a way to increase output power without decreasing performance or causing increased failure rates due to facet degradation. The internal power level also determines whether gain saturation occurs with consequent transverse multimode operation. Thus, as the internal power level increases beyond a certain point gain saturation becomes a problem. Antireflection coatings allow higher output powers to be obtained without increasing the internal power levels beyond this threshold. Not only is the output power double that of an uncoated device, but single mode operation is assured at up to twice the level previously obtained.

Antireflection coatings alone, however, do not provide the optimal solution to obtaining higher output powers from laser diodes. With the decreased reflectivity at the front facet more optical gain is required to reach the lasing threshold of the diode. A high-reflectivity coating on the back facet can increase the reflectivity to 90 or 95 percent. By combining a high-reflectivity coating on the back facet of the diode with the antireflection coating on the front facet, higher output powers may be obtained

without increasing the lasing threshold. The effective efficiency of the laser is also increased because nearly all the light exits at the front facet.

2.1.2 Eliminating absorption at the mirror facets

Another technique for increasing the output power of a diode laser is to form nonabsorbing regions adjacent to the mirror facets. By eliminating absorption at the mirror facets the threshold at which degradation of the facet occurs is increased. These nonabsorbing mirror regions are formed by creating areas of higher bandgap energy adjacent to the facets than in the lasing region. This technique is more difficult than the two previous methods discussed. Nonabsorbing mirrors are formed by regrowth of a cap of material of higher bandgap at each end of the optical cavity²⁷ or by zinc, or some other p-type dopant, diffusion throughout while excluding the region directly adjacent to each mirror facet^{28,29}. The lasing light is then reflected at the mirrors but not absorbed in the region near them. Power outputs have been reached that are four to five times those achieved for the same laser without nonabsorbing mirrors.

2.1.3 Current confinement considerations

As technology has evolved to permit higher output powers from diode lasers, as discussed in the previous sections, the limiting factor in reliable performance is no longer so much facet degradation but damage arising from the large amounts of power being dissipated in the diode. Higher operating powers require higher drive currents and thus more power dissipation in the laser diode. If the drive current can be made to be more efficient then higher operating powers do not require as high a

drive current and therefore there is less power dissipation in the device. The drive current can be made more efficient by confining it tightly to the active layer so that more of the injected current contributes directly to lasing. With the metalized stripe contact, current confinement is somewhat removed from the active layer and spreading occurs. For more efficient current confinement, regions of high-resistivity or reverse-biased p-n junctions may be formed on either side of the lasing region to prevent current from spreading beyond this area. Ways of confining current include:

1. preferential dopant diffusion-- a p-type dopant such as zinc or cadmium is diffused through an n-type capping layer forming a narrow current path surrounded by reverse-biased p-n junctions
2. proton implantation-- protons are implanted on either side of the desired current path creating damaged regions of high resistivity restricting the current flow to the desired path
3. inner-stripe confinement-- the lasing structure is grown over a channel etched into planar material of p-type substrate restricting the current flow with reverse-biased p-n junctions formed on either side of the channel
4. regrowth of reverse-biased p-n junctions-- for devices with a discontinuous active layer, current flow is controlled by growing p-n junctions on either side of the mesa that are reverse-biased when current is injected.

2.1.4 Formation of phase-locked arrays of diode lasers as a source of even higher power

A desire for even higher optical power from diode lasers has led to the development of one-dimensional arrays of mutually coupled diode lasers. Despite the techniques described above which have been developed to fabricate high power diode lasers there remain inherent limits on the level of reliable output power. To achieve output powers in the hundreds of milliwatts, in a near diffraction-limited beam, it becomes necessary to consider arrays of lasers rather than single element devices.

Arrays were investigated as early as 1970 when the coupling of two adjacent stripe geometry lasers was experimentally observed³⁰. Several years later coupling of adjacent diode lasers was considered theoretically³¹ but, it wasn't until 1978 that a five element gain-guided array was demonstrated by Scifres et al.³². It wasn't until 1981 that phase-locked arrays of index-guided lasers were reported^{33,34}. These arrays could then only operate under restrictive conditions such as low-duty-cycle pulsed mode at room temperature³³ or CW mode at 77 K³⁴. The next advance came with the improved capability of metal-organic vapor-phase epitaxial (MOVPE) growth to produce quality quantum-well heterostructures. These devices have low threshold current densities and early examples were able to operate with CW power in the hundreds of milliwatt range⁴. It wasn't until 1982 that an array of index-guided lasers was able to maintain CW operation reliably at room temperature³⁵. With this array of index-guided lasers, single longitudinal mode operation was observed. Much effort since then has been focused on new designs for these index-guided arrays^{10,16,18,19,23,35-42} to promote array operation in which the desired single lobed far-field pattern is achieved.

2.2 Fundamental Array Types

There are essentially two classes of array lasers-- gain-guided and index-guided arrays. A gain-guided laser differs from an index-guided laser in the method of optical-mode confinement and carrier confinement: a gain-guided laser relies solely on the injected carrier profile for its lateral optical-mode confinement while the index-guided laser has built-in dielectric waveguides which serve to confine the lateral optical modes. Within the index-guided array classification there are at least five different fundamental types. Six fundamental array types are depicted schematically in Figure 2.1. where they are listed in chronological order with the gain-guided array being the first array to be developed.

The gain-guided array (Figure 2.1a) is one of the simplest of all the array structures; the current being confined by high-resistivity regions formed by proton implantation, for example. The remaining array types shown in Figure 2.1 are all index-guides which, by definition, are lasers with real refractive index waveguides. The ridge-guide structure (Figure 2.1b) was one of the first index-guide arrays to be developed³⁴. Planar double heterostructure material is chemically etched to form the ridge-guide structure. The variations in the cladding layer thickness are sufficient to provide a variation in the effective index and optical mode confinement^{18, 18, 19, 39, 41}. One of the next structures to be developed was the Zn-diffused array^{35, 43}. Zn is diffused into planar double heterostructure material through both the p-type cladding layer and the p-type active layer. The Zn lowers the refractive index of the material forming a dielectric waveguide in which the nondiffused regions are the high index regions of the lateral guide. Following the development of the Zn diffused array was that of two array types grown on channeled substrates (Figure 2.1d,e). These struc-

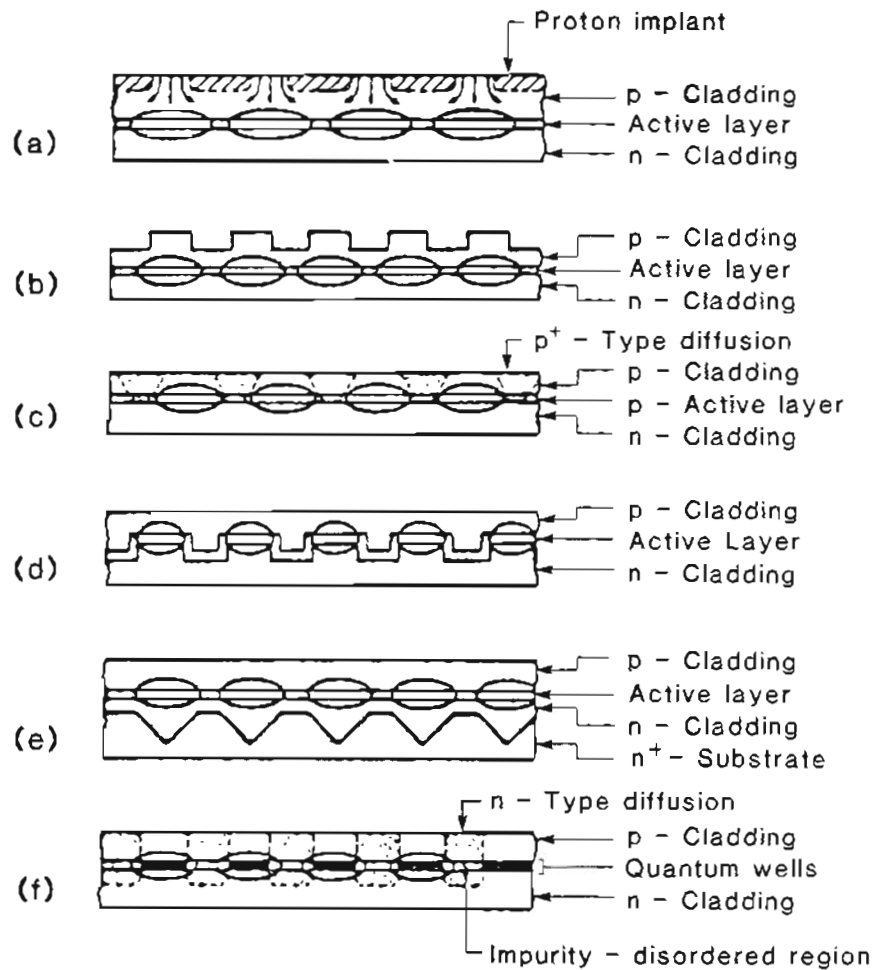


Figure 2.1 Fundamental array types. Schematic representation of phase-locked arrays with gain-guided (a), and index-guided (b-f) structure formed by: (a) proton implantation; (b) chemical etching of ridge-type waveguides; (c) p-type-dopant diffusion; (d) MOVPE over channeled substrates; (e) LPE over channeled substrates; and (f) quantum-well-structure disordering induced by n-type-dopant diffusion. [22]

tures exploit the properties of metal-organic vapor-phase epitaxial (MOVPE) and liquid-phase epitaxial (LPE) crystal growth techniques. With MOVPE the channel structure is preserved (Figure 2.1d) and a constant thickness active layer with periodic bends results⁴⁴. These bends in the active layer provide lateral optical mode confinement⁴⁵. The channel structure is not preserved with LPE growth (Figure 2.1e). For the LPE structure, a V-groove channeled substrate is used. As the n-type cladding layer is grown the channel is filled in creating a cladding and/or active layer of nonuniform thickness²⁸. The most recent array design, the impurity-disordered array, employs quantum-well-structure disordering induced by preferential n-type dopant diffusion (Figure 2.1f). A quantum-well laser has an active layer comprised of alternate thin layers ($< 200 \text{ \AA}$ each) of GaAs and AlGaAs. The multiple layers comprising the quantum well become a single layer when an n-type dopant such as Si is diffused into the structure. This new single layer composite material has a bandgap and index of refraction intermediate between those of the original layers⁴⁶. Regions where Si was not diffused become the high-index regions of lateral dielectric waveguides.

3. OPERATIONAL CHARACTERISTICS OF PHASED ARRAY LASERS

Since operation of the first phased array lasers was demonstrated there has been a major effort to understand the physics behind their operation. Scifres et al. note in their pioneering study⁴⁷ that it is not reasonable to consider the laser array as a series of isolated narrow stripe lasers. Individually, these narrow stripe lasers have non-Gaussian or double lobed far-field patterns⁴⁸⁻⁵⁰ which are a result of the real refractive index antiguiding due to the spreading of the optical modes into the surrounding, unpumped regions of higher refractive index. In contrast, these surrounding regions are not relatively unpumped in a coupled multiple stripe (CMS) laser. In a CMS device the individual emitters are not isolated and factors such as lateral charge conduction and diffusion between emitters⁵¹ must be considered. Since the CMS laser discussed by Scifres et al⁴⁷. is a gain-guided array, lateral optical mode confinement is weak and the optical mode beneath each stripe contact couples with those of its neighbors. It has been shown both theoretically⁵¹ and experimentally⁵² that a significant charge density exists over 10 μm from stripe edges. For this reason, Scifres et al⁴⁷. suggest that the charge density between the stripes may be significant and would thus alter the mode calculations. It follows that the charge density under the two end emitters will differ from that of the central emitters and will most likely be asymmetric.

This asymmetry of the outer emitters was not considered in the first analysis⁴⁷

where the observed experimental results were interpreted by modeling the array as one of identical radiators. The individual lasers of the array were considered to be the equally spaced slits of a transmission diffraction grating. The observed diffraction pattern from this uniformly illuminated grating provides a point of comparison for the observed radiation patterns of a CMS laser. This simple diffraction theory allows interpretation of some experimental results^{33, 47, 53} such as the double lobed far-field pattern corresponding to out-of-phase operation, but lacks the capability of determining the allowed modes of the array.

Coupled-mode analysis provides insight into the allowed modes of the array and was the next step in the development of the theoretical foundations of array operation. Otsuka⁵⁴ was the first to apply the coupled-mode analysis to understand the behavior of phase-locked arrays. An infinite array of emitters with an infinite aperture was considered. Only two normal modes or eigenmodes of the array were found. These were the same two modes predicted by simple diffraction theory: 0° and 180° -phase-shift. When an array of finite extent is considered with coupled-mode analysis more eigenmodes are predicted than just the two modes corresponding to 0° and 180° -phase-shift. Butler et al. published the first investigations of coupled-mode analysis for an array of N emitters⁹. They found that for an array of N emitters, N normal modes or array modes are allowed. For each of these array modes there is a near-field amplitude profile that is nonuniform across the array. In previous studies^{47, 54} the near-field amplitudes of each emitter were assumed to be the same. The amplitude profile will be uniform only for the case of an infinite array or a pair of emitters⁵⁵. The coupled-mode analysis developed by Butler et al. was used to understand previously published experimental results. Other groups have independently developed coupled-mode theories^{8, 56} and recent work seems to indicate that this formalism fits

the observed behavior well^{2, 39, 57}.

A new development in the theory of operation of these arrays is the addition of optical gain and loss considerations to the coupled-mode analysis. The work discussed previously pertains to arrays of mutually coupled dielectric waveguides. Since the arrays are comprised of lasers, gain-loss spatial profiles should be incorporated into the theory. These factors influence which array mode has the lowest lasing threshold and is thus the preferred mode of operation of the array. This is of significance because the desired single lobed far-field pattern corresponds to the fundamental mode, (in-phase). Thus, there is a preferred mode of operation and an understanding of how to predetermine that mode of operation of the device is of great importance.

3.1 Simple Diffraction Theory

As mentioned briefly in the overview of this chapter, simple diffraction theory as applied to arrays can be understood by analogy with a transmission diffraction grating. An array of identical apertures of width s with period D forms the grating. The radiation pattern produced by a plane wave transmitted through the grating is the far-field pattern. This is proportional to the Fourier transform of the near-field intensity pattern. When the array is comprised of identical elements the far-field pattern is equivalently the product of a sampling function of period λ/D with the radiation pattern produced by a single aperture of width s . These patterns are shown in Figure 3.1. Note that several lobes fall under the envelope defined by the radiation pattern of a single radiator.

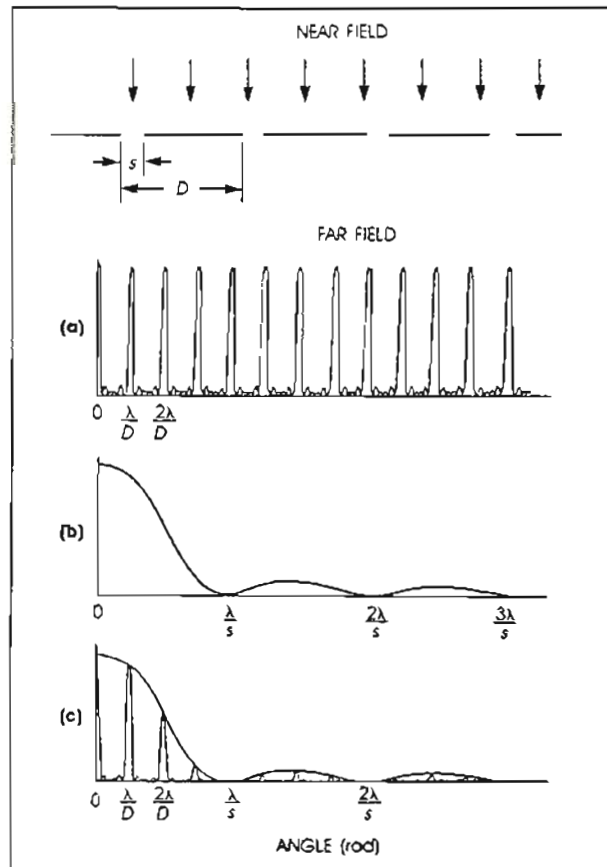


Figure 3.1 Array far-field pattern from simple diffraction theory. The near-field depicts a plane wave moving toward a periodic aperture array. Curves (a)-(c) are used to determine the far-field pattern: (a) sampling function for a periodic array; (b) radiation pattern of a single aperture; (c) far-field pattern, which is formed by taking the product of curves (a) and (b). [61]

This is a somewhat simplified view of the situation for several reasons. An analogy with an array of apertures of width s with period D is not realistic since the optical field of each emitter spreads beyond the aperture width s and is not uniform in s . The extent of an individual optical field is closer to the period D , for a gain-guided array, than the aperture width s . The resulting far-field pattern includes only one or two lobes within the envelope defined by the radiation pattern of this single, broader radiator.

Another unrealistic simplification is that there is no provision to include the relative phases of the individual emitters of the array or the phase-shifts within an emitter. If the lateral modal field pattern is the same for each of the emitters and the phase of each is shifted by ϕ then the radiation intensity pattern is given by⁴⁷ :

$$I(\theta) \propto \cos^2\theta |E(\theta)|^2 G(\theta) \quad (3.1)$$

where θ is the angle with respect to the normal to the facet, $\cos^2\theta$ is an inclination factor, $E(\theta)$ is the Fourier transform of the near-field pattern for a single emitter, and $G(\theta)$ is the sampling function given by:

$$G(\theta) = \frac{1 - \cos [N(k_0 D \tan\theta + \phi)]}{1 - \cos (k_0 D \tan\theta + \phi)} \quad (3.2)$$

For both of these equations, D is defined as the stripe periodicity, ϕ is the phase shift, and $k_0 = 2\pi/\lambda_0$. A phase shift of zero degrees between adjacent stripes produces a symmetric intensity pattern centered about $\theta = 0$. The intensity pattern is centered about

$$\theta = \tan^{-1} (-\phi/k_0 D) \quad (3.3)$$

for a nonzero phase shift. For a phase shift of $\phi=\pi$ the sampling function, $G(\theta)$ is small in the forward direction ($\theta = 0$) with side lobes at

$$\theta_{\phi=\pi} = \pm \tan^{-1}(\lambda/2D) \quad (3.4)$$

3.2 Coupled-mode Analysis

Coupled-mode analysis follows simple diffraction theory in the effort to understand and describe the observed behavior of phase-locked diode laser arrays. Coupled-mode analysis provides an explanation for the discrepancy noted between experimentally observed far-field patterns and those expected based on simple diffraction theory. With coupled-mode analysis it is possible to define the allowed modes of an array of N identical emitters where it is assumed that the emitters are weakly coupled together. The splitting of the oscillation frequency, due to the interaction between the emitters, can be determined in terms of the coupling strength. The development of the coupled-mode analysis that is given here is based on the work of Butler et al. ⁹, the first published work on coupled-mode analysis of coupled stripe semiconductor lasers.

The first step in the analysis is to describe the electric field distribution or wave function of the array. The array wave function may be expanded in terms of the fields of the individual waveguides. These fields are coupled through changes in the dielectric constant induced by the presence of the neighboring waveguides. Weak coupling is assumed between the waveguides. The electric field distribution of the array may be written as the superposition of the electric fields of the individual emitters forming the array. Thus, for an array of N emitters the electric field distri-

bution of the array is given by

$$\Psi(x,y,z) = \sum_{m=1}^N A_m(z)\Psi^m(x,y,z) \quad (3.5)$$

where $\Psi^m(x,y,z)$ is the electric field of an individual emitter and $A_m(z)$ is a complex coefficient describing the amplitude and phase dependence of the emitter for the allowed modes of the array. The individual emitter wave functions are normalized so that $\langle \Psi^m | \Psi^m \rangle = 1$. The wave functions Ψ^m may be separated and written as⁵⁸

$$\Psi^m(x,y,z) = u^m(x)v^m(y)e^{-\gamma z} \quad (3.6)$$

where $u^m(x)$ is the transverse component, $v^m(y)$ is the lateral component, and γ is the propagation constant.

With the assumed field solution for the array defined, this may be substituted into the wave equation

$$\nabla^2 \Psi + \left[k_0^2 \kappa(x,y) + \gamma^2 \right] \Psi = 0 \quad (3.7)$$

where k_0 is the free-space propagation constant ($k_0 = 2\pi/\lambda$) and $\kappa(x,y)$ is the complex dielectric constant. A set of equations are then obtained which describe the modes of the array. To determine which of these are the allowed modes the constraint of orthonormality of the modes is applied resulting in the eigenvalue equation

$$\sum_{n=1}^N k_0^2 c_{nm} A_m(z) - 2\gamma \frac{\partial A_m}{\partial z} = 0 \quad (3.8)$$

where the second-order term $\partial^2 A_m / \partial z^2$ is neglected because of the weak z dependence of the amplitude coefficients $A_m(z)$. The c_{nm} are the coupling coefficients which are determined by calculating the lateral overlap integrals with the dielectric variation

averaged in the transverse direction⁵⁸. If only nearest neighbor coupling is considered, the number of nonzero coupling coefficients is substantially reduced. The only surviving coefficients are the $c_{n,n\pm 1}$ so the equation is reduced to a bidiagonal matrix equation in c . If the z dependence of the amplitude coefficients $A_m(z)$ is separated out and written explicitly as $A_m(z) = a_m e^{-(\partial\gamma)z}$ then the eigenvalue equation may be solved to determine the eigenvalues $\partial\gamma$ and the eigenvectors a_m . These solutions are

$$\partial\gamma_L = (-k_0^2 c / \gamma) \cos(m\theta_L) \quad (3.9)$$

$$a_m^L = \sin(m\theta_L) \quad (3.10)$$

for the N allowed array modes. The L_{th} array mode may then be written as

$$\Psi_L(x,y,z) = \sum_{m=1}^N \sin(m\theta_L) u^m(x) v^m(y) e^{-(\gamma + \partial\gamma_L z)}. \quad (3.11)$$

The individual emitter field functions are now weighted by the envelope function determined by the eigenvalue equation of the array which considered the effect of the interaction of the neighboring elements. Figure 3.2 shows the possible normalized amplitudes of the individual emitters in a ten element array for each of the allowed modes of operation from $L=1$ to $L=10$. The $L=1$ mode is the in-phase mode or 0° phase shift mode, and the $L=10$ mode is the out-of-phase mode or 180° phase shift mode. In addition to these two modes, there are eight other modes that are predicted by the coupled-mode analysis. The envelope function which determines the individual amplitudes for an array operating in the L th array mode is $\sin \left[L\pi y / (N+1)S \right]$ where S is the distance between emitters and the origin is located to the left of the

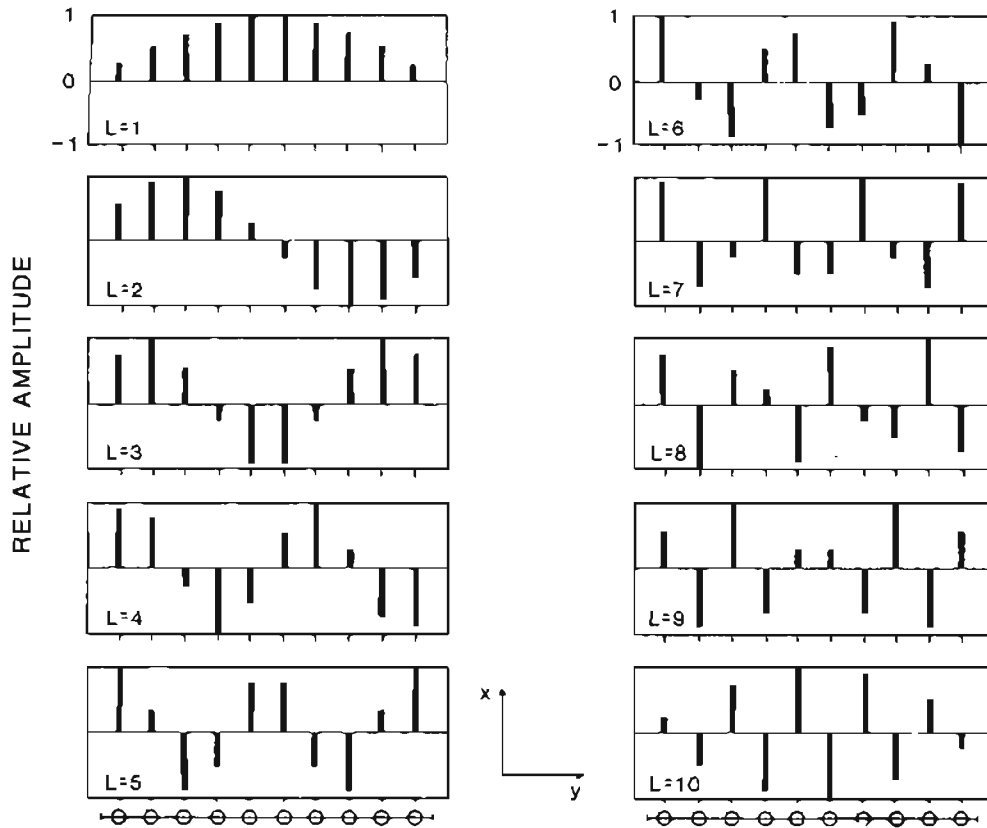


Figure 3.2 Normalized amplitudes of the allowed modes. [9]

first emitter at a distance S from it. It is interesting to note that it is the coupling between the individual elements of the array that causes the amplitudes of each of the emitters to differ.

The possible far-field patterns for an array of N emitters are determined by summing the contributions to the field, preserving the phase variation, from each of the individual emitters as was done in simple diffraction theory⁹. The far-field intensity distribution is⁵⁶

$$F(\Theta) = |E(\Theta)|^2 I(\Theta) \quad (3.12)$$

where Θ is defined as the angle with respect to the normal to the facet, $E(\Theta)$ is the far-field distribution for an individual emitter and $I(\Theta)$, the grating function, is a function characterizing the array and describing the effect of coupling of adjacent emitters in the array. The array-grating function in the coupled-mode analysis for the array mode L is given by⁹

$$I(\Theta) \equiv I_L(u) \propto \left[\frac{\sin \left[N(u + \Theta_L)/2 \right]}{\sin \left[(u + \Theta_L)/2 \right]} - (-1)^L \frac{\sin \left[N(u - \Theta_L)/2 \right]}{\sin \left[(u - \Theta_L)/2 \right]} \right]^2 \quad (3.13)$$

where $u = k_0 S \sin \Theta$. Figure 3.3 shows the possible lateral far-fields of a ten-element array for each of the allowed modes of operation from $L=1$ to $L=10$. As anticipated, the patterns for the $L=1$ and $L=10$ modes closely match those predicted by the simple diffraction theory. Simple diffraction theory cannot, however, predict the other allowed modes.

In addition, the coupled-mode equations make possible the determination of the splitting of the oscillation frequency of the individual emitters in the array as a func-

tion of the coupling strength. There is a splitting about the center frequency of the individual lasers due to the interaction between the emitters. If the coupling strength is c then this splitting is given by⁹

$$(\lambda_1 - \lambda_L)/\lambda_0 \approx c(\cos\Theta_1 - \cos\Theta_L)/n_e^2 \quad (3.14)$$

where λ_0 is the wavelength of the uncoupled emitters and n_e is the average effective index of an individual emitter. The largest splitting occurs between the $L=1$ and $L=10$ modes since the $L=1$ mode corresponds to the lowest lasing energy and the $L=10$ mode to the highest. For this case, $(\cos\Theta_1 - \cos\Theta_{10}) \approx 2$; assuming a coupling coefficient of $c = 10^{-3}$ and $\lambda_0 = 0.83\mu\text{m}$, the splitting is on the order of 1.3\AA . This splitting is much smaller between either the first two or last two modes; for a ten stripe array the splitting is about 6% of the maximum value for the array which is $<0.1\text{\AA}$ ⁹. If the number of emitters in the array is increased this splitting is decreased; a forty-stripe array, for example, could have a frequency splitting as small as 10^{-3}\AA . With a splitting so small it could be possible to have two modes operating degenerately. If the natural linewidth of an individual laser is broader than this splitting then there will be only one mode operating. Butler et al⁹. state that it is possible for a number of array modes to mix coherently, to form composite modes which are the sum of the individual array modes (with relative phases preserved), if there is some nonlinearity between the emitters. Referring back to Figure 3.3, note that the position of the far-field lobes is shifted for sequential array modes. Thus, if two modes are operating simultaneously, the resulting far-field lobes will be significantly broader. The existence of these composite modes may explain why most phase-locked arrays^{35, 36, 47, 59} have far-field lobe widths that are two to three times the diffraction limit.

4. DYNAMIC RESPONSE OF SEMICONDUCTOR DIODE LASERS

The transient response of diode lasers to a modulated drive current will be considered in this chapter. Diode lasers, and in particular phase-locked arrays, are potentially useful for high data rate communication either via optical fiber or in satellite-to-satellite systems, as well as for optical recording at high data rates, high speed printing, and many other applications. Semiconductor lasers respond quickly and efficiently to changes in the drive current. For a laser below threshold, the light output (spontaneous emission) depends only on the injected carrier concentration. The output intensity responds to a current step with a time constant determined largely by the carrier recombination time. In contrast, for a laser running at or above threshold, the optical response to a current step involves interaction of the photon population in the cavity and the fraction of injected carriers in excess of the equilibrium concentration. Thus, in order to examine the transient and the modulation responses of semiconductor lasers both the carrier and photon populations must be considered.

To model the physical response to changes in the drive current the concentration of injected carriers and the change in the photon population need to be examined. As the current is increased the injected carrier concentration increases, initially. The increase in the carrier concentration stimulates the local rate of light emission. Light emission may be in two forms, emission into the resonator and emission of light

through the mirror facets however, the output of light through the facets depends on the size of the photon population in the resonator. Thus, the rise in the photon population lags behind the increased generation rate of photons. This delay is small but is not insignificant. Thus, the response to a change in the drive current has at first two distinct steps -- first, an increase in the injected carriers and second, an increase in the photon population.

The interaction between the populations of both injected carriers and photons, and the delay due to the accumulation time of the photon population leads to oscillation. The system tends to oscillate between the electron and photon populations with a natural resonance frequency normally on the order of 1 GHz. The optical resonator provides little damping since its Q is large when the laser is driven above threshold. The spontaneous recombination time of the carriers provides the only significant source of damping with a decay time close to 5 ns⁶⁰. So, the resonant behavior, or relaxation oscillation, is observed as a transient oscillation in response to laser switching on.

4.1 A Physical Model of the Transient Response

A more detailed description of the response is given here by considering as input a step function of current which delivers current beyond the threshold level. When the step function of current is applied there is a delay in the optical response as the population of the injected carriers builds. The injected carrier population must increase to slightly beyond the threshold level before any lasing emission may be observed. Several factors determine the length of this delay: the carrier recombination time, the amount of current overdrive in the step function and the characteristics of the previous current pulse. What is meant by current overdrive is the extent

beyond threshold that the laser is driven from pulse to pulse.

Figure 4.1 shows the time dependence of the photon population density and the injected carrier concentration during the switch-on period of a semiconductor laser. As the carrier concentration increases beyond its threshold value, switch-on begins and emission increases nearly exponentially from the low level of spontaneous emission to its maximum value. The carrier concentration reaches its maximum at the end of the switch-on period. The duration of this period is dependent on the photon lifetime in the resonator, the injected carrier recombination time and the extent of overdrive in the current pulse. During this switch-on period the injected carrier concentration increases substantially beyond its equilibrium value which in turn causes the photon population to increase beyond its equilibrium value toward the end of the initial phase of switch-on. The transient oscillations mentioned earlier are also excited during this time.

After switch-on the laser emission spectrum evolves in time as shown in Figure 4.1. The temporal behavior of the spectrum, however, is not directly correlated to the transient behavior of the total emitted intensity. Initially, the laser's spontaneous emission has a broad spectrum with a bandwidth of several hundred angstroms⁸⁰ which is composed of a large number of modes. As the emission becomes predominantly stimulated emission the modes adjacent to the mode that will eventually dominate increase temporarily. At the beginning of the switch-on they increase but more slowly than the main mode. The general trend is to narrow the overall linewidth. The linewidth continues to narrow even as the emission undergoes transient oscillation. These satellite modes oscillate as well but their oscillations tend to decrease in amplitude with respect to those of the main mode. It may take up to 20 ns²⁵ before the mode spectrum of the laser settles into a single mode form.

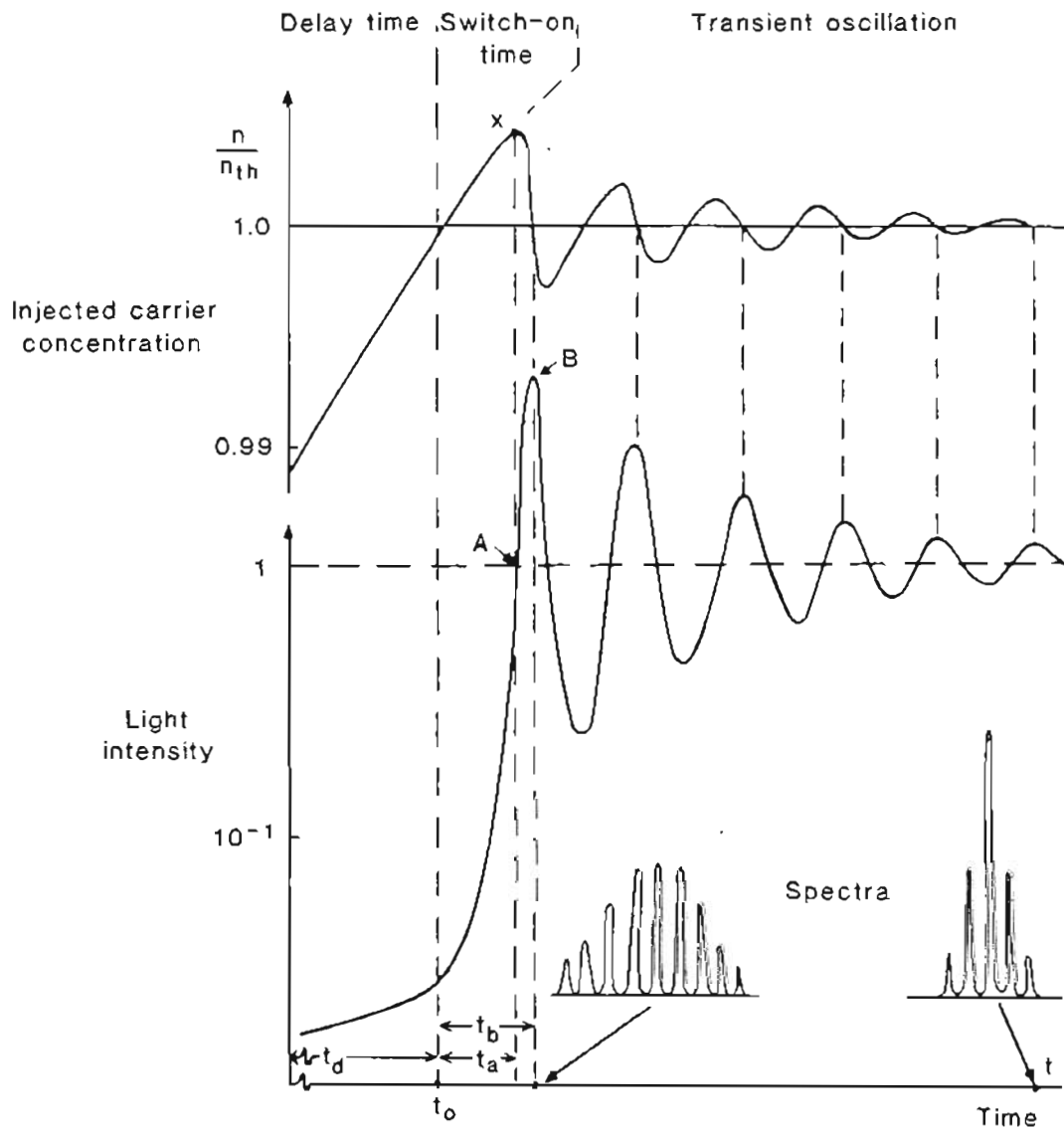


Figure 4.1 Time dependence of photon density and injected carrier concentration during switch-on. [60]

5. EXPERIMENTAL STUDIES

The previous chapters have presented information on the development of array lasers, discussed the theory of operation and the dynamic response of the arrays under pulsed operation. This chapter describes the experimental studies conducted. Section 5.1 gives an overview of the experiment. Section 5.2 provides details on the method of data extraction from the recorded video signal. Section 5.4 discusses the data transfer process and the creation of array files. The fifth section, 5.5, includes a discussion of the statistical software. Section 5.6, the final section, gives a brief description of the software developed for graphic display of the intensity information and of the corresponding results derived from it.

5.1 Overview of the Experiment

The design of this experiment evolved from that originated by DeFreez and Elliott^{6,7} in the first streak-camera measurements of the fast pulse response of phase-locked, multiple quantum well diode laser arrays. The use of a streak-camera is a significant departure from the more traditional approach of observation of the emission with a photodiode. The streak camera allows real-time single pulse measurements with a time resolution of a few picoseconds²⁵ making temporal studies of rapidly evolving events such as phase-locking possible. In addition, streak camera analysis makes possible the simultaneous observation of the evolution of the intensity

profile for each of the individual emitters in the array. This feature of the streak camera system is essential for the studies of the noise properties of the emission in the near-field.

It is possible to obtain intensity profiles for individual pulses and integration of a sequence of these gives the optical response averaged over a number of pulses. Statistical analysis may be done on these intensity profiles providing information on the transient response of the array. In the earlier work by Defreez and Elliott simultaneous observation of at most two portions of the radiation pattern were possible since the temporal analyzer of the Hamamatsu C979 streak camera used in their experiment allows for the definition of either one or two spatial windows. Video frame grabbing capability was added to the streak camera system thereby making full use of the intensity information available on each of the individual emitters in the array.

The streak camera video frame-grab system used to measure the time evolution of the light intensity from the array is illustrated in Figure 5.1. The current pulser and the streak camera were triggered synchronously by a video frame pulse extracted from the free-running video output of the vidicon by the sync-stripper (Colorado Video model 302-2). This method of triggering ensures that the output from the streak camera coincides with the beginning of a video frame. Consistent positioning of the streak trace at the beginning of a video frame is essential for any type of temporal analysis.

Intensity profiles were recorded in frames separated by 1s time intervals and retained with a video cassette recorder (Panasonic VCR model AG-6200). These stored streak traces could then be digitized with a video frame grabber (Robot model 850). The digitized images were accessed by software developed by Robert Carey of Sunset Labs, Inc. for our Apple IIe computer which reduced the data from a 256 by

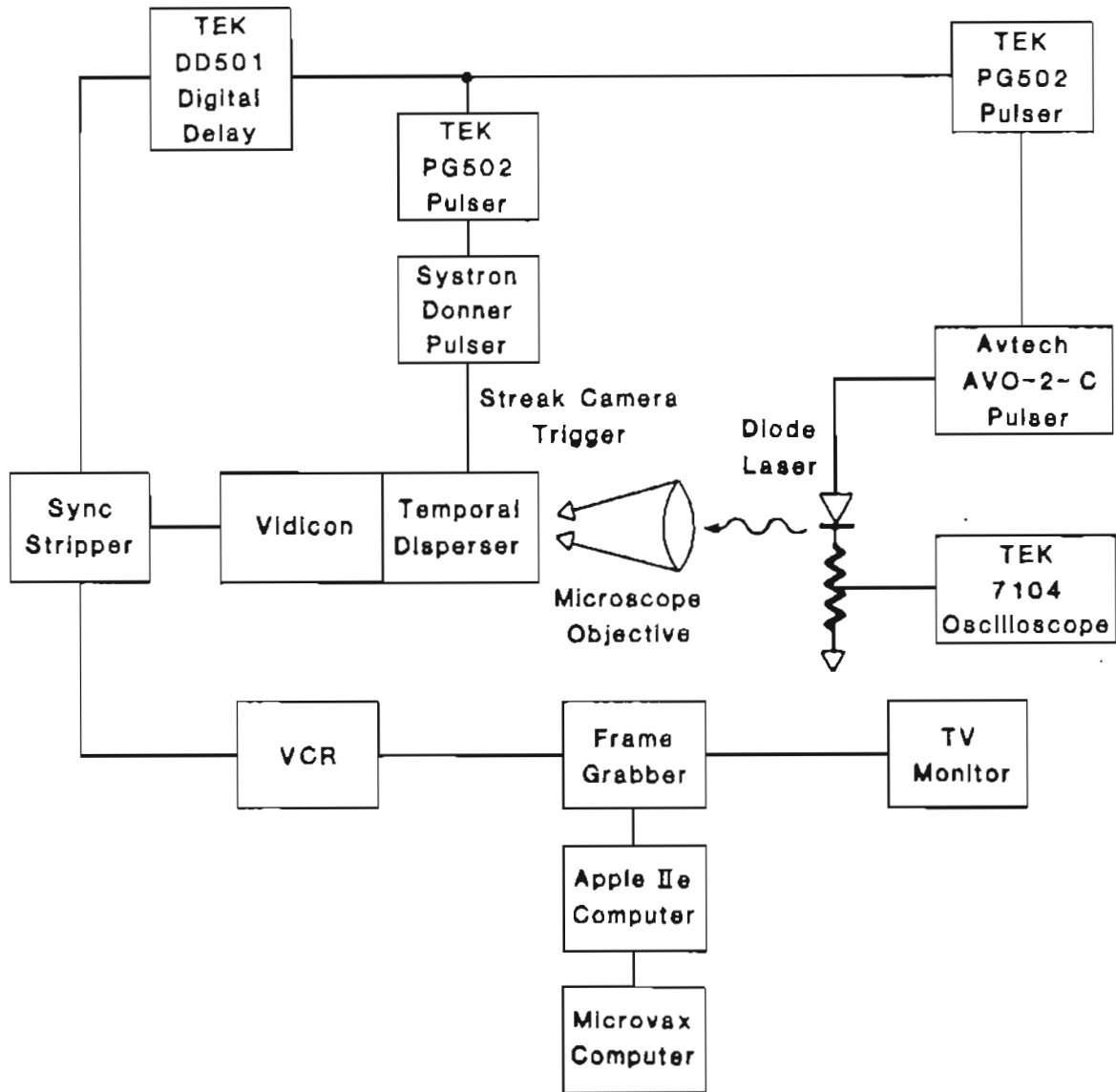


Figure 5.1 Schematic diagram of the streak camera video frame-grab system.

256 array of intensity data to an $256 \times N$ array where N represents the number of windows defined to partition the data. For near-field measurements on ten stripe devices ten windows would be defined, each window enclosing the intensity profile for an emitter. These windows were all of equal width to ensure that the same amount of background would be present in each of the individual intensity profiles.

Software on the Apple IIe determined an average intensity for each window for each of the 256 time channels. This average intensity data was written to files on floppy disks. Typically images were processed in this manner for twenty frames recorded under a given set of conditions. The average intensity data stored on the floppy disks was transferred electronically to a MicroVAX computer for in-depth analysis of the near-field time evolution. Statistical analysis could then be done on these twenty individual frames and on their average intensity profile in an environment much more suited to the extensive computation and file manipulation involved in the analysis.

5.2 Details of the Method of Data Acquisition

Before any measurements of the time evolution of the light intensity can be obtained several characteristics of the laser must be determined. Typically the packaging of the laser was not designed for high frequency current modulation and it needs to be modified. Usually, this is accomplished by removing the thin ($25 \mu\text{m}$ diameter) gold contact wires and replacing them with a broad ($100 \mu\text{m}$ wide) gold strap. This modification reduces the high frequency inductive loading that would preclude a fast risetime current pulse. Current has to be injected into the laser array with a device that has a fast enough response time so that the rise time and shape of

the current pulse is as close as possible to that of a square wave. The theoretical studies on the dynamics of semiconductor lasers consider a square wave pulse as the form of the injected current profile⁶⁰. To get a smooth, clean square pulse shape it is necessary that the impedance of the probe and laser match that of the current pulser (50 Ω). Most of the laser arrays examined in this study had a resistance between 13 and 17 Ω as measured with a curve tracer. A curve tracer is used so that the voltage through the laser can be limited to 2 volts in this case. Once the resistance of the laser diode is determined an impedance matched current source may be constructed. A semi-rigid SMA cable provides the hot lead of the current source while a carbon resistor of the appropriate value (between 37 and 33 Ω) soldered to the outer conductor of the SMA cable provides the path to ground. All leads are kept as short as possible to minimize inductive effects. With the proper current source in place the lasing threshold of the array may then be determined. The waveform of the current pulse driving the laser may then be checked to see that it closely approximates a square wave.

Current is injected into the laser via a pressure contact between these two leads of the current source and the gold foil covered pads on either side of the mounted laser. Both the shape and the amplitude of the current pulse need to be monitored. Current through the laser diode is monitored on a Tektronix 7104 oscilloscope by placing a high frequency (1.5 or 3.0 GHz.) oscilloscope probe across the resistor. The high frequency probe is necessary as the pulse width is 50 ns with a short rise time. The current pulser, an Avtech AVO-2-C, also provides a monitor pulse which is a scaled version of the output current pulse driving the laser. This monitor pulse serves as a trigger for the oscilloscope as well as a measure for comparison of the shape of the pulse through the laser. The initial response to the current pulse is especially

interesting, making the most critical portion of the current pulse the first few ns.

Once it has been determined that clean square wave current pulses can be injected into the laser the lasing threshold must be determined. This can be accomplished in two ways: one, observe the structure that develops in the far-field pattern as the emission becomes coherent or two, measure the light output (L) as a function of current (I) and identify the threshold from the L-I curve. As the current to the laser is increased the far-field pattern, as viewed with an ir viewer (FJW Industries) on a paper screen, makes a transition from being just a diffuse glow (spontaneous emission) to a three lobed pattern (lasing). The current value at which this structure evolves marks the current threshold. The second method requires the use of a photometer. A line extrapolated from the linear region of the LI curve gives the current threshold.

With this preliminary work completed the laser and current probe can be integrated into the system. For the near-field studies the image of the output array facet is imaged on the object plane of the streak camera's optics with a microscope objective (20X, 0.4 NA).

As mentioned in the previous section, the streak camera and current pulser were triggered synchronously by a video frame pulse extracted from the free-running video output of the vidicon by the sync-stripper. The vidicon puts out a frame pulse every sixtieth of a second. This frequency is higher than desired since it would not permit sufficient time for the streaked image on the phosphor screen to decay to the background level between pulses. To decrease the frequency a Tektronix DD501 digital delay unit was set to generate a pulse after receiving 60 such frame pulses thus giving the triggering signal a frequency of 1 Hz. The output of the DD501 is insufficient to trigger either the pulser or the streak camera so a pair of Tektronix PG502 pulse

generators were used to create a signal with the right characteristics for each of the triggering circuits. A variable delay was needed for the streak camera trigger so the output of the PG502 was input to a Systron Donner pulse generator with a variable delay on the output pulse. This delay could be adjusted while viewing the streaked trace on a monitor allowing the trace to be positioned in time such that the beginning of the trace occurred near the top of the video frame. The ability to finely adjust the triggering delay during the course of a data run is essential as there is some drift with time.

Jitter present in the triggering electronics is minimal in absolute terms but when the time frame of the experiment is considered it becomes more of a problem. An extremely sensitive touch in adjusting the various triggering levels minimizes the problem but does not eliminate it. Triggering instabilities must be compensated for in software which will be discussed in the next section.

Final alignment of the laser and optical system can now be done. Alignment is critical: the laser and microscope objective must be at the same height as the center of the streak camera's input optics to avoid any off axis distortion. The image is roughly focused on the streak camera by adjusting the position of the microscope objective (mounted on a 3D translation stage) while viewing the image with an ir viewer. Final focusing is completed while operating the streak camera in focus mode. In this mode the image is not streaked and it is possible to obtain the spatial variation of intensity across the array: Figure 5.2 is an example of this for the SDL laser C500. When the image is fully focused it appears as a horizontal array of bright spots each one corresponding to the emission of an individual emitter in the array. As the image is slightly defocused the spots should broaden and decrease in intensity symmetrically across the array indicating that the output facet of the array is parallel

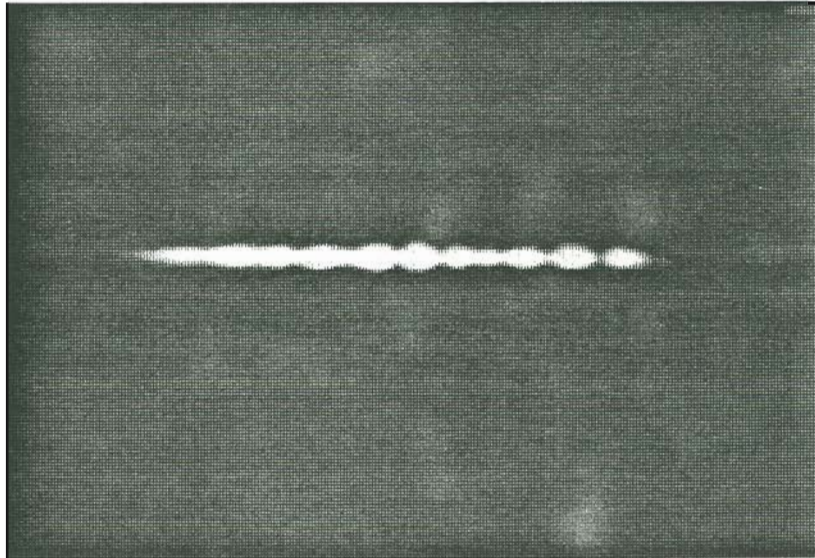


Figure 5.2 Spatial variation of the intensity across the array.
(SDL laser C500)

to the input plane of the streak camera. It is also important that the image of the array facet be horizontal since vertical displacement corresponds to time and cross correlations among the emitters would be of little value if the image were skewed. At this point it is possible to determine whether all emitters are functioning and whether or not there is an even intensity distribution across the array. For the gain guided arrays studied it was found that the central emitters in the array were more intense than the outer emitters, especially the end emitters. In some cases these end emitters were only faintly visible.

The streak camera can be switched to operate mode after the laser and optics have been aligned and focused. While viewing the television monitor the triggering delay for the streak camera trigger can be adjusted so that the streak trace is initiated at the beginning of a video frame and hence is visible on the monitor. The optical density of the neutral density filters placed at the input of the streak camera can be adjusted in combination with the gain adjustments of the camera to optimize the video signal. The signal to noise ratio is best using low to mid-range gain on the streak camera. It is desired to obtain data with a good dynamic range where the signal is maximized but not saturated; saturation of the signal causes information to be lost.

There are effectively three components of the system which have contrast and brightness adjustments, each of them independently causing the image viewed on the television monitor to be altered. The television monitor and frame grabber have contrast and brightness controls. The streak camera's output signal can be modified by changing the neutral density filters and by adjusting the gain setting; this is effectively changing the contrast and brightness of the signal. With all of these independent opportunities to modify the video signal before it is observed on the

monitor, it is imperative that there be some means to know the nature of the signal the streak camera is receiving.

An investigation was made to understand how the various components of the system biased the video signal. A grey scale generated by the frame grabber, independent of the settings of the contrast and brightness controls, was used as a video signal. This grey scale was recorded with the VCR in the same way that data is normally acquired. Several frames of the grey scale were frame grabbed (while varying the contrast and brightness settings of the frame grabber) with windows positioned within each shade of the scale to determine what affect these settings have on the dynamic range of the video signal. It was found that there was a significant difference in the range of the digitized average intensity profiles for the various frame grabber settings. It was found to be insufficient to determine non-biasing settings of contrast and brightness at which to record the data because much of the time the data would be saturated.

By looking at the taped image of the grey scale with an oscilloscope it was possible to determine what the black and white shades of the grey scale correspond to in absolute terms; in voltages. Knowing these upper and lower limits of the grey scale, individual frames could be analyzed, in real time, to see that the video signal falls within the accepted range of the grey scale from black to white. It is imperative that this signal has the maximum dynamic range possible without saturation. By placing the oscilloscope in line after the streak camera the intensity of the video signal incident on the streak camera can be checked to see that it is not saturating the camera. After the data has been recorded, the oscilloscope is placed in line after the frame grabber so that the contrast and brightness settings may be adjusted to optimize the signal being digitized.

5.3 Extraction of Data from Analog Video Signal

The process of extracting the data from the VCR tape begins by playing back the tape and observing the pulse to pulse behavior of the laser array under varying pump current levels and at different positions in the 50 ns pulse. At this point in the experiment, it has not yet been viewed since the tape is made with the monitor turned off to prevent the light it emits from entering the streak camera. The VCR used in the experiment has the capability of stepping through the tape a frame at a time. Two fields comprise a frame. One of the fields will be significantly brighter than the other since the image on the phosphor screen of the streak camera decays with time. Thus, alternate fields will be of the same relative intensity level. The data is extracted by stepping through the tape and selecting alternate fields to be digitized. When a field has been selected the image is frame grabbed, or digitized. This digitized image is accessed by the Apple IIe software which can then do some preliminary data analysis.

Primarily this analysis consists of data reduction. Rather than work with a 256 by 256 array of pixels, the array is reduced to an N by 256 array where N may denote, for example, the number of emitters in the array. This is accomplished by defining windows around each of the emitters in the array and then determining the average intensity across each window for each of the 256 channels or rows of pixels (each row of pixels represents a time interval of 22 ps). The windows are all set to the same width so that there are no problems with varying amounts of background signal being incorporated into these average values. The windows are drawn such that the right edge of one window forms the left edge of the next. These window positions remain constant throughout an entire data set with a particular laser. The

N by 256 array of average intensity values is written to N files on floppy disks for each of the fields in the data set. Typically twenty fields are processed for each data set to insure a representative sample of the transient response under those particular conditions, and to allow a reasonable average response to be determined. This average response is computed numerically by a straight summation of the intensity profiles comprising the data set. An average response allows one to determine if any of the behavior observed in the individual intensity profiles is random and then, if there are subtle effects being obscured by this random noise.

To achieve a meaningful average response for a temporal event such as the transient response of the array under pulsed operation it is necessary that all of the streak traces in the data set begin at precisely the same position in time with respect to the current pulse. The resolution of the streak camera operated in the slowest sweep speed is 22 ps/channel. A shift of even a couple of channels from pulse to pulse is intolerable, meaning that the electronics must be stable to within a few tens of picoseconds. This requires that there be essentially no jitter in the triggering electronics. With the equipment being used this requirement could not be satisfied. It was possible to minimize the drift in the position of the streak traces with respect to the current pulse by optimizing the adjustment of the triggering levels and output pulse shapes of the pulse generators. The remaining drift was compensated for with software.

To adjust for the triggering instability in software one requires as input a record of when the laser turns on for each trace. An analysis of several intensity files revealed that numerically determining when the laser turns on is quite difficult if the data is not digitized under optimal levels of contrast and brightness (ensuring a signal range from black to white). Under these optimal conditions the background level is

zero and the number of zeros in the file corresponds to the number obtained by counting the scan lines on the monitor before the laser turns on. In this case it would be straight forward to determine numerically when the laser turns on. If, for whatever reason, there is some bias in the video signal then this background level is no longer zero. In this situation it is much more difficult to determine when the signal rises above this background level. How steep a slope is required in the signal data before the laser is considered on? How long should this rise in intensity persist before it is considered lasing emission as opposed to noise? These problems are avoided by a visual determination of when the laser turns on. While viewing the intensity profile on the monitor one can observe when the laser turns on and count the number of scan lines between the top of the video frame and the point at which the laser emission is observed to begin. The monitor used gives an under-scanned view of the video frame which ensures that the first observed scan line is in fact the first scan line of the frame. A record is made of this triggering delay information for each of the fields as they are being digitized. Once a data set has been extracted from the tape, a triggering delay file made and, average intensities determined and written to files on floppy disks then these files can be transferred electronically to the MicroVAX for in-depth analysis.

5.4 Data Transfer and Creation of Array Files

The data transfer process involves reading the individual emitter reduced intensity files (average intensity across the window) from floppy disks on the Apple IIe and transmitting this data to the MicroVAX where the triggering compensation software determines the maximum length of the array files to be prepared for a given data set. Part of the rationale for forming these array files is to limit the number of files that

need to be accessed each time a calculation is made. For a typical data set of twenty files, two hundred files representing the intensity profiles of the individual emitters must be transferred. Formation of array files permits a reduction in the number of these files to twenty. Another reason for creating array files is that it allows the intensity data for a given field to be normalized to one. This normalization is essential for the graphics software which will be discussed in a later section.

The data transfer process begins on the MicroVAX with the program "max.trig.f". This program reads the triggering data file and creates an output file in which the maximum triggering delay is the first element followed by the delay values for each of the intensity profiles in the data set. When the array files are formed this output triggering file is accessed to determine the starting point of the intensity profile array and its length.

Next the connection to the MicroVAX is established using a modem plugged into the Super Serial card of the Apple IIe, and the data transfer program run (see Appendix A for a listing of the code). Essentially, the program toggles the Apple between two states: terminal emulation mode and data communication mode. In terminal emulation mode the Apple reads the data files on the floppy disks. Then, in data communication mode commands may be executed on the MicroVAX such as editor commands which allow a file on the MicroVAX to be opened and data appended to it. The data is then ported to the MicroVAX through the, now transparent, Super Serial card and modem connection to the opened file. Once all of the intensity data files for a given field have been transferred a shell script, "datin.shell", is executed on the MicroVAX which calls the program that forms the array file, "mkarray.wnd.trg.f" (see Appendix B), and then removes the individual intensity files that were used to form the array. Control returns to the Apple in terminal emulation mode where it

begins to read and transfer the next field's data files. The data transfer program was designed to make the process essentially automated since it takes a few hours to transfer the two hundred files comprising a data set even with software control of the transfer.

5.5 Statistical Analysis Software on the MicroVAX

Visually, the streak traces observed on the monitor give a qualitative view of the fast pulse response and thus are invaluable in providing insight into the processes responsible for such behavior. With the video frame grabbing capability of this system it is now possible to make some quantitative observations of the transient response. The statistical analysis software was designed with the goal of understanding the physics of the transient response of the phased array diode laser. To this end, the analysis performed includes:

- discrete Fourier transforms (DFT) for each emitter of the array for each field in the data set
- auto- and cross-correlations among the individual emitters in the array for each field in the data set
- averages of both the discrete Fourier transform and correlation results for the data set
- the average intensity profile for the data set
- both Fourier transforms and correlations on this average intensity profile

- the intensity profile of the array as a whole for each field in the data set

- the average response from each emitter for each field in the data set

5.5.1 The discrete Fourier transform

Knowing the discrete Fourier transform (DFT) of the sequence of intensity values for each of the emitters in the array may allow association of a physical process with an observed frequency. For example, lasing wavelength splitting caused by multiple transverse mode operation is expected and should appear as beating in the time domain. Analyzing different portions of the 50 ns pulse provides further information about what process may be responsible for a given spike in the DFT spectrum. Relaxation oscillations, for example, would only be present in the initial portions of the pulse. Multiple frequencies may be present in the DFT spectrum at the beginning of the pulse but as time goes on and the response is stabilizing, it is reasonable to expect fewer frequencies in the spectrum and possibly different ones than those observed for the beginning of the pulse. Comparisons between data taken under similar conditions with different lasers will help to confirm any possible assignments of physical process to observed frequency.

5.5.2 The auto- and cross-correlation

The calculation of the auto- and cross-correlations provides information about the strength of coupling, or interaction, among the individual emitters in the array and on the competition between the array modes. An array operating in phase should show strong correlation among the individual elements. Any phase shifts observed in the position of the peaks of the correlation profile would certainly be of

interest. This change in the cross correlation with time reflects a shift in the relative phases of the two emitters and yields information on the stability of phase locking. A correlation profile that appears to be a combination of two or more separate units would indicate that portions of the array were operating independently and that in phase operation of the entire array was not possible. Physically, this type of behavior could be explained by increased spacing among several of the emitters or other non-uniformities or defects in the emitters themselves.

5.5.3 The algorithms

A brief description of the algorithms for the discrete Fourier transform and correlation calculations is given below. These calculations are performed within sub-routines of the main data analysis program, "statc.crl.trg.F". A complete listing of the code for "statc.crl.trg.F" may be found in Appendix C.

Discrete Fourier transform. The finite discrete Fourier transform (DFT) of a sequence of N complex numbers $z_j, j = 0, 1, \dots, N-1$ is defined by:

$$\hat{z}_k = \frac{1}{\sqrt{N}} \sum_{j=0}^{N-1} z_j \times \exp \left[-i \frac{2\pi jk}{N} \right] \quad (5.1)$$

for $k = 0, 1, \dots, N-1$. The transform is periodic with period N hence, $\hat{z}_k = \hat{z}_{k \pm N}$ and specifically, $\hat{z}_{-k} = \hat{z}_{N-k}$. If the original sequence is expressed as a complex number with real and imaginary components $z_j = x_j + iy_j$ then the transform $\hat{z}_k = a_k + ib_k$ may be written in terms of sines and cosines as:

$$a_k = \frac{1}{\sqrt{N}} \sum_{j=0}^{N-1} \left[x_j \cos \left[\frac{2\pi jk}{N} \right] + y_j \sin \left[\frac{2\pi jk}{N} \right] \right] \quad (5.2a)$$

$$b_k = \frac{1}{\sqrt{N}} \sum_{j=0}^{N-1} \left[y_j \cos \left[\frac{2\pi jk}{N} \right] + x_j \sin \left[\frac{2\pi jk}{N} \right] \right] \quad (5.2b)$$

When the original sequence is real, $z_j = x_j$, then:

$$\begin{aligned} \hat{z}_k &= \frac{1}{\sqrt{N}} \sum_{j=0}^{N-1} x_j \exp \left[-i \frac{2\pi jk}{N} \right] \\ &= a_k + ib_k \\ &= \frac{1}{\sqrt{N}} \sum_{j=0}^{N-1} \left[x_j \cos \left[\frac{2\pi jk}{N} \right] \right] + \frac{i}{\sqrt{N}} \sum_{j=0}^{N-1} \left[x_j \sin \left[\frac{2\pi jk}{N} \right] \right] \end{aligned} \quad (5.3)$$

The DFT of a real sequence is a Hermitian sequence with the properties: $a_{N-k} = a_k$, $b_{N-k} = -b_k$, $b_0 = 0$, and if N is even, $b_{\frac{N}{2}} = 0$.

The DFT subroutine calculates the discrete Fourier transform of each column in the intensity data array. This corresponds to a DFT in the time domain since the columns contain intensity information as a function of time for a single emitter. The data in the two dimensional array is read a column at a time into a real one dimensional array required by the Numerical Algorithms Group (NAG) library routine "c06eaf" which computes the result. Each of the individual columns of intensity data is a real sequence and consequently the resulting DFT is a Hermitian sequence. The modulus of the resulting DFT is the quantity of interest. These results are normalized before being written to a file.

Correlation. The correlation of two vectors x and y is defined by:

$$w_k = \sum_{j=0}^{N-1} x_j y_{k+j}$$

where x and y are real with period N . When x and y are the same, the auto-correlation is formed.

The correlation subroutine calculates the correlation of the intensity data from each of the emitters with that of the central emitter, emitter number five. Before the

correlations are computed, the mean of each of the columns of data in the intensity array is determined and subtracted off from each data value in the respective column. The data in the two dimensional array is read two columns at a time into the one dimensional arrays that the NAG library routine c06ekf requires. The correlation must be normalized so that the relative intensities of the two emitters involved is not a factor in the magnitude of the correlation. The normalization of w_k is done as follows:

$$w'_k = \frac{w_k}{\left[\sum_{j=1}^N x_j x_j \right]^{1/2} \left[\sum_{j=1}^N y_j y_j \right]^{1/2}} = \frac{\sum_{j=0}^{N-1} x_j y_{k+j}}{\left[\sum_{j=1}^N x_j x_j \right]^{1/2} \left[\sum_{j=1}^N y_j y_j \right]^{1/2}} \quad (5.4)$$

where x and y are real with period N. With this compensation for the varying intensity levels of the emitters completed, the result array must be normalized again so that a graphic display of the results is possible. The correlation values lie between negative one and one so if one is added to each value the range shifts to lie between zero and two. Now these values can easily be normalized to one to make possible the graphic display of the correlation results for all of the emitters simultaneously.

5.6 Graphic Display

Much information may be gained through graphic presentation of the intensity data and corresponding results. Initially, the intensity profiles, (depicting the average intensity across each of the windows defining the emitters), for the data set would be plotted. A menu driven graphics program, "gr", was developed for the MicroVAX by Paul Turner, at OGC, which allowed these intensity profiles to be plotted with a laser printer. Because of the similarity of the plot parameters and the menu driven

operation of "gr", controlling software was developed to expedite the process. A similar approach was taken with regard to the graphic display of the DFT and correlation results. As an example, the controlling programs for these result files may be found in Appendix D. Several other result files were handled in a similar manner including, the plots of the average intensity of the individual frames.

The ability to generate halftone prints of individual frames of data was added to the graphic analysis. Robert Carey developed the machine language programs on the Apple IIe that access the frame-grabber memory to produce the 256 by 256 array representing the image. Richard DeFreez and David Bossert then developed the necessary software to generate a halftone image from the 256 by 256 array produced by the Apple IIe.

With this increased capability it became possible to consider working with the full intensity image rather than the intensity profiles. There are limitations on this however, as the amount of data to be transferred to the MicroVAX and to be processed is increased significantly. A three-dimensional (3-D) plot of the intensity surface would be a useful and informative means to view the intensity data. A UNIX graphics program "plot3d" was obtained and ported to our MicroVAX by Mark Foster of the OGC Computer Science and Engineering Department. The required software was written to put the intensity data in the form required by "plot3d".

6. RESULTS

The previous chapter presented a detailed discussion of the experimental studies conducted. This chapter contains a representative sample of the results of those studies. Section 6.1 gives the near-field optical response. The discrete Fourier transform and correlation results of the near-field data are presented in Section 6.2. In Section 6.3, both the near- and far-field optical response of a Y-guide array is given .

6.1 Near-field Optical Response

The near-field optical response of several different gain-guided diode laser arrays was observed and recorded as described in the previous chapter. Streak camera data was taken for pulsed injection currents of both $1.5I_{th}$ and $2.0I_{th}$ (from zero bias current). For one of the laser arrays, the near-field optical response was observed and recorded for three different temporal positions within the duration of the pulse-- the beginning, middle, and end of the current pulse. For each of the temporal positions within the pulse, the variation in the optical response from pulse to pulse is significant. A representative sampling of the intensity profiles is included in this section to give an impression of the range of the variation in the optical response from a particular laser under fixed conditions.

Two of the lasers studied will be examined here. The first of the laser arrays was fabricated by Xerox from double heterostructure material with a multiple

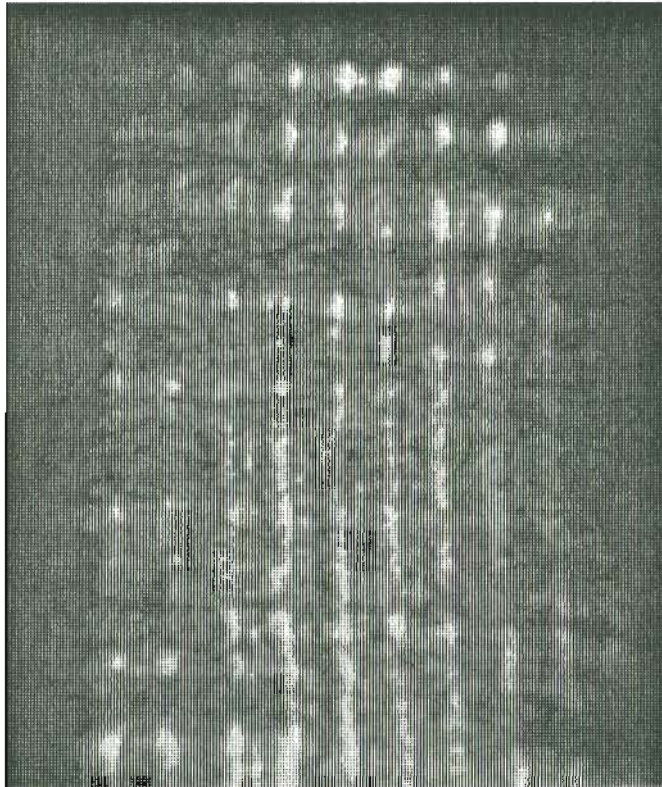
quantum well active layer. The second laser array was fabricated by Spectra Diode Labs. Intensity information on these lasers is grouped according to the particular laser array. Differences in the pulse to pulse response may thus be readily examined.

6.1.1 Xerox laser 3-C-2

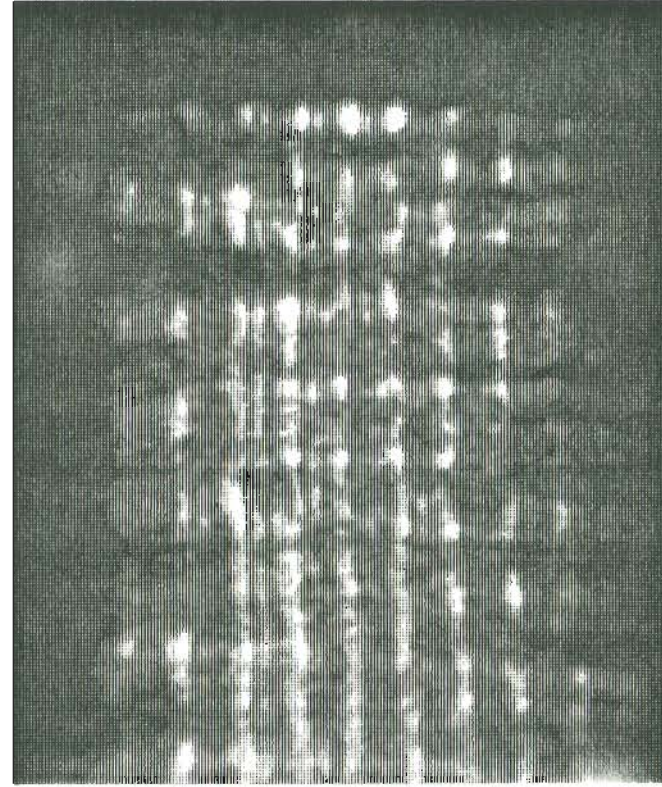
Intensity information presented on this laser includes data taken with pulsed current levels of $1.5I_{th}$ from zero bias current. Figure 6.1 is a halftone reproduction of the near-field intensity versus time of the ten emitter gain guided array for two different current pulses. The frame on the left corresponds to the fifth pulse in the set and the frame on the right to the fifteenth. The total time represented in each of these frames is 5.5 ns. The time scale for these halftones begins with zero at the top and increases to 5.5 ns. at the bottom of the frame. Lasing begins in the upper region of the frame and as time progresses the light output is streaked downward across the frame. The lasing emission is definitely nonuniform both spatially, across the emitters, and temporally, throughout the duration of this portion of the current pulse.

Considering the spatial variation first, there are obvious differences in the intensity between the central and outer emitters. If the leftmost emitter is the first emitter, then the tenth emitter is nearly unrecognizable. The streak trace of the tenth emitter is only visible after the others are already established, and even then is very faint. Weakly lasing outer emitters is typical behavior for all of the gain-guided laser arrays studied.

Of all the arrays examined, this laser gave the strongest indications of phase-locking as it is apparent from looking at the halftones of Figure 6.1 that the optical



(a)



(b)

Figure 6.1 Time evolution of the near-field pattern for Xerox laser 3-C-2 at $1.5I_{th}$ (beginning of pulse). Half-tone (a) represents frame 5, (b) frame 15.

intensity between the emitters is significant. This appears as narrow stripes in between each of the stripes representing the output of the emitters. The intensity between the stripes defined by the emitters is correlated in time in the same way as that of the emitters. That is, the spiking observed occurs at the same temporal positions as for the emitters. It is significant that this spiking is observed. Initially several sharp spikes are observed; these correspond to the relaxation oscillation peaks. Beyond this point in time spiking behavior persists but the spikes are less well defined and there seems to be an overall background level developing such that the intensity observed between the spikes is non-zero.

This phenomena may be seen more clearly in Figure 6.2 which is an intensity profile of the array for the fifth frame. This data is obtained by forming an average intensity across a window defining the emitter for each of the ten emitters in the array, as discussed in the previous chapter. In this graph the temporal axis is given in units of pixel number; each pixel represents 22 ps. The well correlated relaxation oscillations may be identified as well as the increased "background" level of emission with the more rapid, less pronounced spikes.

Figure 6.3 gives the average intensity of frame five. It is apparent from this figure that the emission of the array as a whole is not stabilized in the first 5.5 ns of a current pulse. Four well defined relaxation oscillation peaks may be noted. Following these oscillations, the overall emission of the array averages out at about 75 % of the maximum output of one of the relaxation oscillation peaks.

The next figure, Figure 6.4, is an expanded view of the intensity profile for two adjacent emitters, emitters four and five. This figure demonstrates the near exact correlation between adjacent emitters. Even fine structure on some of the spikes has its counterpart on the adjacent emitters intensity profile. Although the spiking is

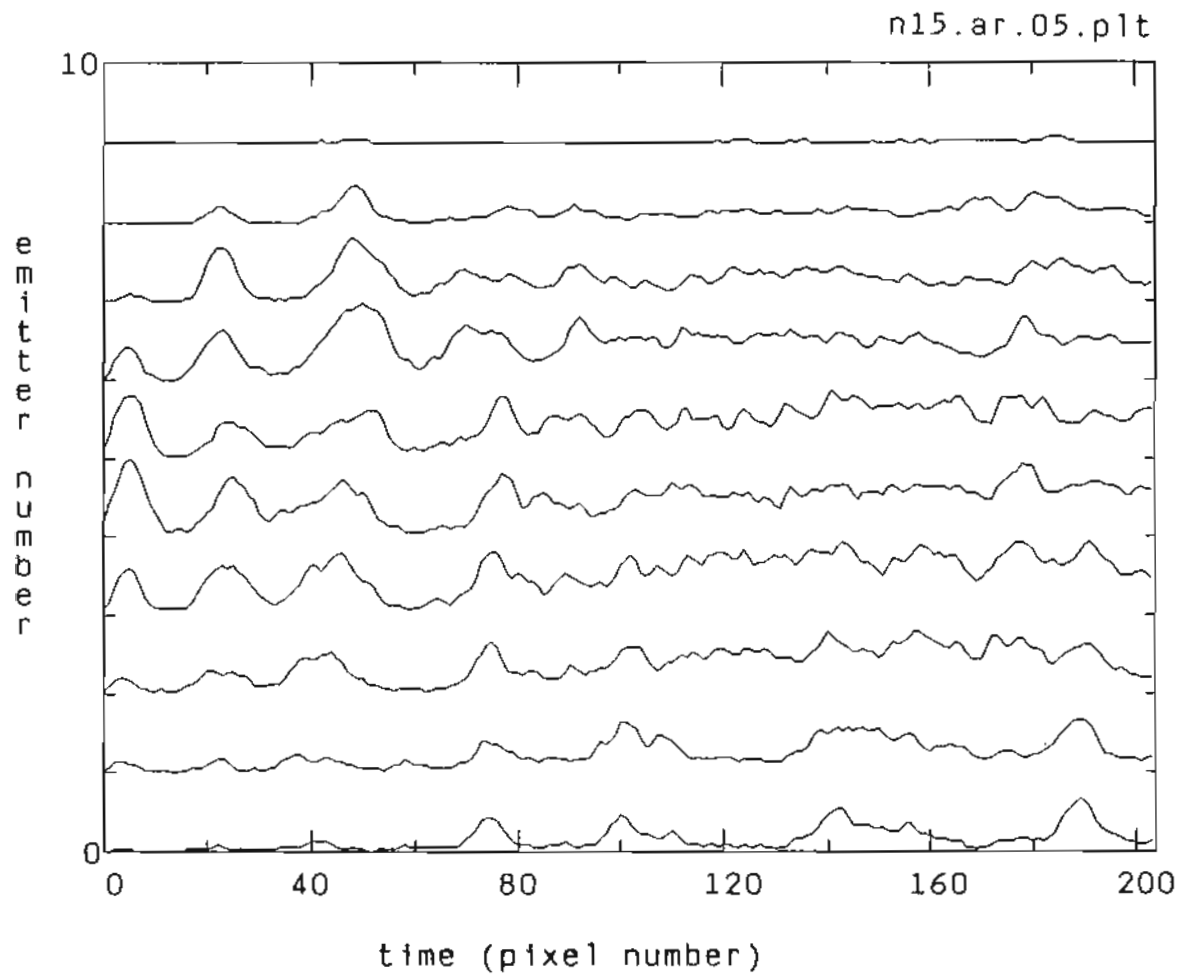


Figure 6.2 Intensity versus time profile for frame 5.
(one pixel equals 22 ps.)

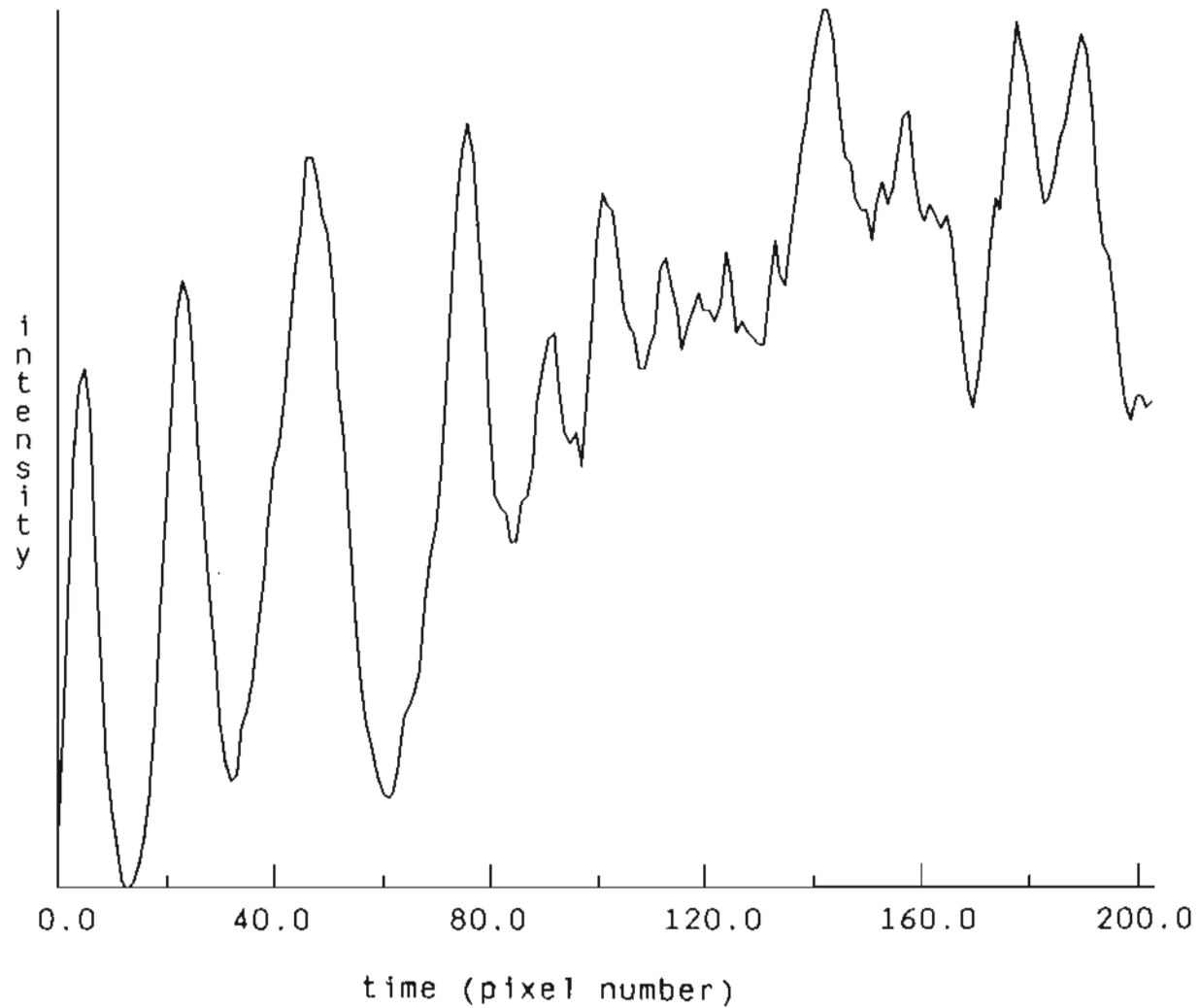


Figure 6.3 Average intensity of the array for frame 5.
(one pixel equals 22 ps.)

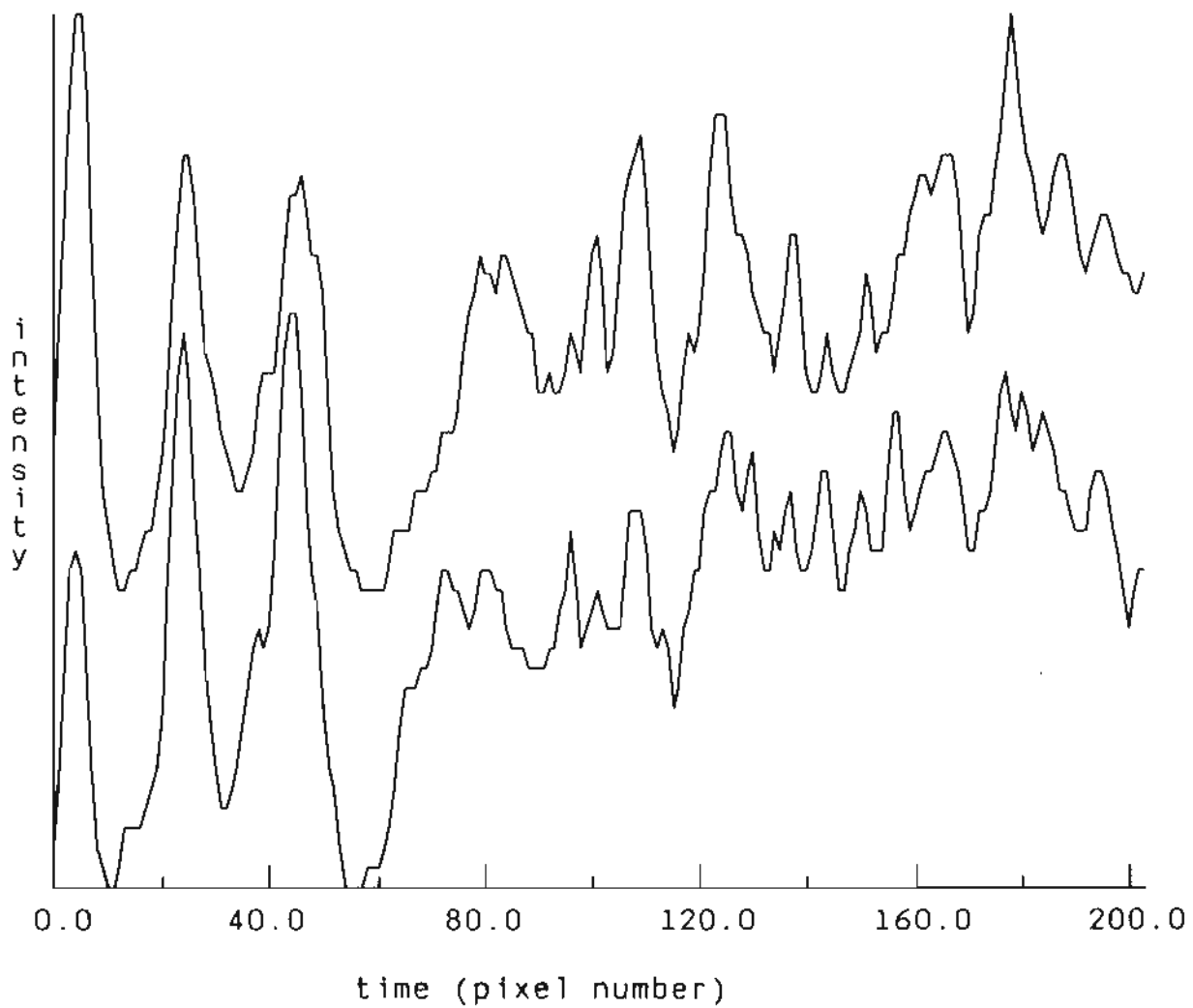


Figure 6.4 Intensity versus time profile for emitters 4 and 5.
(one pixel equals 22 ps.)

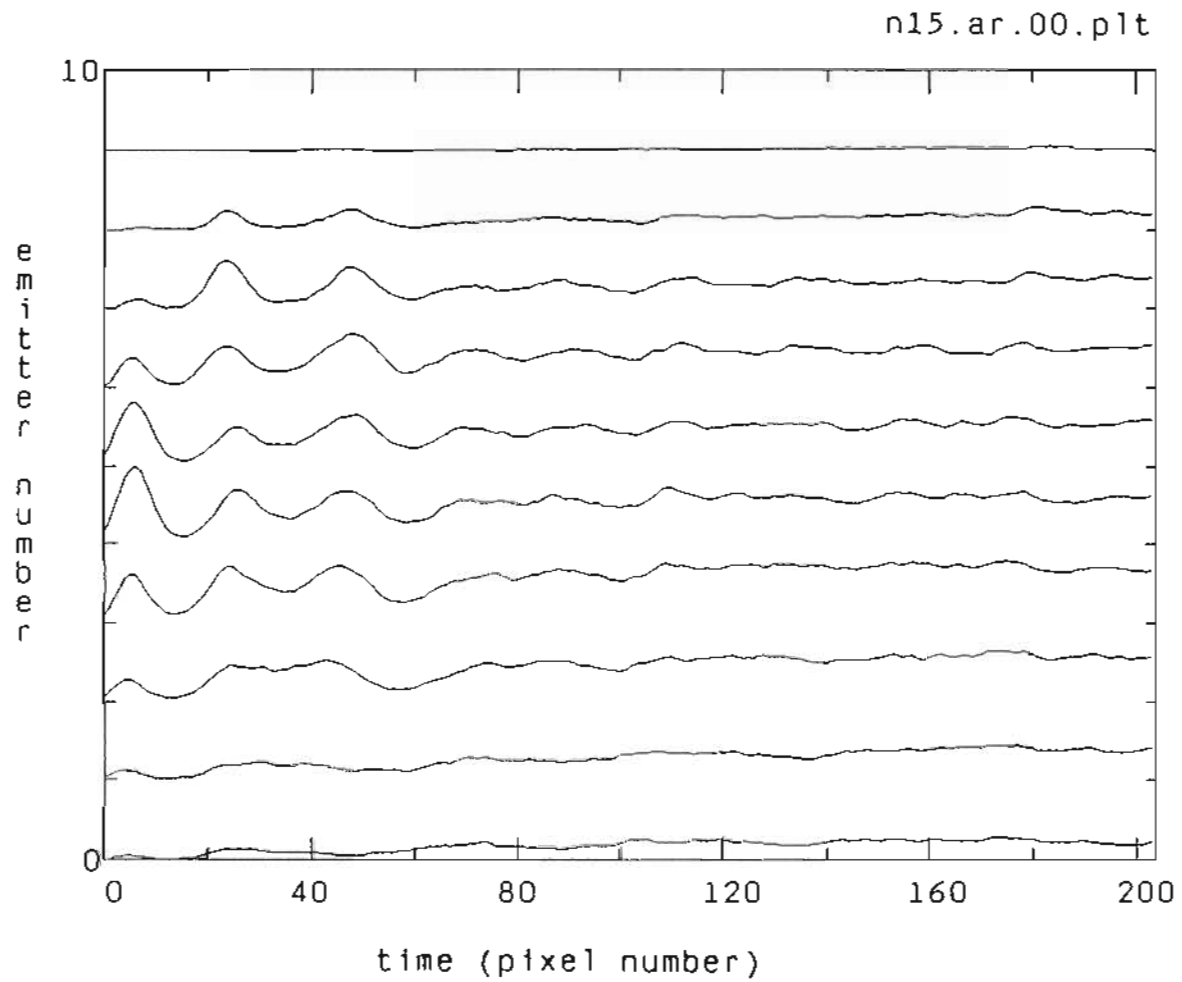


Figure 8.5 Average intensity versus time profile.
(one pixel equals 22 ps.)

directly correlated across the emitters within a given frame, nearly all of the spiking beyond the relaxation oscillation peaks averages out when multiple frames in a data set are averaged. Figure 6.5 is the average intensity profile of the array in which twenty frames were averaged. Three relaxation oscillation peaks are visible. The relative flatness of the remaining portion of the intensity profile suggests that the rapid spiking noted in the previous figures is randomly phased.

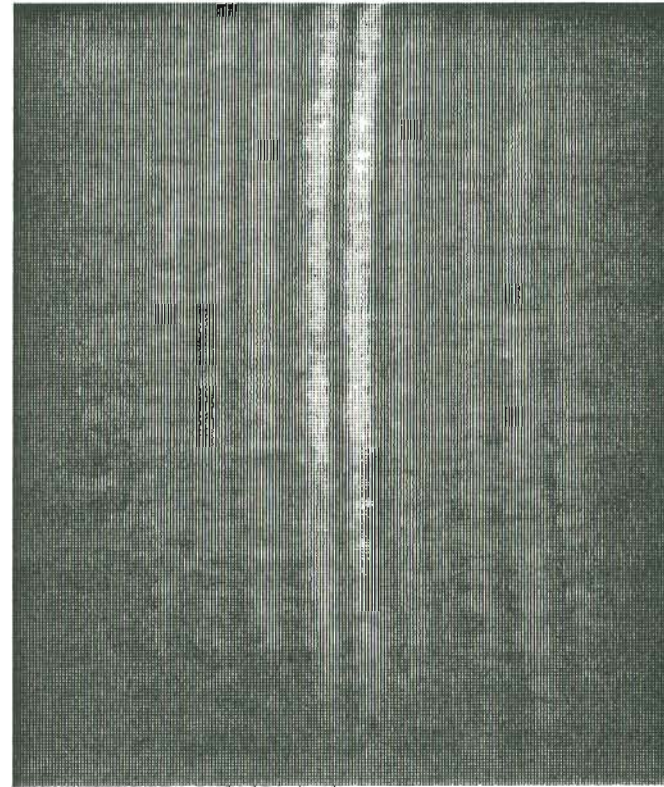
6.1.2 Spectra Diode Labs laser SDL500

Intensity information presented on this laser includes data taken with pulsed current levels of both $1.5I_{th}$ and $2.0I_{th}$ (from zero bias current). At $1.5I_{th}$ the beginning and end of the pulse was studied. At $2.0I_{th}$ the beginning, middle and end of the pulse was examined. The results of the studies at a current level of $1.5I_{th}$ were inconclusive with regard to correlations among the emitters since the array was not lasing strongly at this level. Only the central emitters were clearly visible with the outer emitters only faintly discernible. Figure 6.6 shows two halftones depicting the beginning (left) and the end (right) of the near-field optical response to a current pulse at $1.5I_{th}$. It is evident that the laser does not come on strongly. There is a variation in the delay time of the elements of the array with the central emitters responding more quickly than the outer emitters.

The halftones of Figure 6.7 show the laser array turning on quite strongly with all ten emitters visible in each of the two frames. This figure and subsequent figures depict the near-field optical response to pulsed current at $2.0I_{th}$. At $2.0I_{th}$, rather than $1.5I_{th}$, the SDL laser exhibits behavior more closely related to that of the Xerox laser at $1.5I_{th}$ (compare with Figure 6.1). Similarities include the well defined

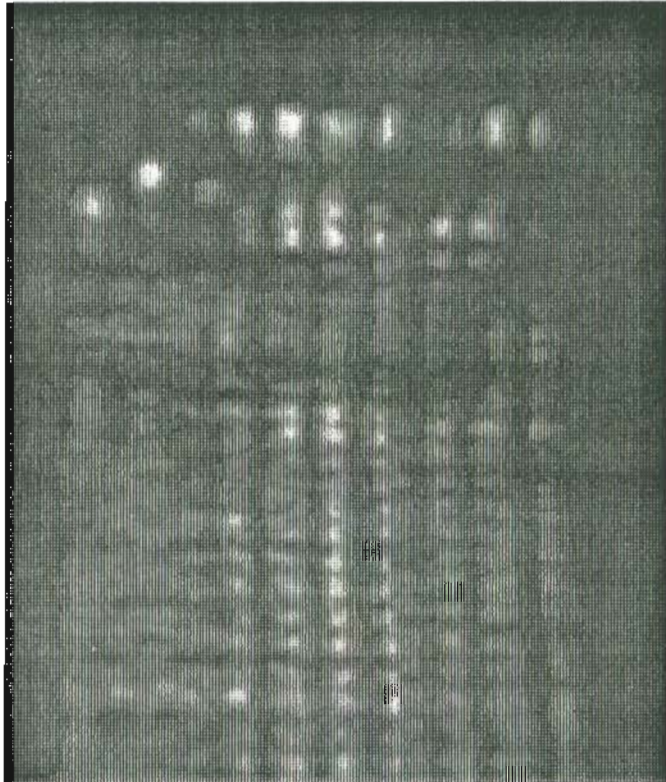


(a)

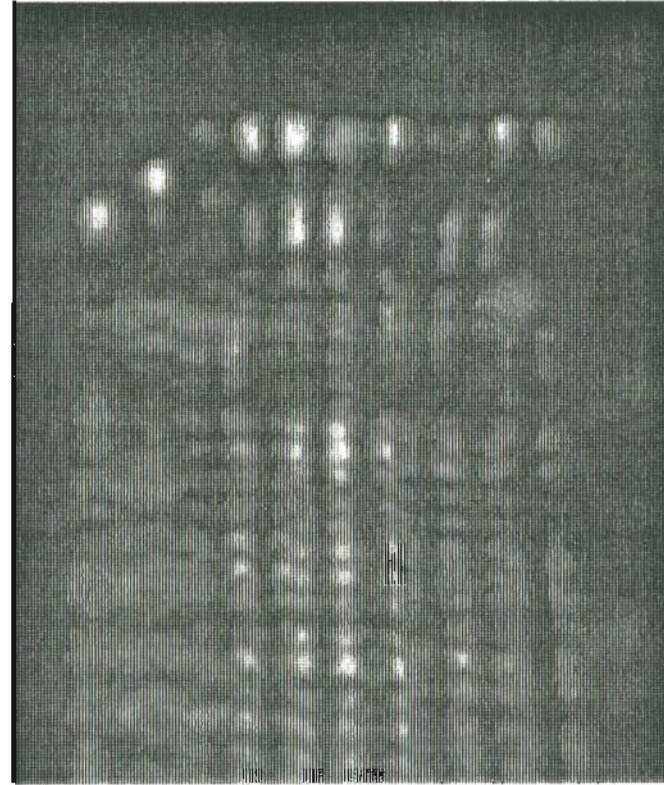


(b)

Figure 6.6 Time evolution of the near-field pattern for SDL laser C500 at $1.5I_{th}$ (beginning & end of pulse). Halftone (a) represents the beginning, (b) the end.



(a)



(b)

Figure 6.7 Time evolution of the near-field pattern for SDL laser C500 at $2.0I_{th}$ (beginning of pulse). Halftone (a) represents frame 10, (b) frame 20.

switch-on of the array, the obvious spiking of the intensity and central emitters with a stronger optical response. There are differences as well; with the SDL laser, the first two emitters turn on after the other emitters and together with the third emitter seem to operate more stably than the rest of the array. The intensity profile of these three emitters has very gentle oscillations and is largely uniform after the initial switch-on. The spiking observed in the remaining emitters of the array appears to be quite periodic and strongly correlated from emitter to emitter across the array. Between the emitters there is less overlap of adjacent optical intensities, with the exception of the first three emitters, than seen with the Xerox laser.

The structure of the near-field optical response may be examined in another way with the use of three-dimensional (3-D) graphics. The same intensity values used to produce the halftone prints of Figure 6.7 are used to generate the 3-D image of Figure 6.8. The intensity scale is in arbitrary units and the time axis is again in units of pixel number. The unlabeled axis defines the spatial dimension with the first emitters on the right side of the plot. Compare the halftone image of the intensity (Figure 6.7) with the 3-D plot (Figure 6.8); note the position of the first two emitters initial spikes to confirm the relative orientation of the two types of plots. The next three figures are the first, second, and third parts, respectively, of the full 3-D image. Intensity profiles of this complexity require either a larger format or segmentation into multiple parts. With these 3-D images it is easier to develop an understanding of the interaction between emitters since the relative height of the intensity profile between emitters is a measure of the interaction or overlap of their optical fields. Recall from the discussion of the halftones of Figure 6.7 that the first three emitters appear to operate more stably than the others after the initial peak. Figures 6.10 and 6.11 demonstrate this observation quite well.

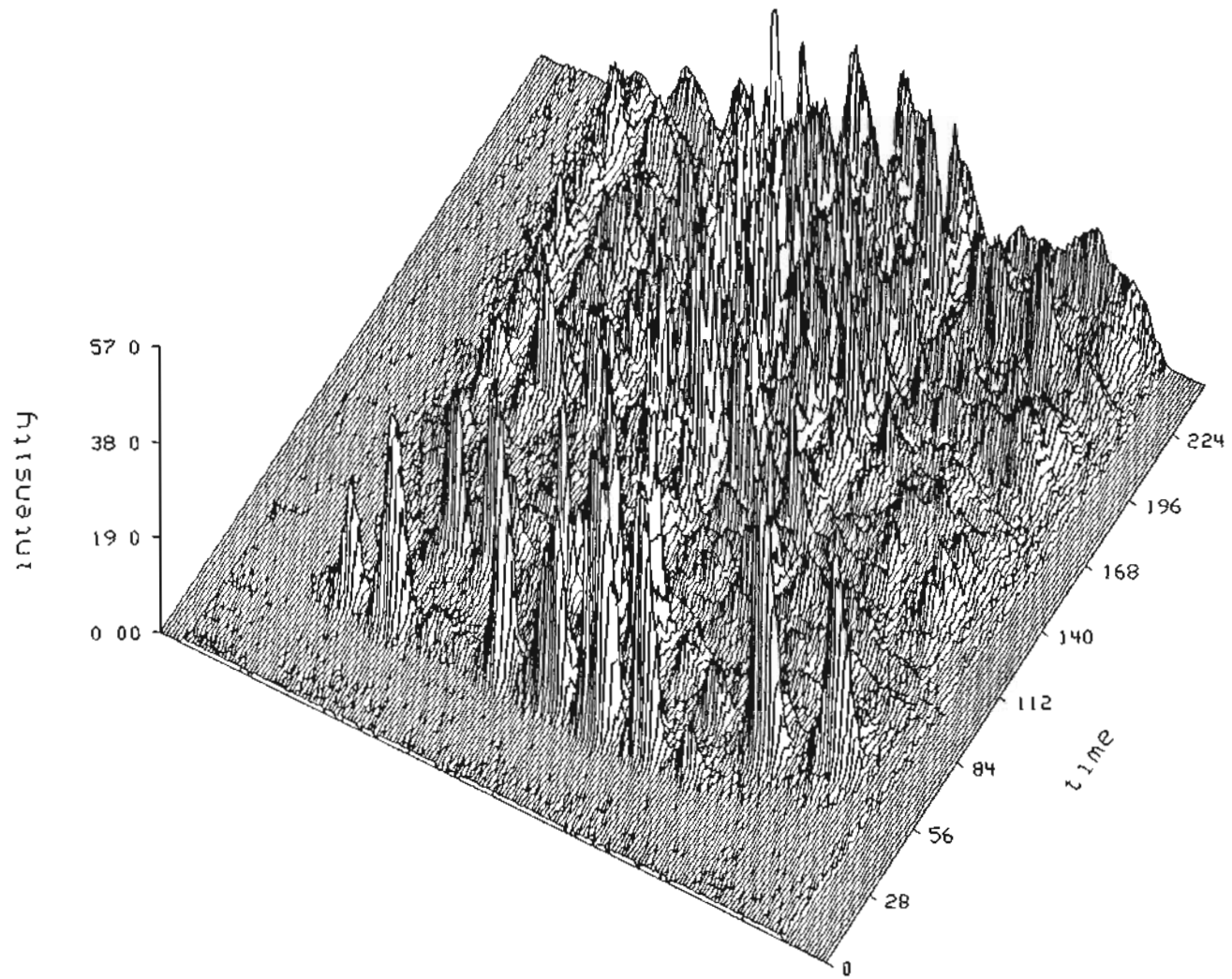


Figure 6.8 Three dimensional plot of the intensity surface for the near-field pattern of Figure 6.7a.

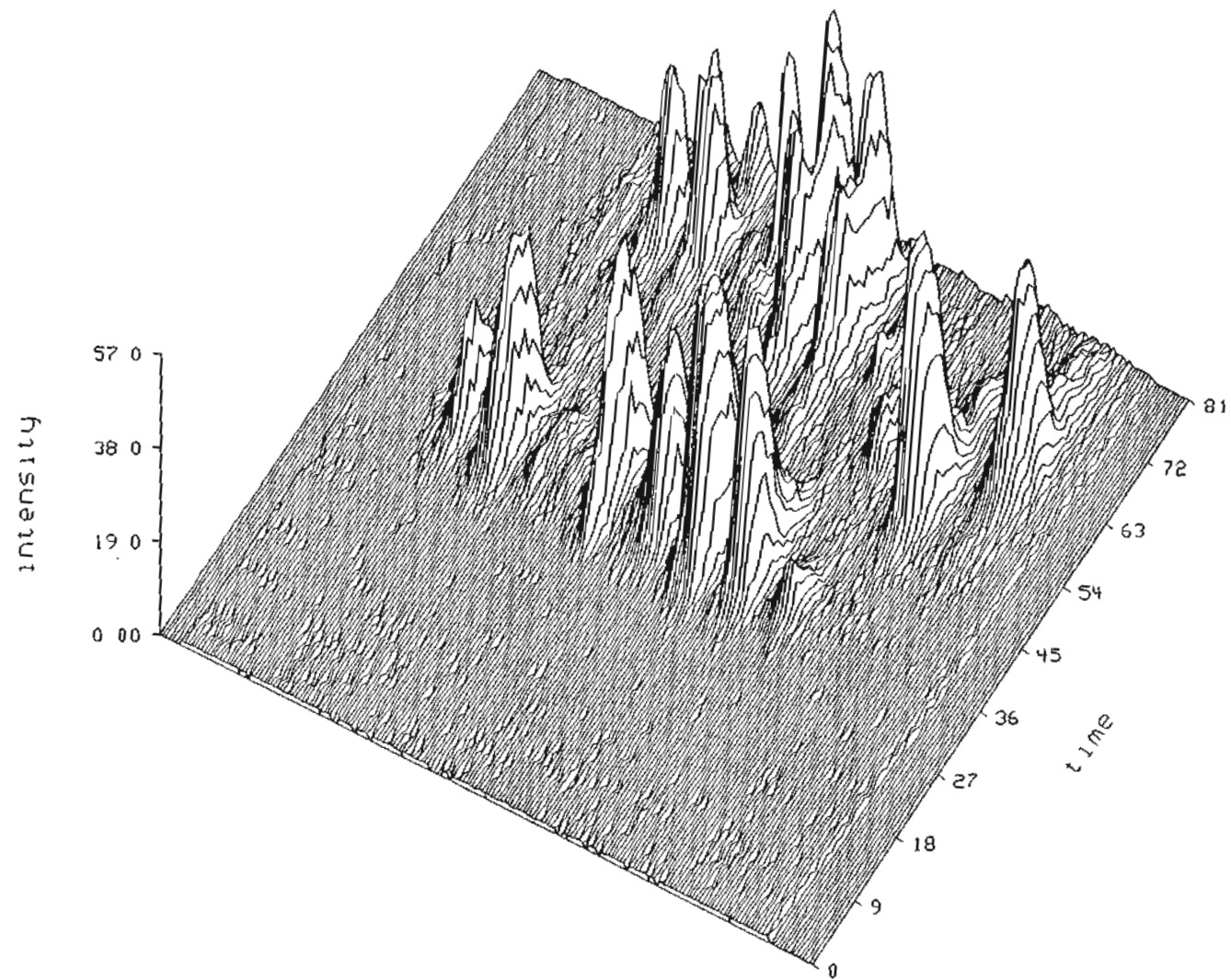


Figure 6.9 An expanded view of the first third of the intensity surface of Figure 6.8.

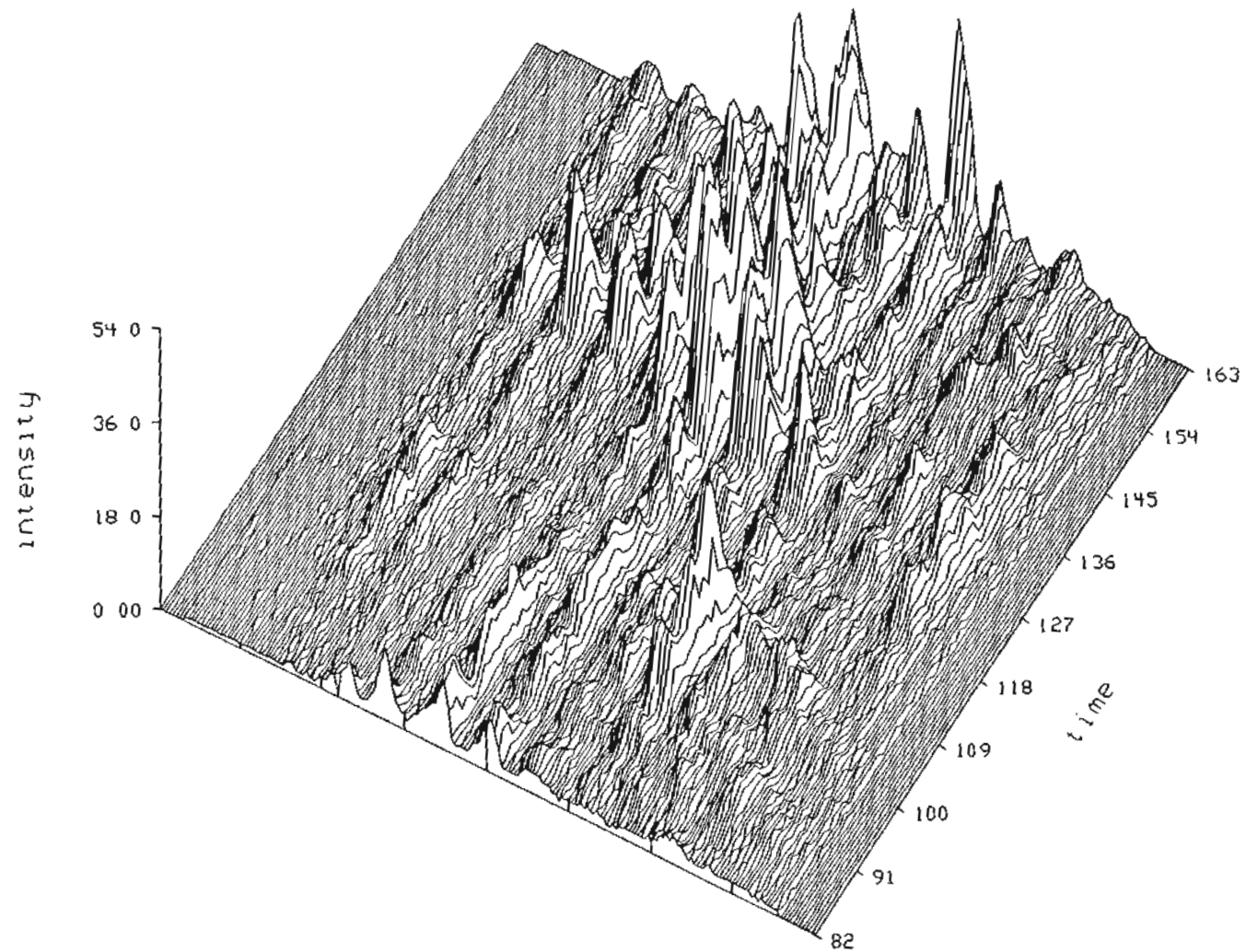


Figure 6.10 An expanded view of the middle third of the intensity surface of Figure 6.8.

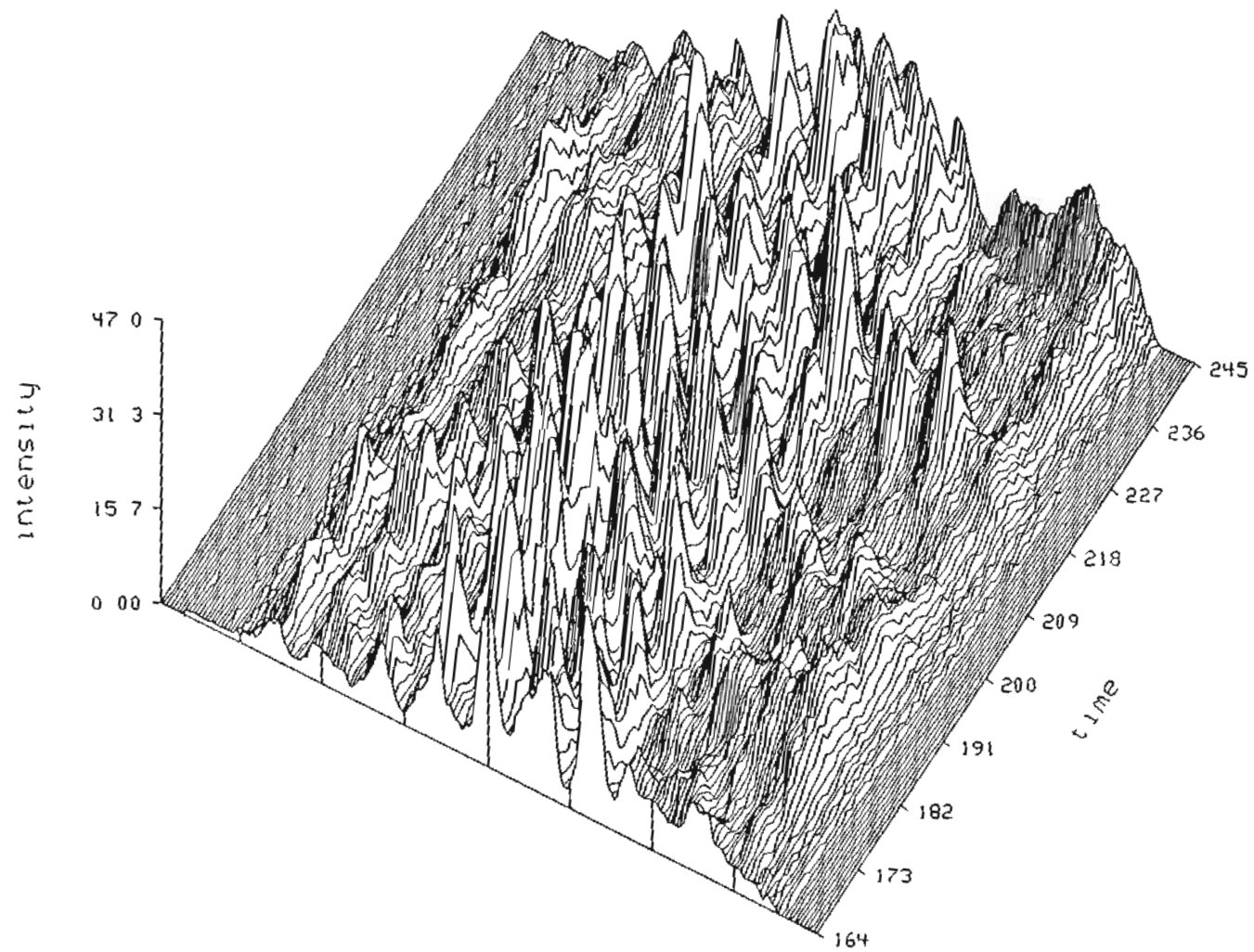


Figure 6.11 An expanded view of the last third of the intensity surface of Figure 6.8.

Another interesting observation to make is to evaluate the average intensity profile of the entire array. This profile is determined by finding the average intensity at each point in time, across all 256 pixels of intensity values. Figure 6.12 shows four such average intensity profiles. Three of them are for consecutive frames in the data set. There is significant pulse to pulse variation even in these average intensity profiles.

Figures 6.13 and 6.14 show the intensity profiles of three of the frames depicted in Figure 6.12 as well as an average intensity profile. This average intensity profile is obtained by forming an average of the twenty intensity profiles of the data set. The rapid spiking of the individual intensity profiles is absent in this average profile. Only two relaxation oscillation peaks may be observed in this average profile compared with three in Figure 6.5 (Xerox laser 3-C-2).

The following series of figures depict the near-field optical response to the middle portion of the current pulse, again at $2.0t_{th}$. In these figures and those for the response to the end of the pulse, it is apparent that there is a problem with the response of the streak camera system at the beginning of the streak trace for emitters nine and ten. The intensity profiles of these emitters are weak at the beginning of the streak trace. Figure 6.15 is a halftone image for this middle section of the pulse response. Compare this figure with Figure 6.7 which gives two halftones for the beginning of the pulse response. Throughout the 5.5 ns duration of this middle portion of the pulse, the response is reasonably consistent. The same periodic spiking observed in the later portion of Figure 6.7 is present here however, the extent of the spiking is greater, spanning the entire array. The first emitter appears to be responding much more strongly than in the beginning of the pulse. The first three emitters seem to be operating with more interaction among them as in the beginning of the

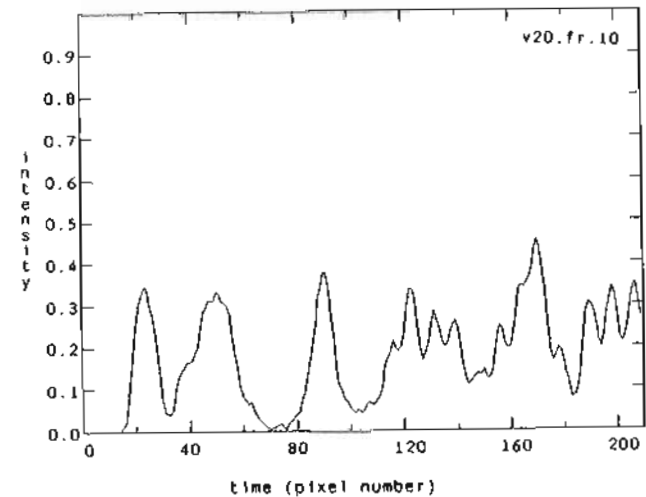
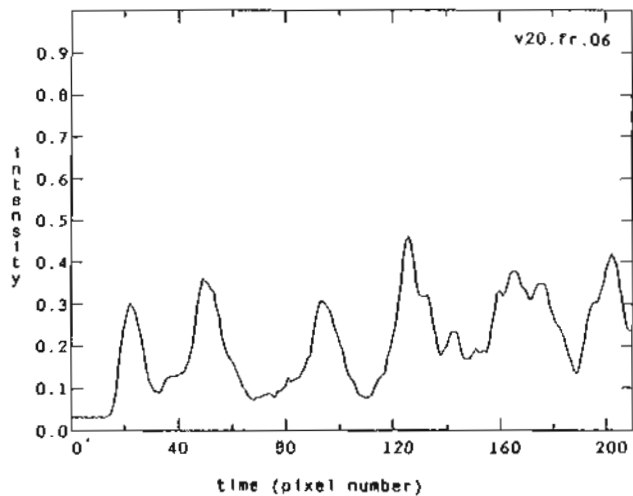
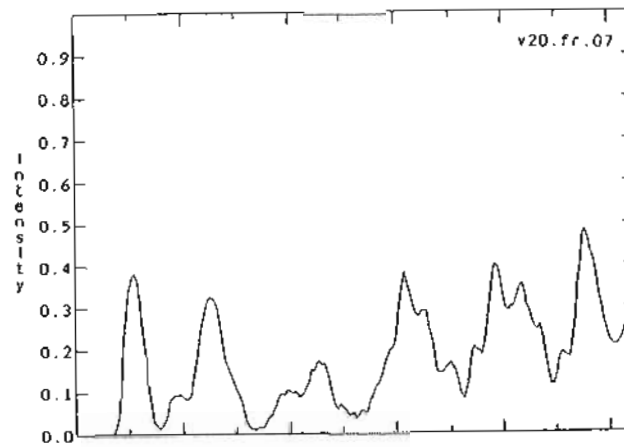
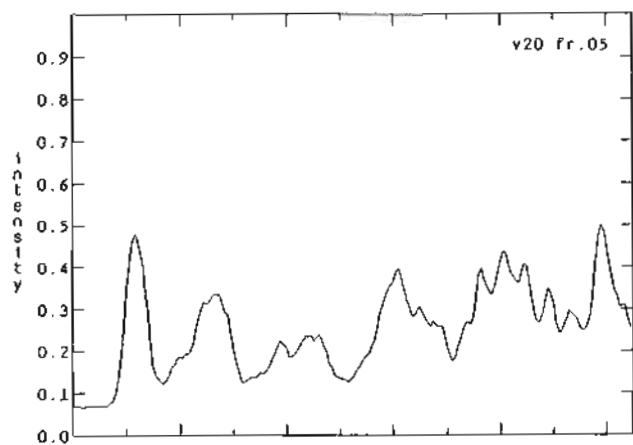


Figure 8.12 Average intensity of the array at the beginning of the pulse for successive pulses. (one pixel equals 22 ps.)

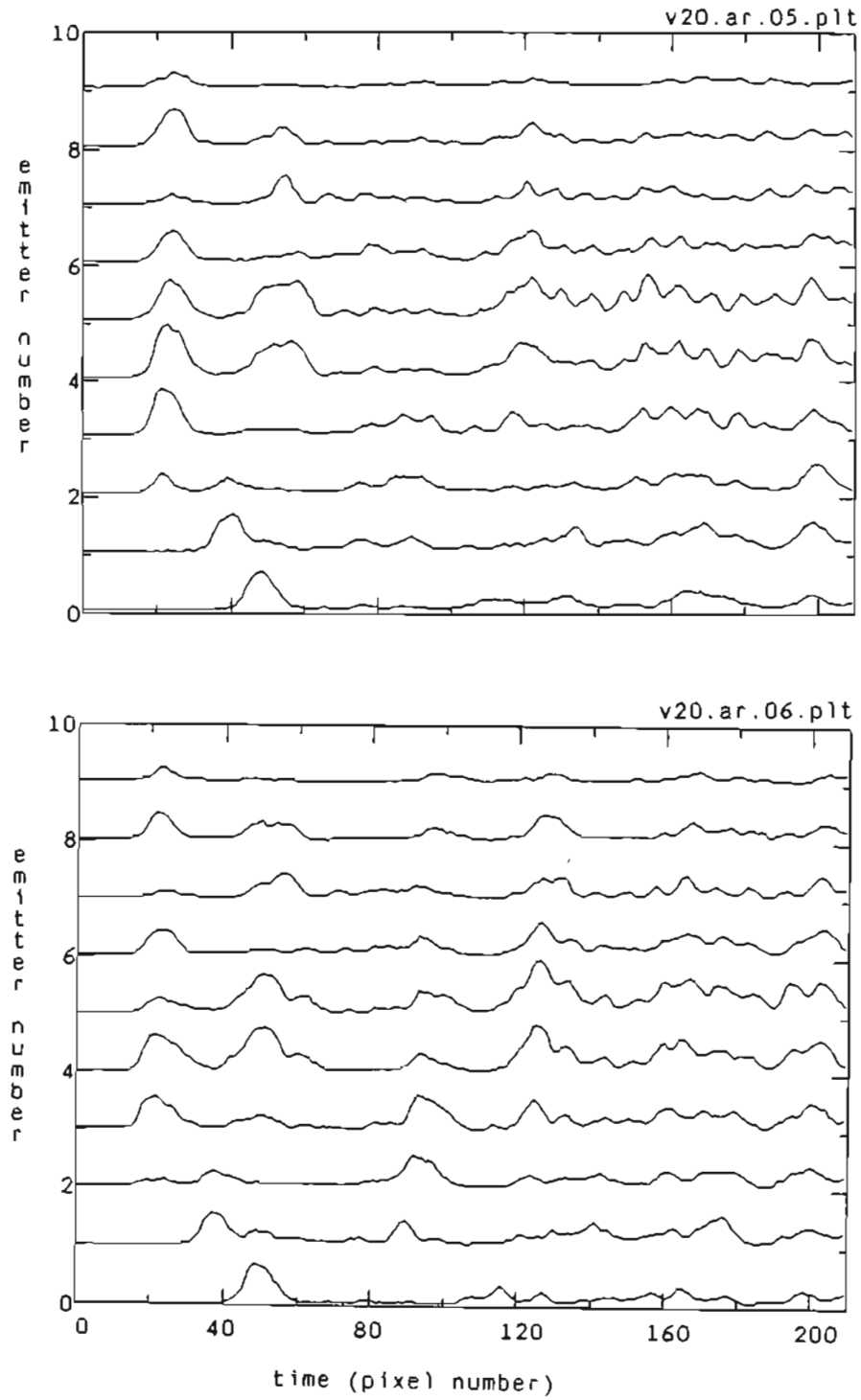


Figure 6.13 Intensity versus time profile for frames 5 and 6. (one pixel equals 22 ps.)

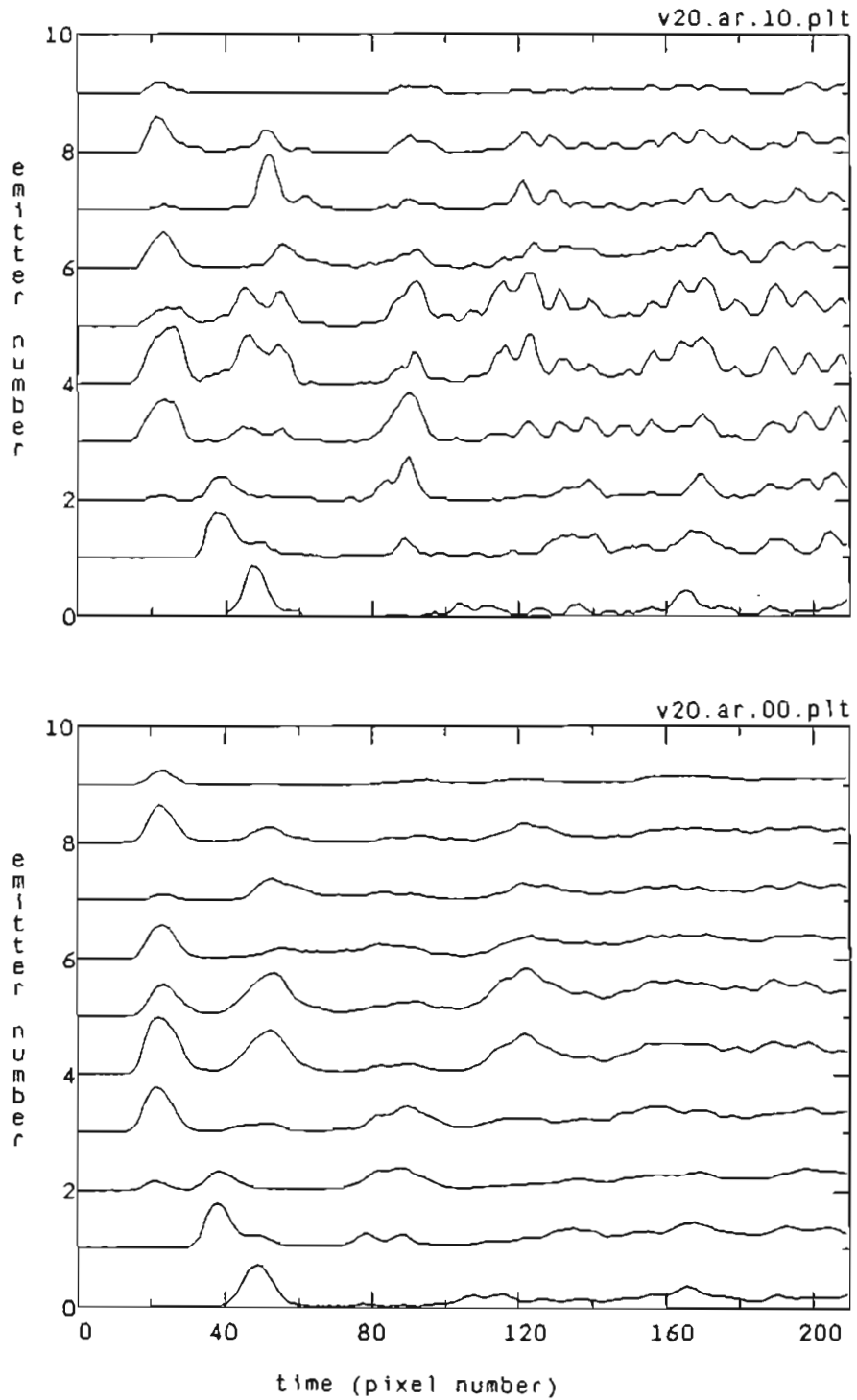


Figure 6.14 Intensity profile versus time for frame 10 and the average profile. (one pixel equals 22 ps.)

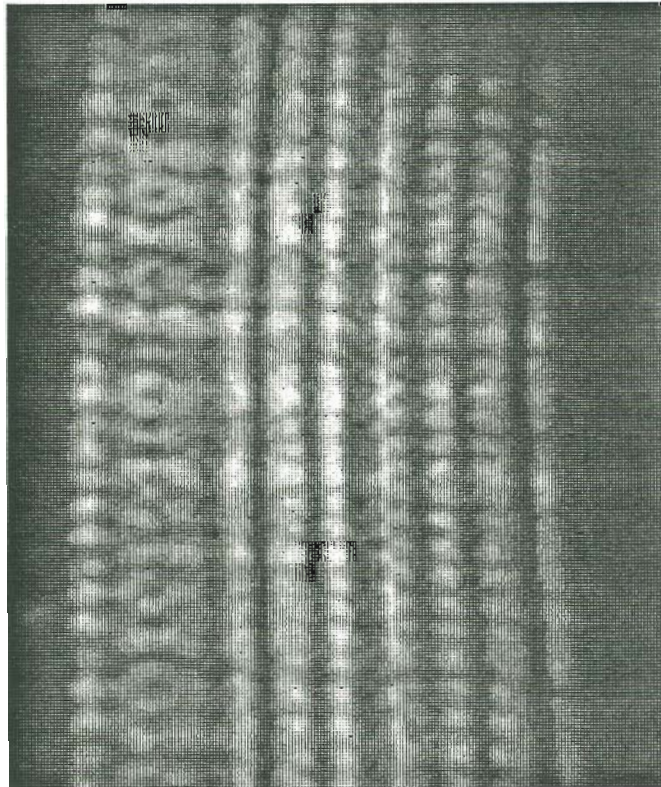


Figure 6.15 Time evolution of the near-field pattern for SDL laser C500 at $2.0t_h$ (middle of pulse).

pulse.

This increased interaction among the first three emitters may also be seen in the 3-D plots of Figures 6.16 and 6.17. The first plot, Figure 6.16, is a full view of the pulse response and the second is an expanded view of the first third of Figure 6.16. The peaks of the first emitters seem to be slightly shifted in time from those of emitters two and three which appear to be directly linked. These two emitters are more directly correlated to the rest of the emitters in the array.

The intensity of the array as a whole is observed in Figure 6.18 where the average intensity for four different frames is shown. Even in the middle region of the pulse response there is significant variation in the response from pulse to pulse. Three consecutive frames are given as well as another frame further along in the data set. Note the evolution of the pulse response in frames three through five; the rapid spiking in frame three gradually develops into the broader, less frequent spikes of frame five. The first third of frame ten is very similar to that of frame five however, the rapid spiking seen in frame three returns for the remainder of the pulse response.

Compare these average intensity profiles for the middle section of the pulse response, (Figure 6.18), to those for the beginning section (Figure 6.12). The spiking observed in the beginning of the pulse seems to be randomly phased across the emitters in the array since the average pulse response for each frame does not show the rapid spiking. This is in contrast to what is observed in the middle of the pulse; here, the rapid spiking remains when an average intensity across the emitters is formed. This affect may be caused by an inability to correct for triggering instability in streak traces initiated after the beginning of the pulse.

The intensity profiles of the individual frames for the middle of the pulse, (Figures 6.19, 6.20), are also very different from those for the beginning of the pulse

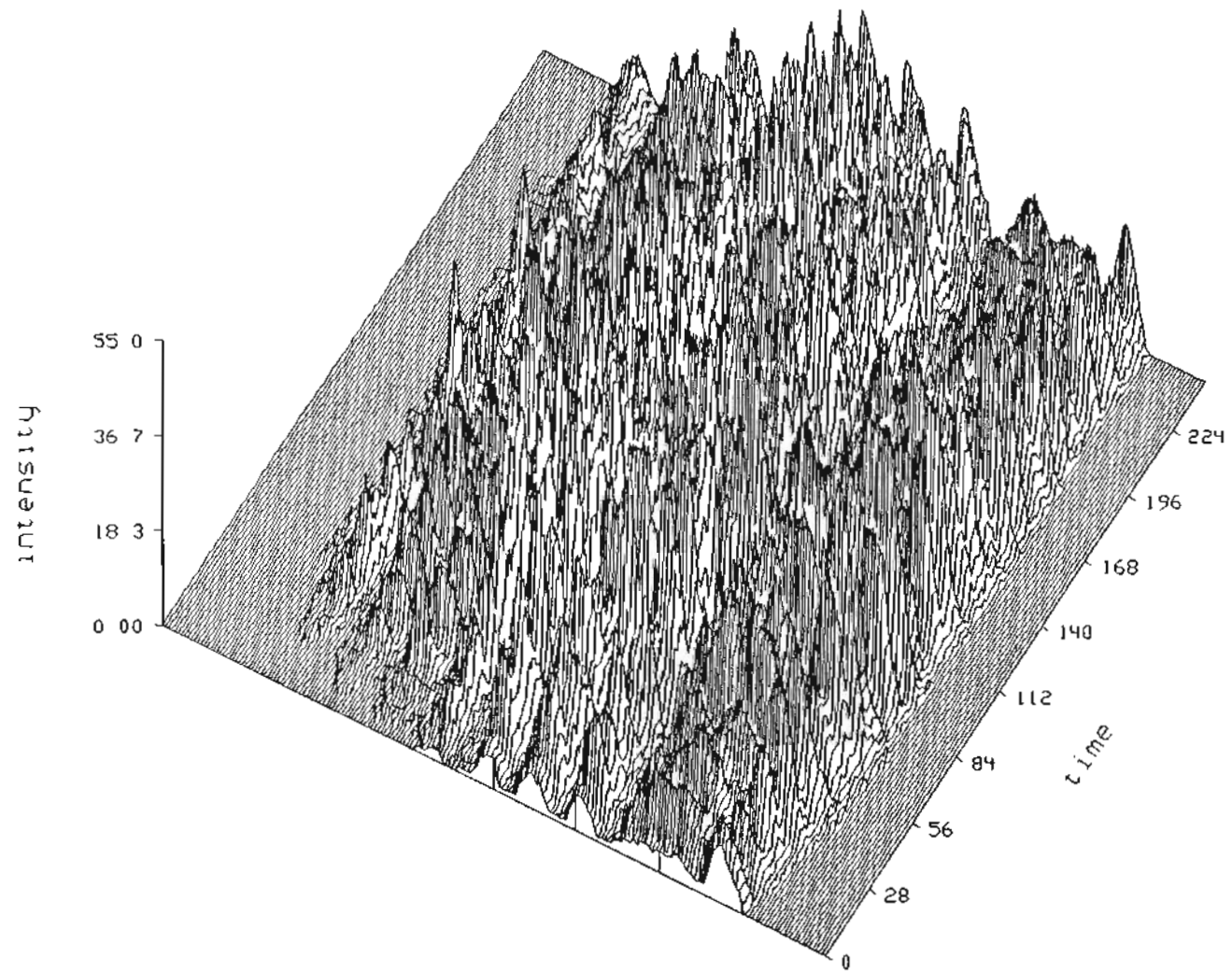


Figure 6.16 Three dimensional plot of the intensity surface for the near-field pattern of Figure 6.15.

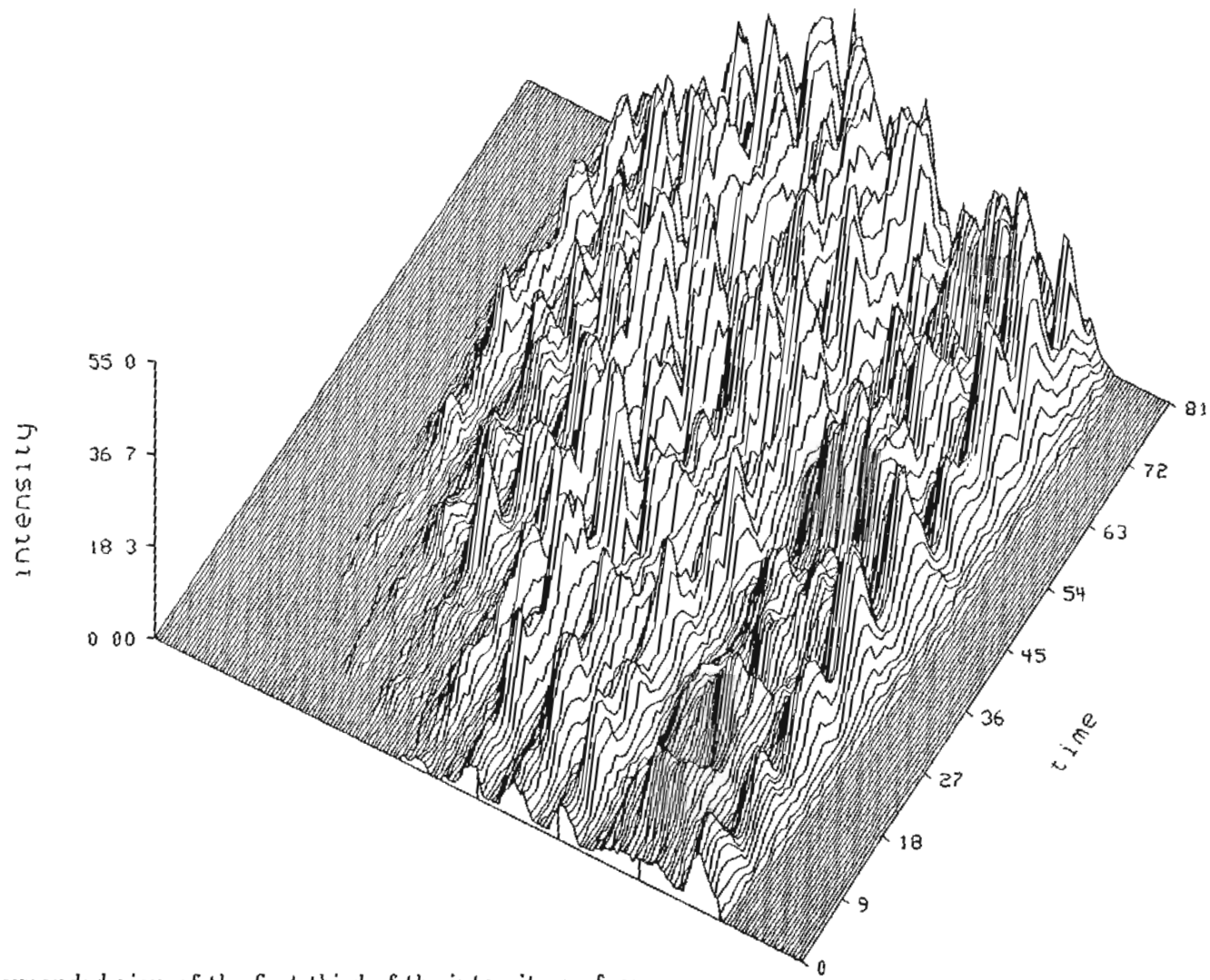


Figure 6.17 An expanded view of the first third of the intensity surface of Figure 6.16.

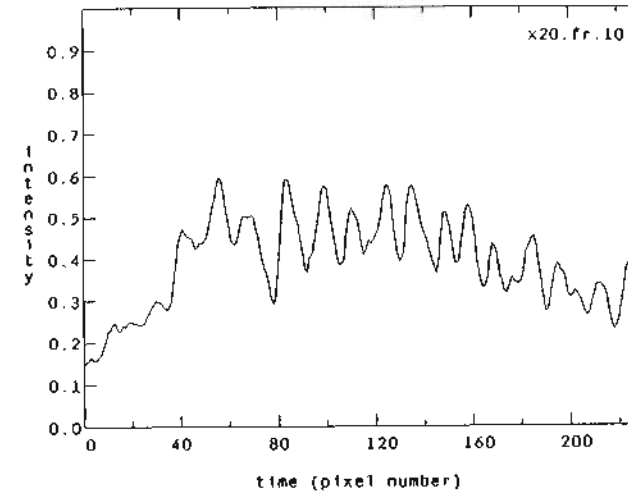
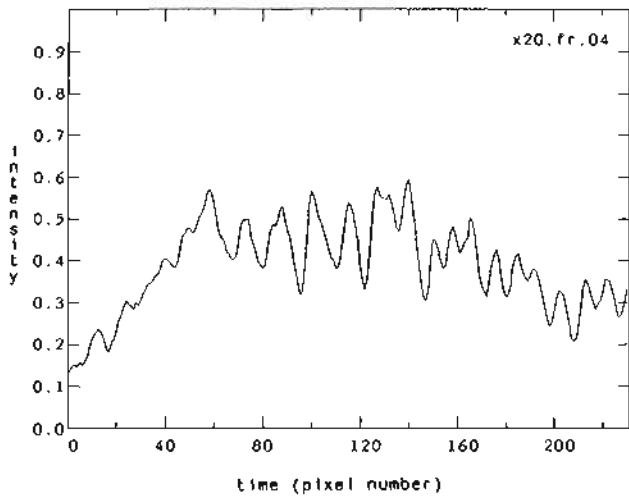
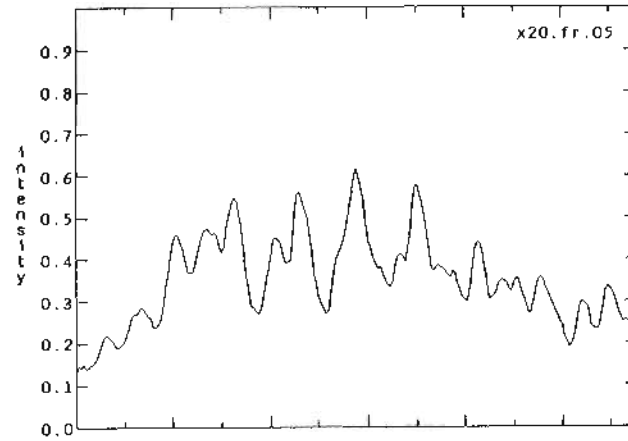
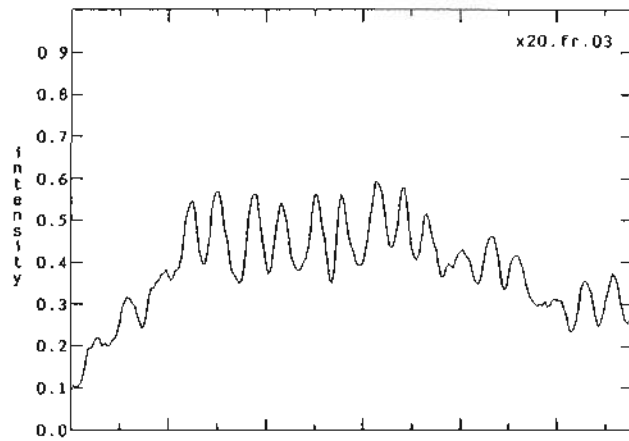


Figure 6.18 Average intensity of the array at the middle of the pulse.
(one pixel equals 22 ps.)

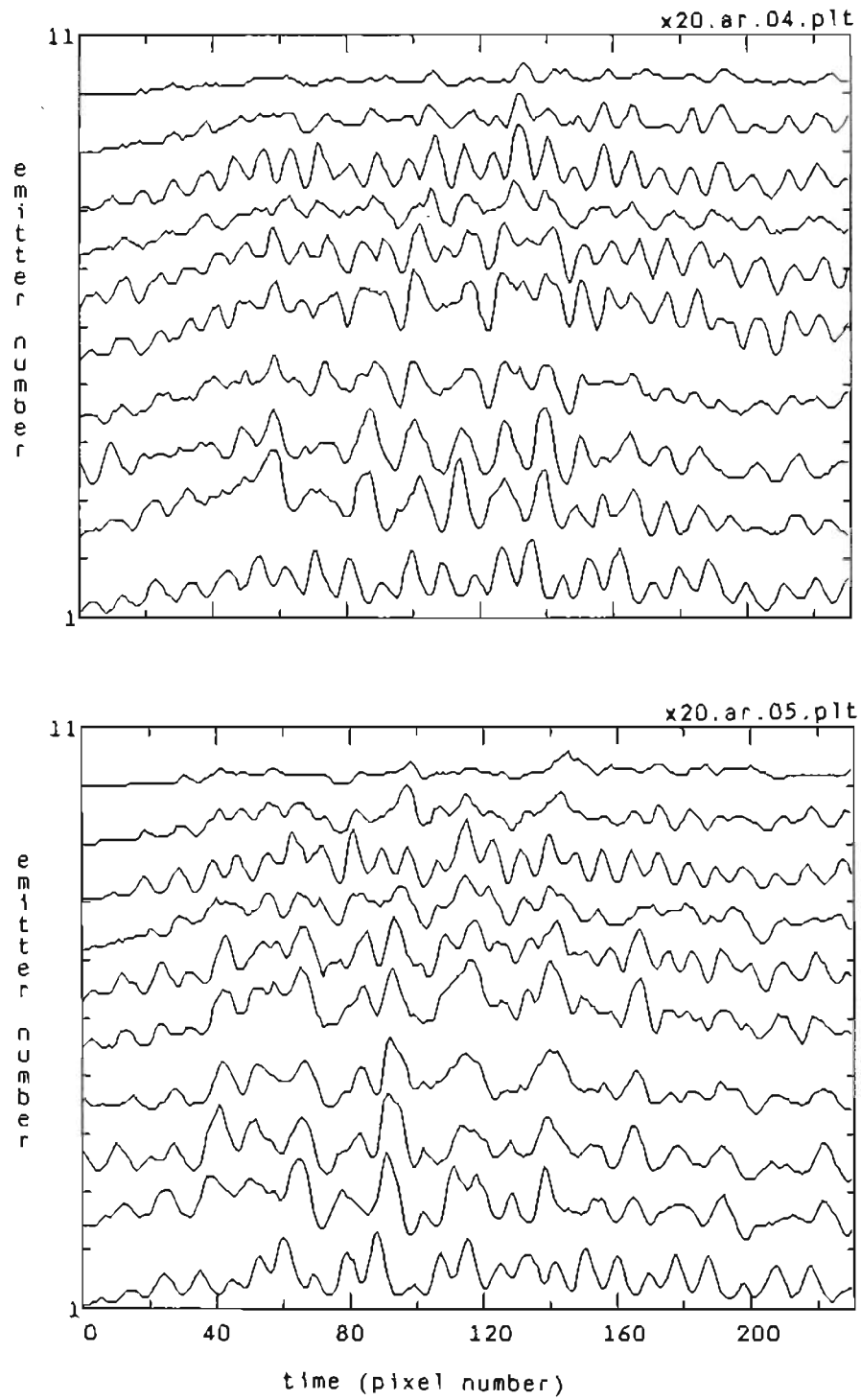


Figure 6.19 Intensity versus time profile for frames 4 and 5.
(one pixel equals 22 ps.)

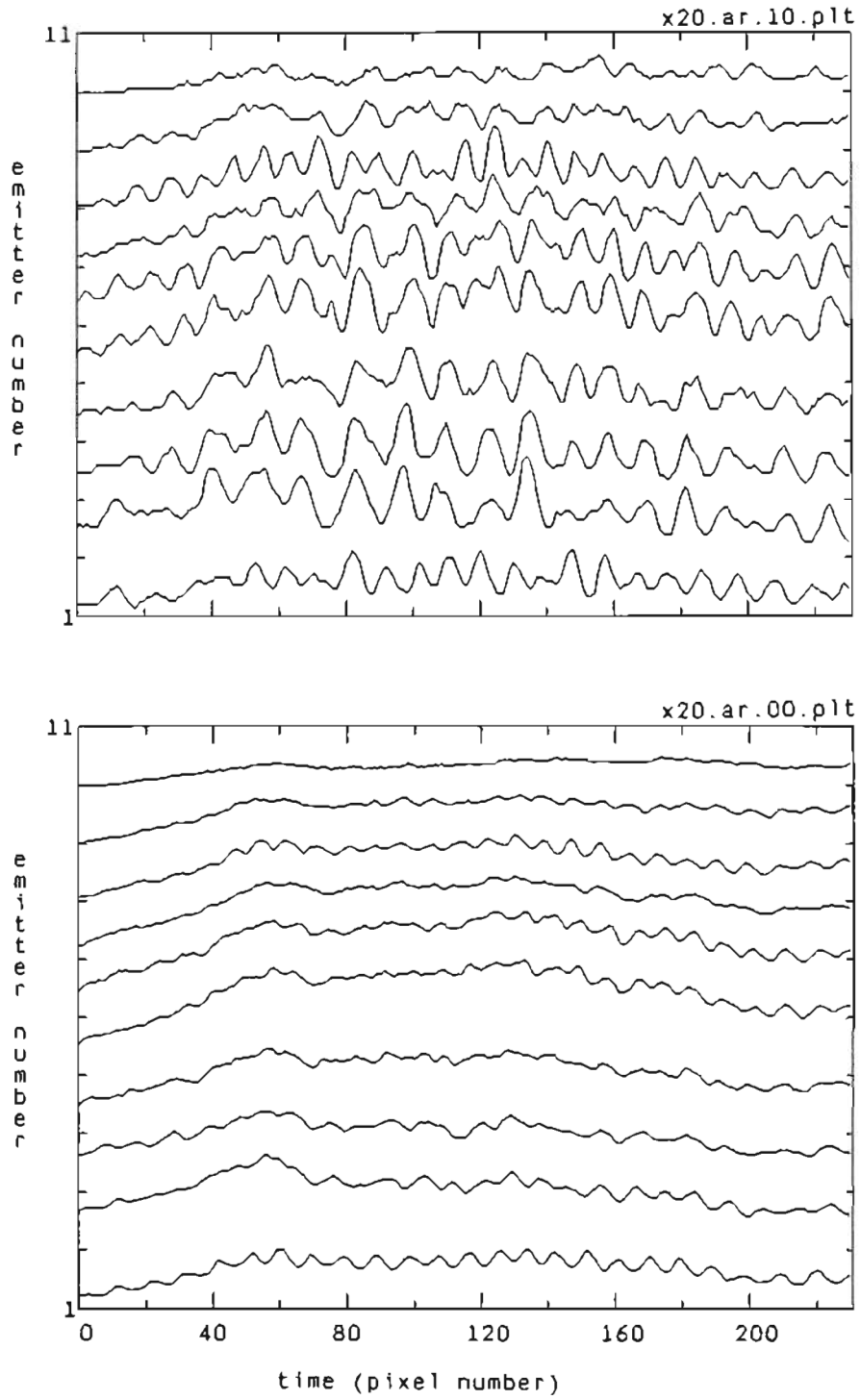


Figure 6.20 Intensity versus time profile for frame 10 and the average profile. (one pixel equals 22 ps.)

(Figures 6.13, 6.14). For the response to the middle of the pulse there seems to be an increase in the overall intensity with rapid spiking superimposed on it. Correlation of the spikes across the array is also quite strong.

The optical response at the end of the current pulse is similar to that for the middle of the pulse. Figure 6.21 is a halftone image of the near-field pattern at the end of the pulse. The rapid spiking characteristic of the middle portion of the pulse, (Figure 6.15), continues through to the end of the pulse. Correlation among the emitters is also strong. Figures 6.22 and 6.23 are 3-D plots of the response to the end of the pulse. A full view of the end of the pulse is given in Figure 6.22 and an expanded view of the first third in Figure 6.23. These plots are very much like those for the middle of the pulse, Figures 6.19 and 6.20.

The basic shape of the plots of the average intensity for individual frames, Figure 6.24, is similar to that for the middle of the pulse, Figure 6.18, however, the characteristics of the spiking is somewhat different. At the end of the pulse the spiking is less rapid and is broader. Figures 6.25 and 6.26 give the intensity profiles for several different frames as well as an average profile for the data set. These are quite similar to those for the middle portion of the pulse. Note that the average profiles for both the response at the middle and at the end of the current pulse are not as reliable as those at the beginning of the current pulse since there is no means of compensating for triggering instabilities in these latter portions of the pulse response.

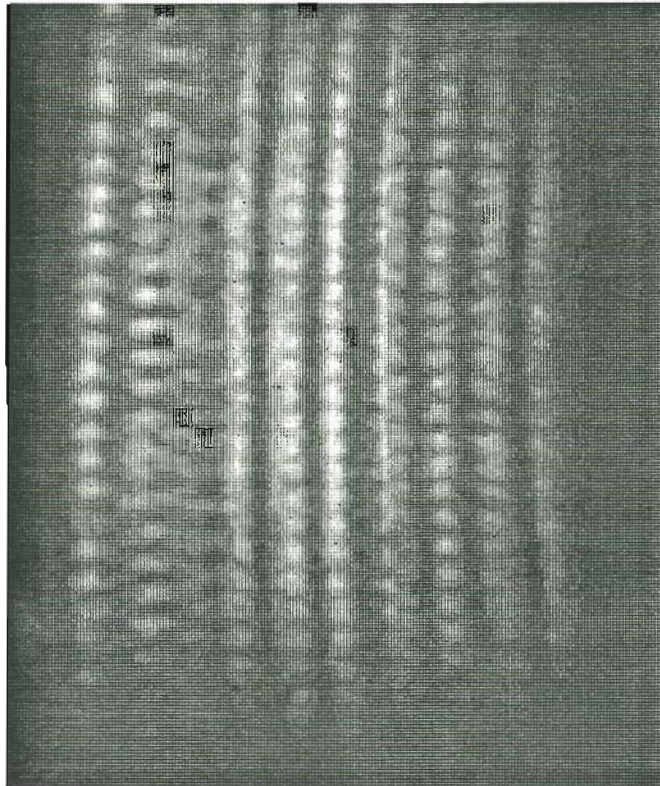


Figure 6.21 Time evolution of the near-field pattern for SDL laser C500 at $2.0I_{th}$ (end of pulse).

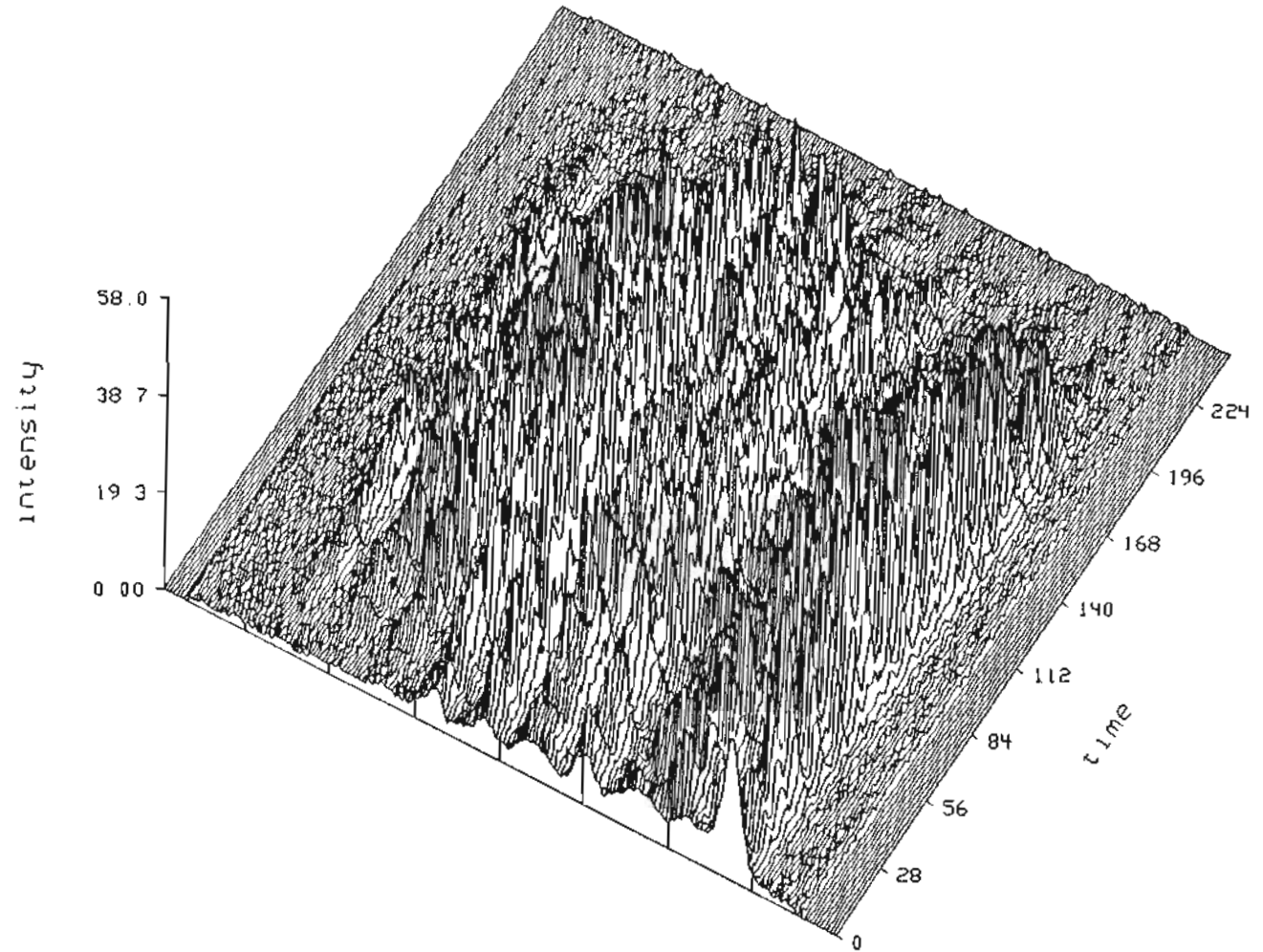


Figure 6.22 Three dimensional plot of the intensity surface for the near-field pattern of Figure 6.21.

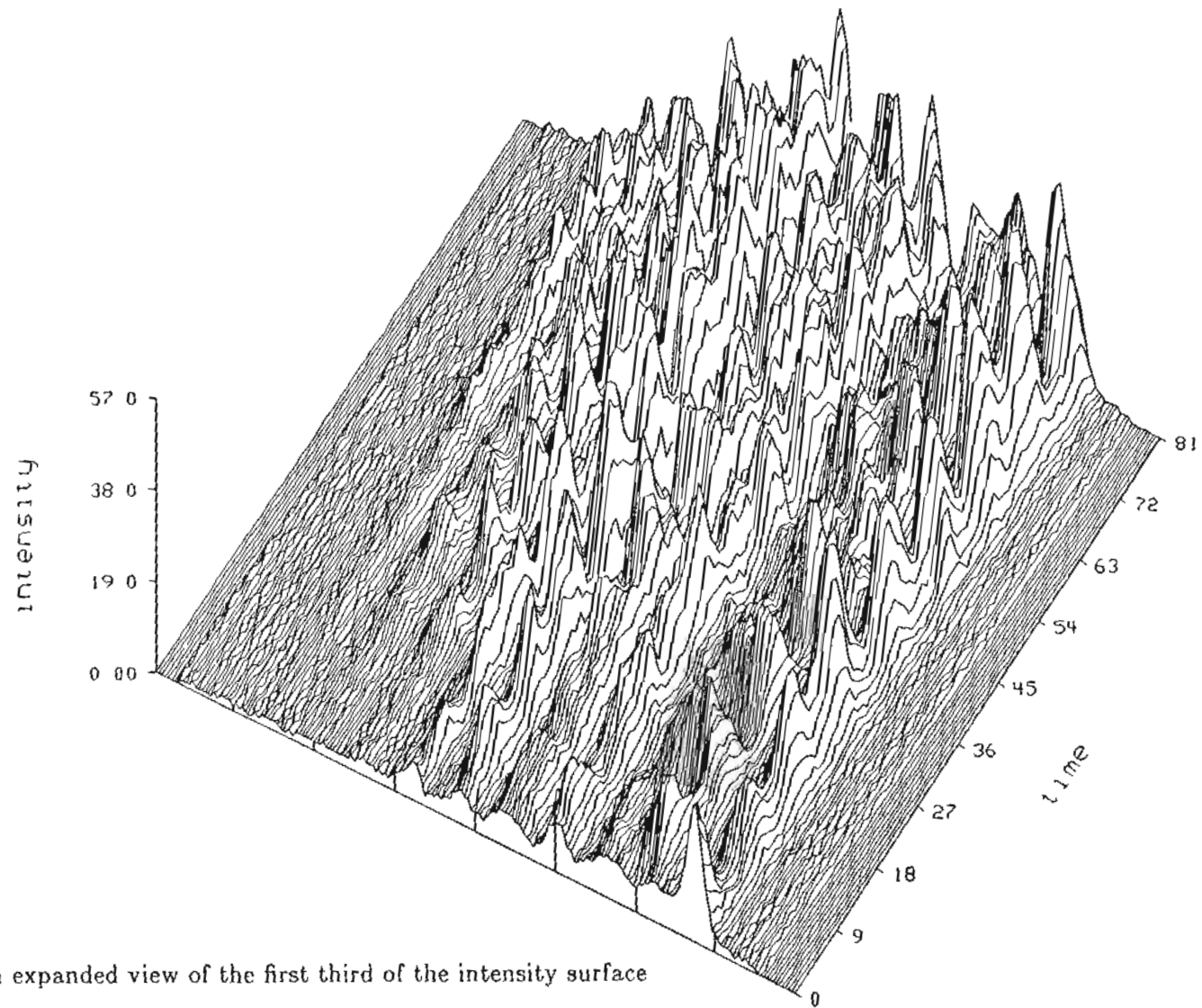


Figure 6.23 An expanded view of the first third of the intensity surface of Figure 6.22.

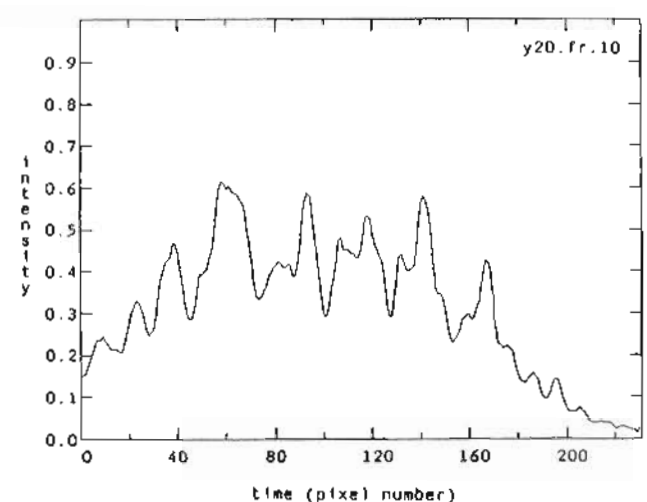
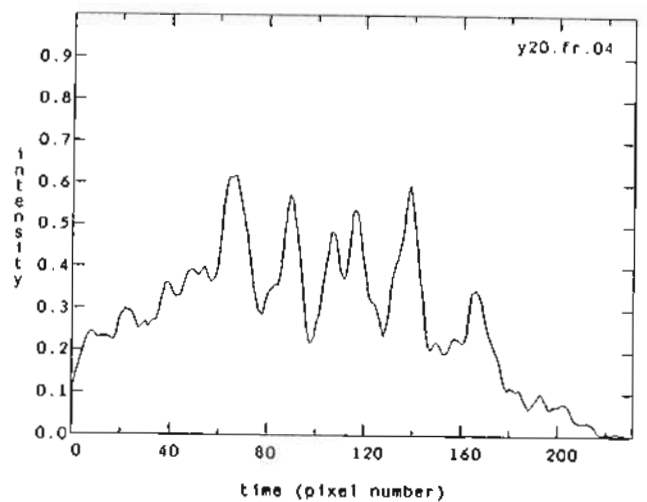
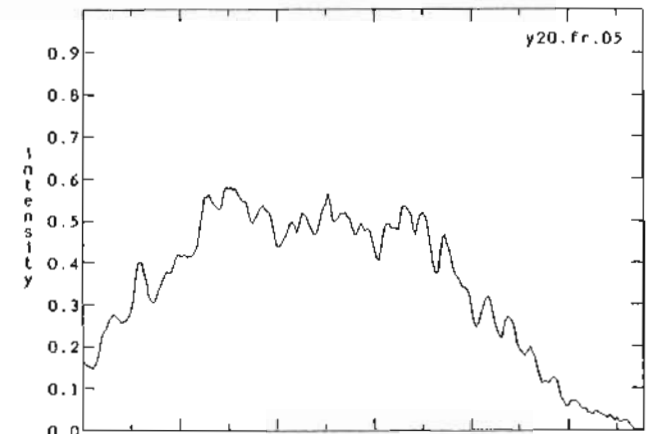
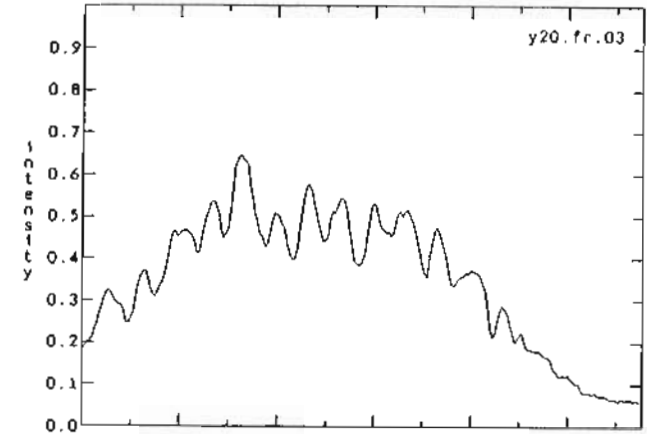


Figure 6.24 Average intensity of the array at the end of the pulse.
 (one pixel equals 22 ps.)

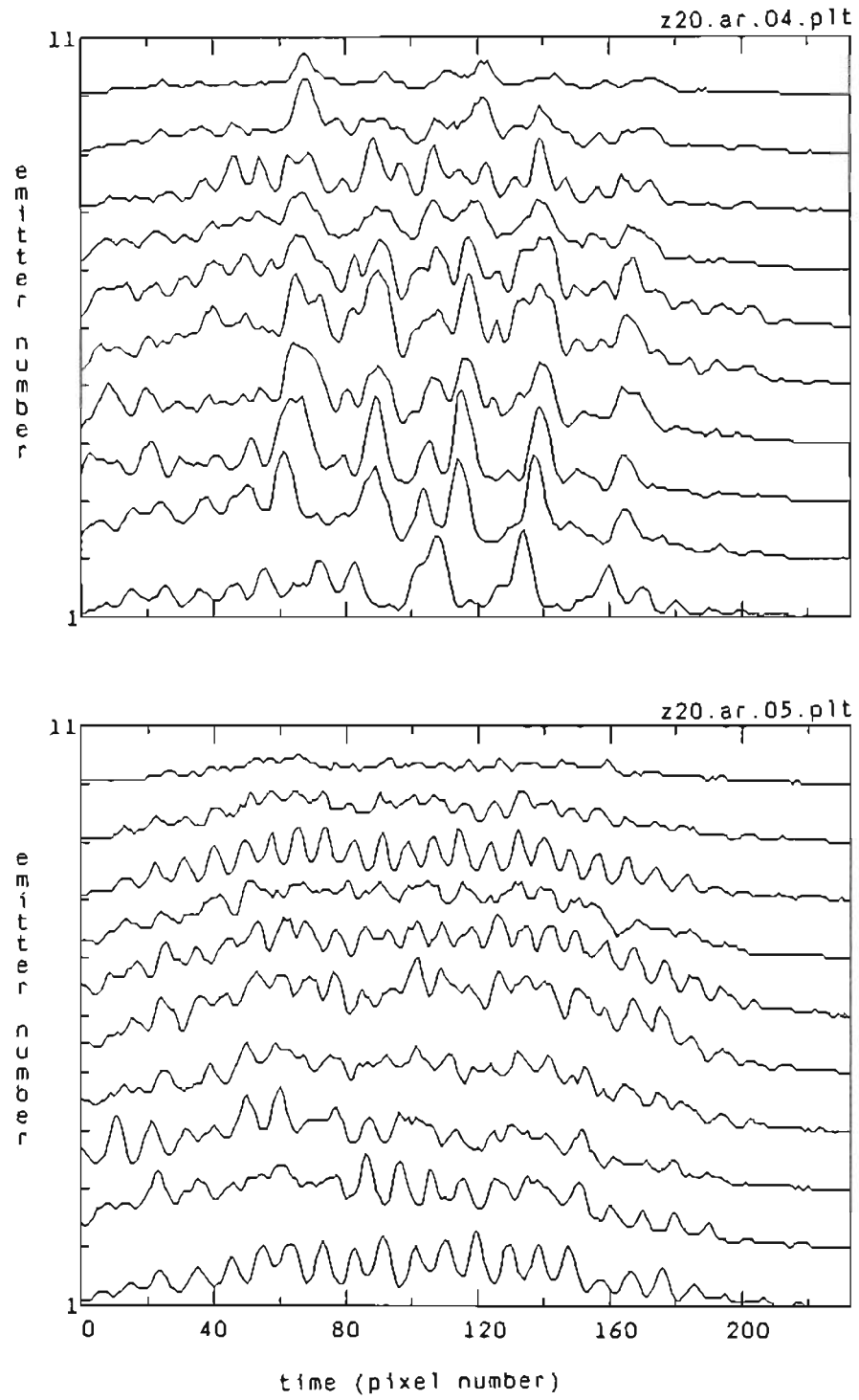


Figure 6.25 Intensity versus time profile for frames 4 and 5.
(one pixel equals 22 ps.)

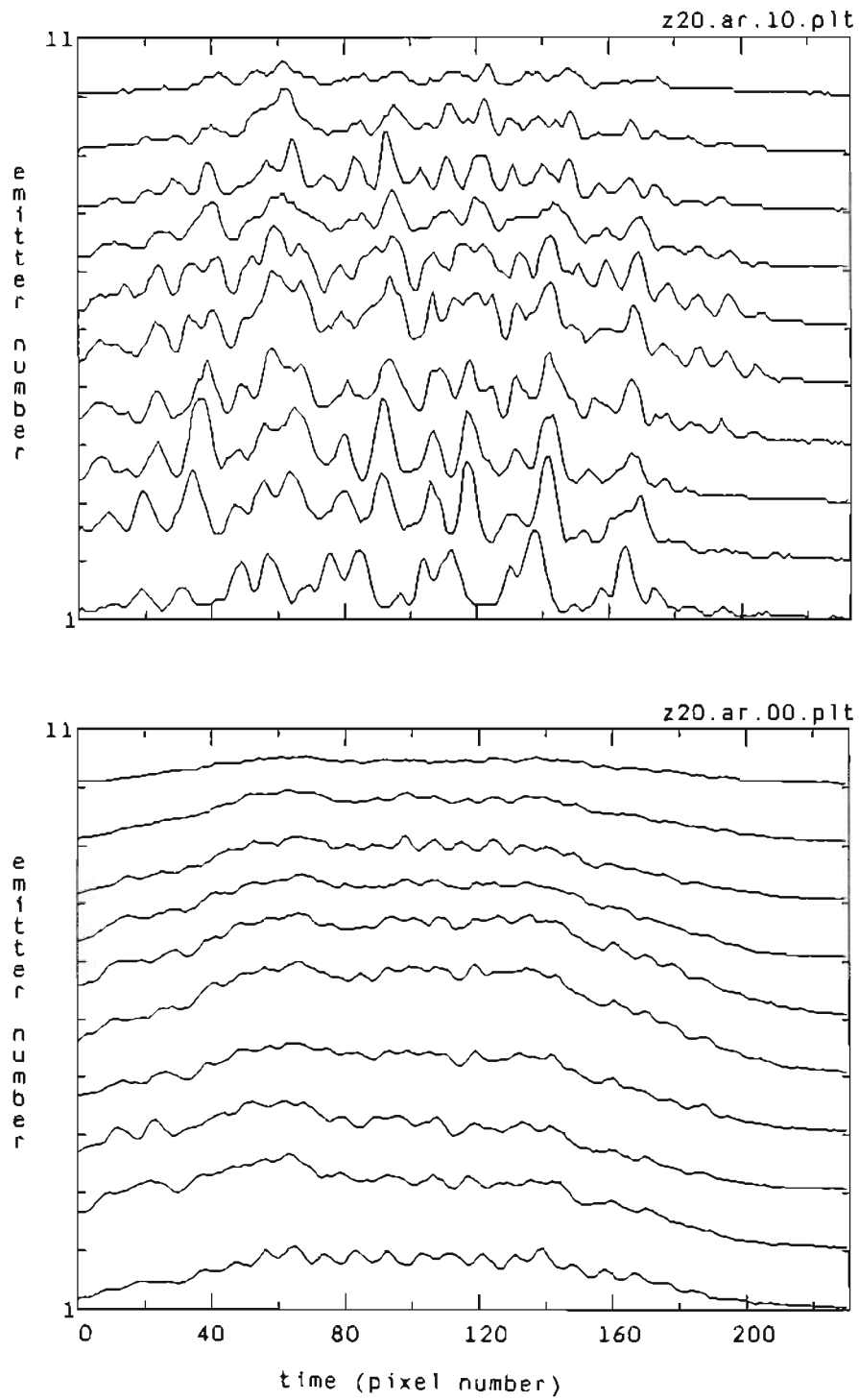


Figure 6.26 Intensity versus time profile for frame 10 and the average profile. (one pixel equals 22 ps.)

6.2 Discrete Fourier Transform and Correlation Results for the Near-field Response

The discrete Fourier transform (DFT) and correlation results presented here were calculated with the data on the near-field response of the SDL C500 array given in the previous section, 6.1.2. Again, the DFT of each column in the intensity data array is calculated. This corresponds to a DFT in the time domain since the columns contain intensity information as a function of time for a single emitter. Both the DFT and correlation calculations are discussed in detail in Section 5.5.3. A representative sampling of the results is included in this section with samples taken from each of the three temporal positions within the pulse response. For the DFT results an average DFT is compared with that of a single frame for each of the three temporal positions. For the correlation results a comparison is made between the results for the three temporal positions.

Figure 6.27 gives the DFT for the near-field response at the beginning of the current pulse. The uppermost plot is the average response for the data set. The middle plot is the DFT for frame ten in the set: compare this with the halftone image of the intensity, Figure 6.7a. The final plot is the DFT for frame twenty of the data set: compare this with the halftone of Figure 6.7b. There is a significant amount of variation in the DFT from pulse to pulse for this beginning portion of the pulse response.

Figure 6.28 gives the DFT for the near-field response to the middle portion of the pulse. The uppermost plot is the average response for this data set. Compare this average response with that of Figure 6.27 for the beginning of the pulse. There are still two dominant frequencies represented but the spacing between them has

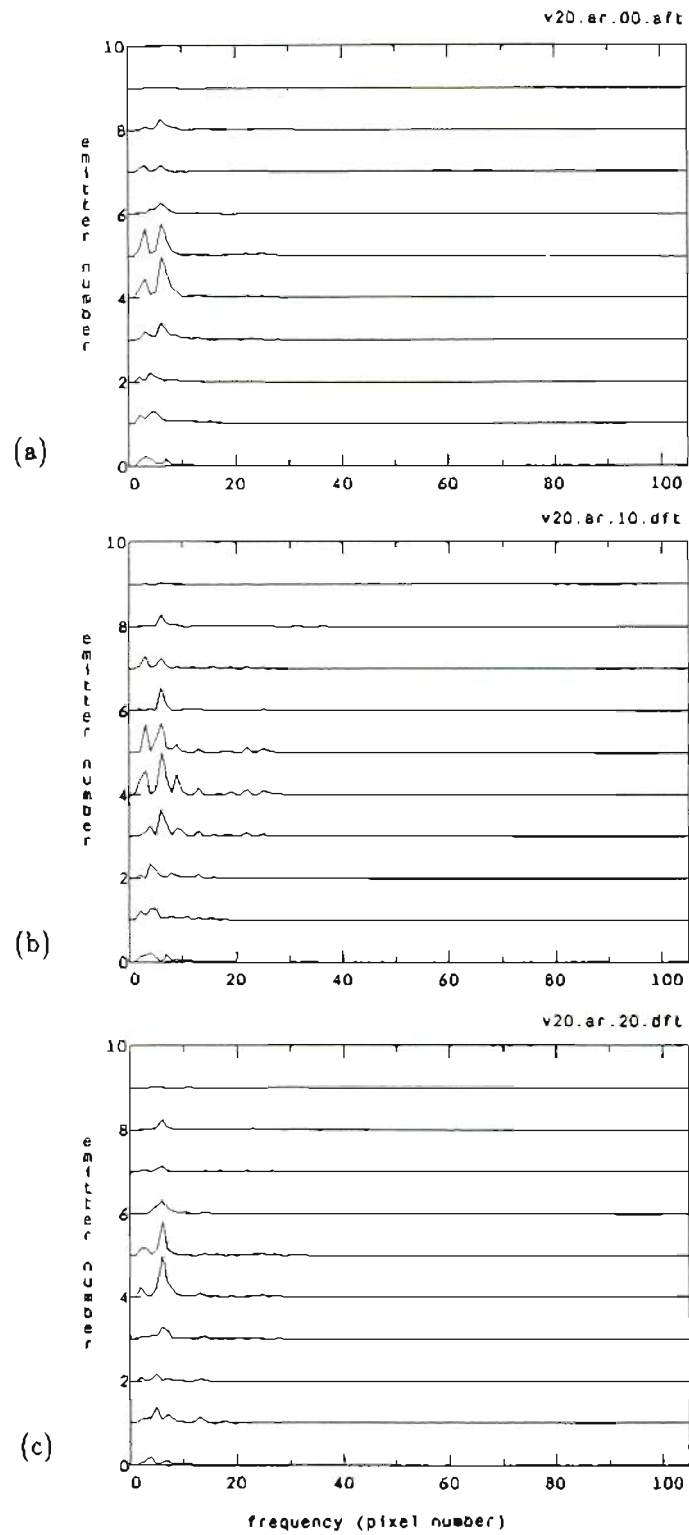


Figure 6.27 Fourier transform of the near-field intensity for SDL laser C500 at $2.0I_{th}$ (beginning of pulse). DFT results shown include: the average (a), frame 10 (b), and frame 20 (c). (one pixel equals 0.19 GHz)

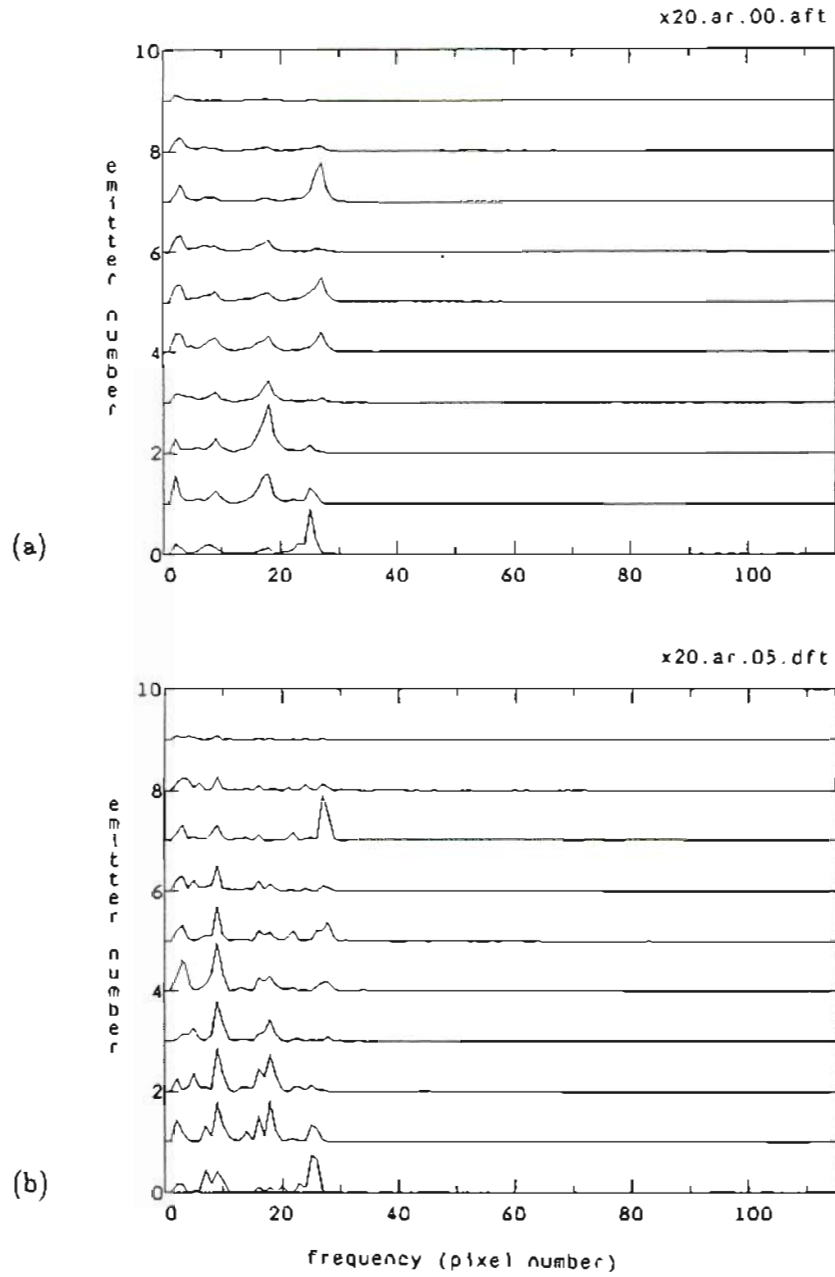


Figure 6.28 Fourier transform of the near-field intensity for SDL laser C500 at $2.0I_{th}$ (middle of pulse). DFT results shown include: the average (a), and frame 5 (b). (one pixel equals 0.19 GHz)

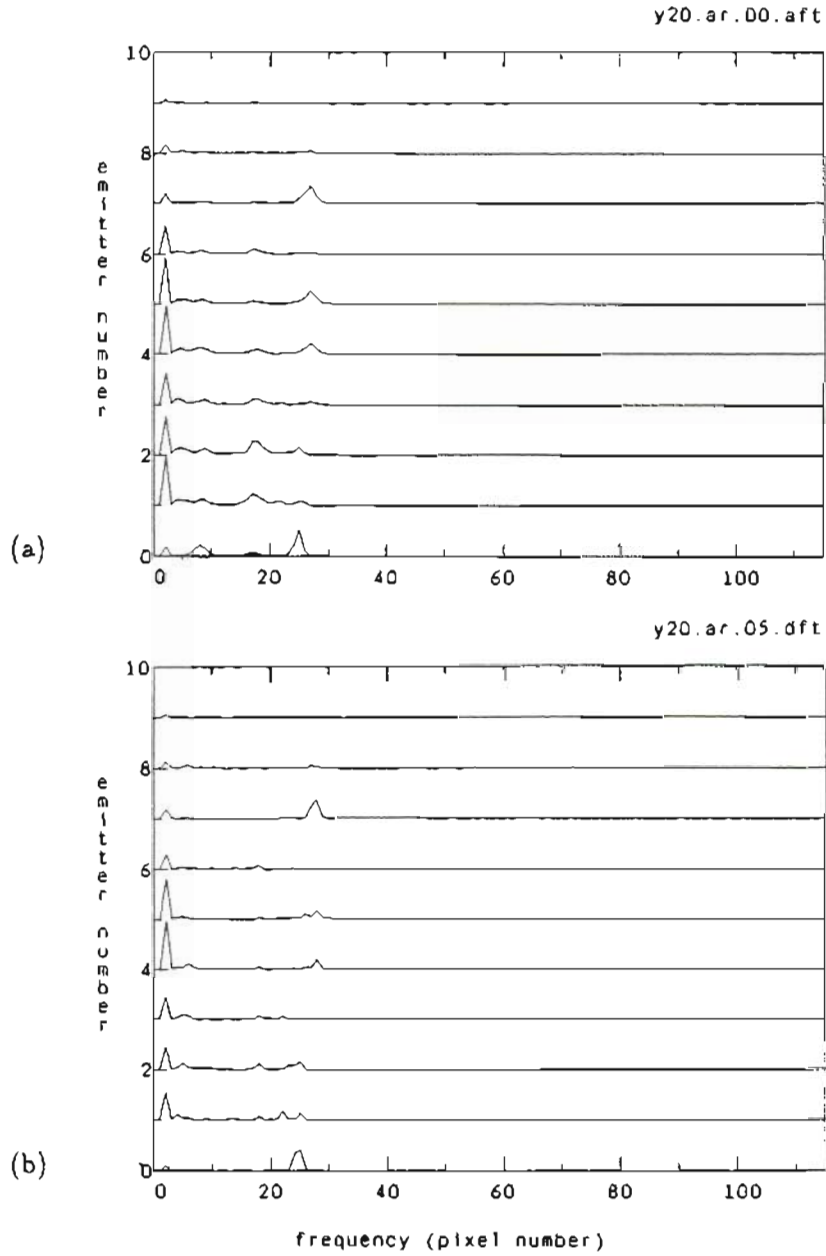


Figure 6.29 Fourier transform of the near-field intensity for SDL laser C500 at $2.0I_{th}$ (end of pulse). DFT results shown include: the average (a), and frame 5 (b). (one pixel equals 0.19 GHz)

increased considerably. In Figure 6.28a the two strongest frequencies are 3.5 GHz and 5.0 GHz. The strongest frequencies represented in Figure 6.27a are 0.58 GHz and 1.4 GHz. The lower plot in Figure 6.28 is the DFT for frame five in the set. The halftone of Figure 6.15 is the corresponding intensity image for frame five.

The near-field response to the end of the pulse is shown in Figure 6.29. The average response is given in the uppermost plot. The first peak in the spectrum (corresponding to a frequency of 0.58 GHz) is much stronger and sharper in this figure, (6.29), than in either of the frames depicting the response to the beginning (6.27) or the middle (6.28) of the pulse. For the end of the pulse, this component of the spectrum clearly dominates. The difference between the average DFT and that of frame five, (the lower plot of Figure 6.29), is less significant than for other regions of the pulse response. For comparison, Figure 6.21 is the halftone image of the near-field response at the end of the pulse for frame five.

Figure 6.30 gives the correlation results for each of the three temporal portions of the pulse response. The uppermost plot corresponds to the beginning of the pulse response, the bottom plot to the end. There seems to be a decreasing amount of periodicity to the correlation plots in going from the beginning to the end of the pulse response. This is most likely due to the decrease in the strength of oscillations and the trend toward stabilization in the response in going from the beginning to the end of the pulse response.

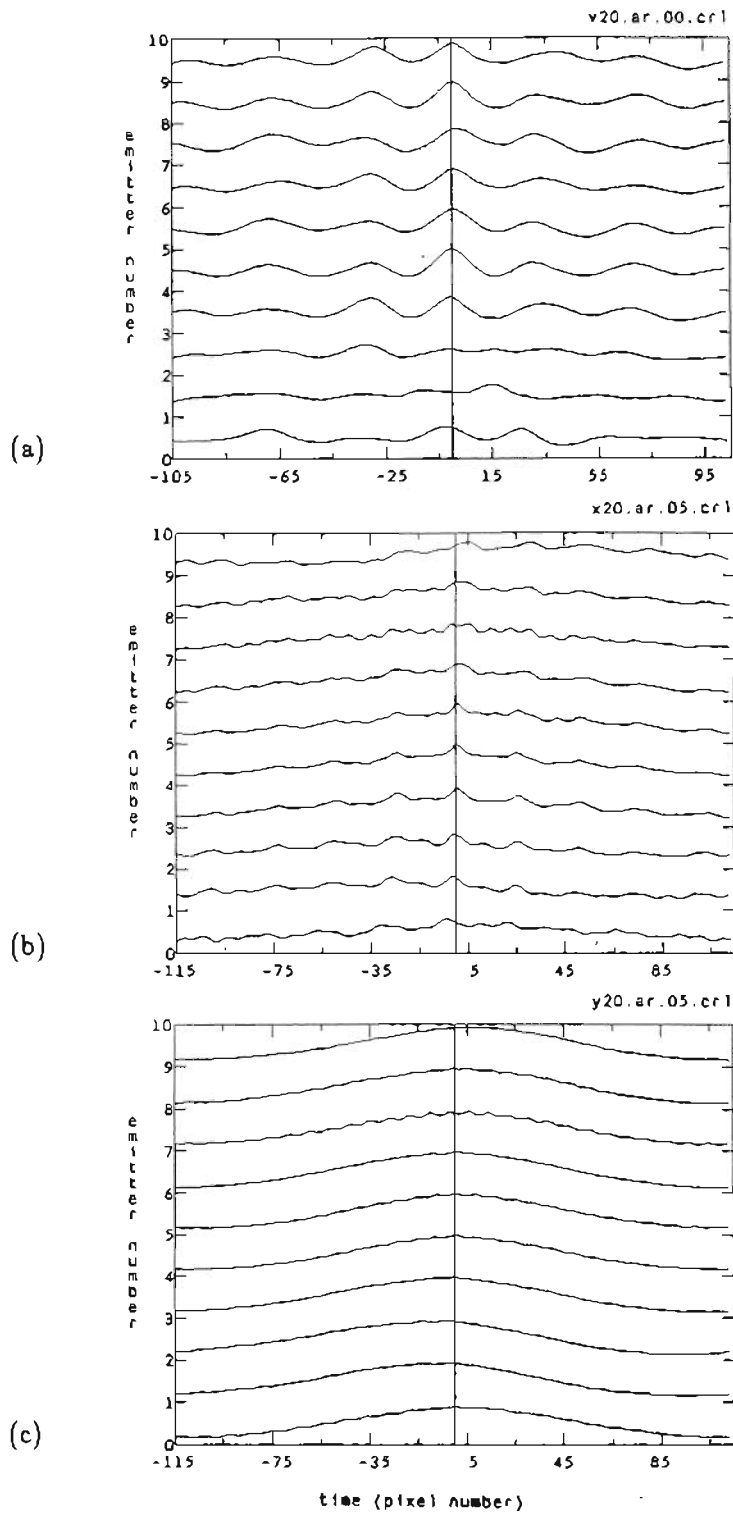


Figure 6.30 Cross correlation between the fifth emitter and the others for SDL laser C500 at $2.0I_{th}$. Results shown include: the beginning (a), middle (b), and end (c) of pulse. (one pixel equals 22 ps.)

6.3 Near- and Far-field Optical Response for a Y-Guide Array

The near- and far-field optical response of a Y-guide array was observed and recorded as described in Chapter 5. Streak camera data was taken for pulsed injection currents of $1.5I_{th}$ from zero bias current. A representative frame in the data set is considered here to allow comparison between the near-field patterns of two different array structures: the gain-guide and the Y-guide. A far-field pattern is included to provide an example of the type of data it is possible to acquire with the streak camera video frame-grab system in addition to the near-field patterns discussed previously.

Figure 6.31 is a halftone image of the near-field response to the beginning portion of the current pulse. The behavior of the Y-guide differs significantly from that of the gain-guides discussed in Section 6.1. The first four emitters of Figure 6.31 appear to be responding as a separate unit, independent of the remaining emitters. The spiking observed in the intensity of these first four emitters is stronger and is less frequent than that of the remaining emitters. It is as if the array is composed of two independent units. Compare the halftone for the Y-guide (Figure 6.31) with those for the gain-guides (Figures 6.1, 6.6, 6.7).

Figure 6.32 is a 3-D plot of Figure 6.31. The rapid spiking of one side of the array (emitters 5-10) may be contrasted with the stronger less frequent spiking of the first four emitters. Figure 6.33 is an expanded view of the first third of Figure 6.32.

The time evolution of the far-field pattern of the Y-guide is shown in the halftone of Figure 6.34. The far-field studies, done here at OGC, on the Y-guide have been described elsewhere²³ in detail. Briefly, Figure 6.34 shows the time evolution of the central far-field lobe and its faint secondary side lobes. The width of the central

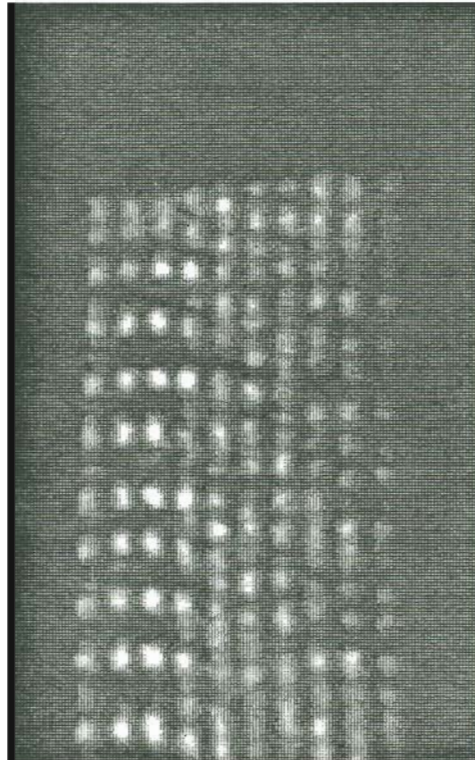


Figure 6.31 Time evolution of the near-field pattern for a Y-guide at $1.5L_{th}$ (beginning of pulse).

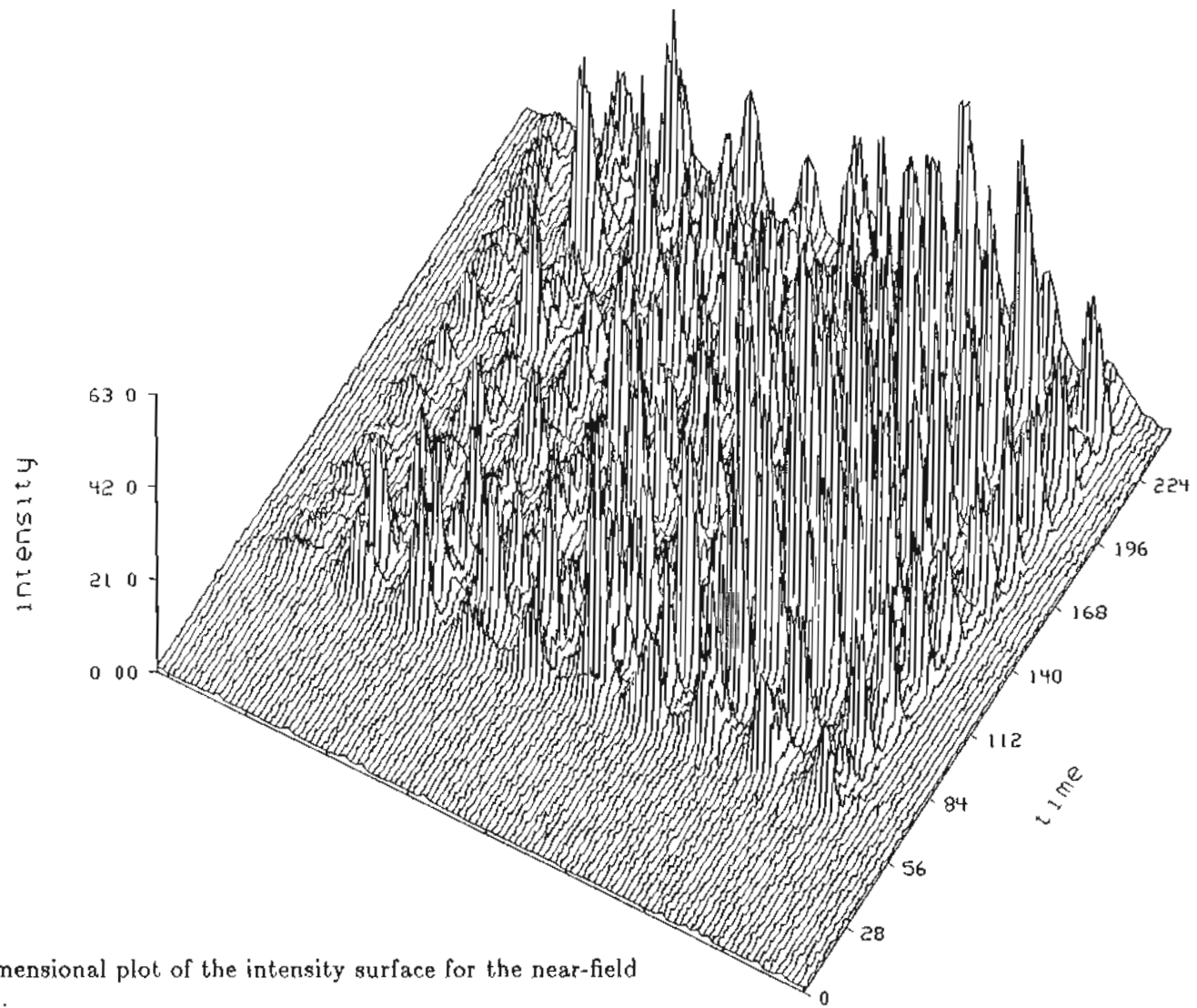


Figure 6.32 Three dimensional plot of the intensity surface for the near-field pattern of Figure 6.31.

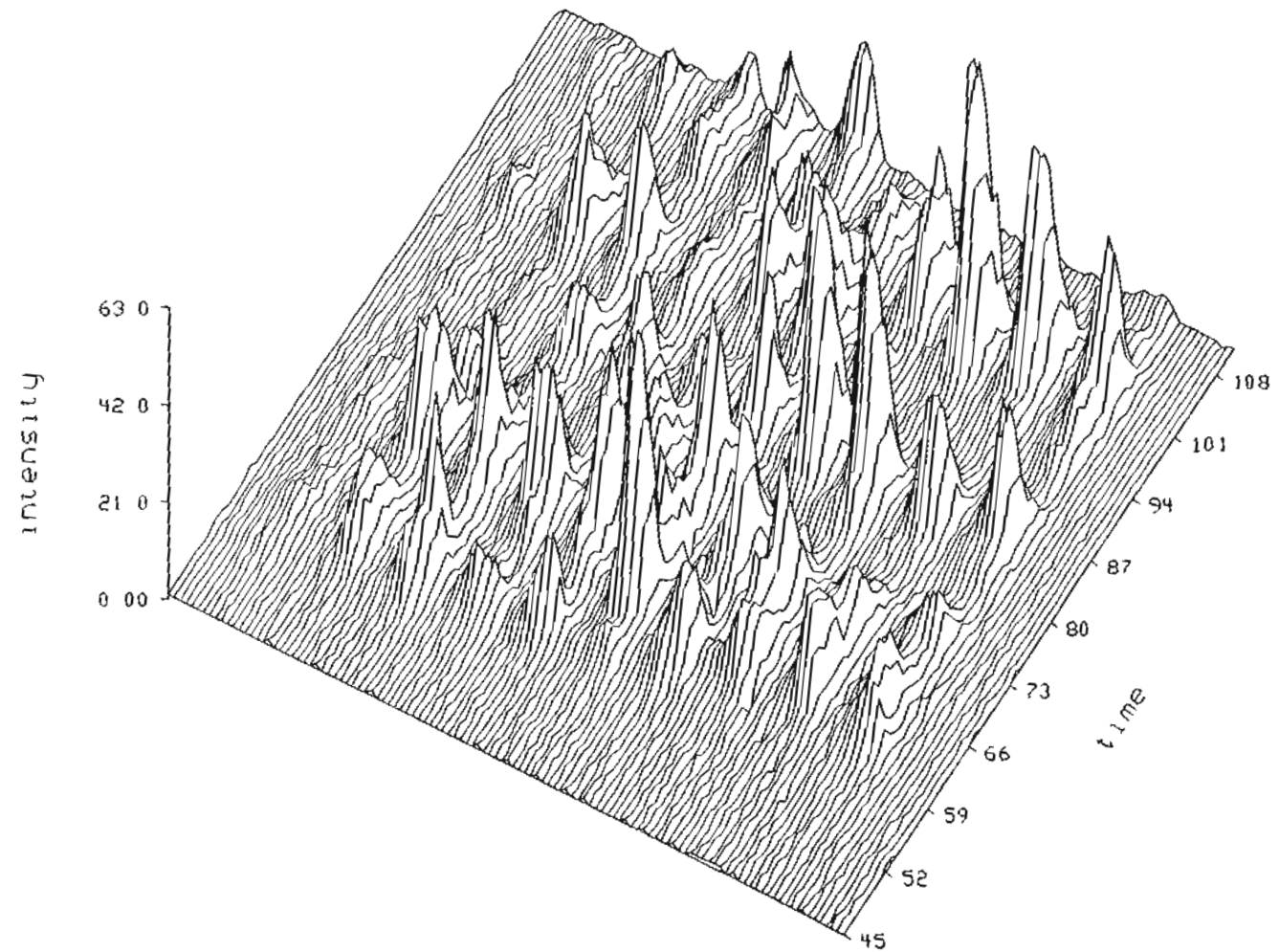


Figure 6.33 An expanded view of the first third of the intensity surface of Figure 6.32.

lobe is approximately $2\text{-}3 \text{ } ^\circ \text{ }^{23}$. From the figure it can be seen that a single-lobed far-field pattern is established simultaneously with the start of laser emission. The time scale of this figure is consistent with the near-field figures: each pixel represents 22 ps. A streak trace recorded at five times the temporal resolution of this trace reveals that the far-field formation time is less than 20 ps^{23} , which implies that the Y-guide is locked in-phase in the same time interval. This is the shortest phase-locking time measured to date.

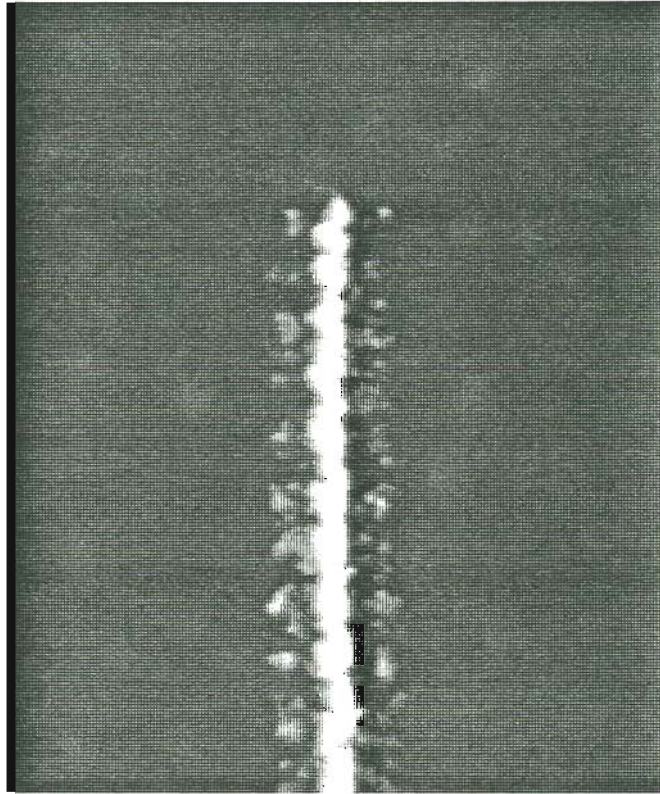


Figure 6.34 Time evolution of the far-field pattern for a Y-guide at $1.5t_h$.

7. CONCLUSIONS

A versatile and powerful streak camera video frame-grabber system for studying the evolution of the near- and far-field radiation patterns of diode lasers has been assembled and tested. Software needed to analyze and display the data acquired with the streak camera video frame-grabber system has been written and the total package used to record and perform preliminary analyses on the behavior of several gain-guided array lasers. The experiments conducted to this end are described in detail in Chapter 5. Examples of the information which can be gathered with this system are presented in Chapter 6.

The figures of Chapter 6 reveal that there is a wealth of information to be gained from streak camera analysis of the behavior of phase-locked arrays. There is significant variation in the optical response from pulse to pulse for a given laser. The characteristics of the near-field radiation patterns differ from one laser to the next, even for two lasers of the same type. This difference is smaller, however, than that observed between arrays of different design such as a gain-guided and a Y-guide.

The statistical programs make it possible to perform discrete Fourier transforms, and auto- and cross-correlations on the individual intensity profiles of the arrays. From this information it may be possible to determine the modal structure of the array emission, i.e., the combination of supermodes in which the array is operating. With information on the interplay of the supermodes in the array it is possible

to predict the shape and evolution of the far-field pattern using the coupled-mode theory. The evolution of the far-field pattern may be monitored directly with the streak camera system thereby allowing a confirmation of the theoretical predictions. It is hoped that the streak camera video frame-grabber system will contribute to the understanding of the effects of variations in array design on the stability and the structure of the near- and far-field patterns of the arrays.

References

1. G. L. Harnagel, D. R. Scifres, H. H. Kung, D. F. Welch, and P. S. Cross, "Five watt continuous-wave AlGaAs laser diodes," *Electron. Lett.*, vol. 22, pp. 605-606, 22 May 1986.
2. T. L. Paoli, W. Streifer, and R. D. Burnham, "Observation of supermodes in a phase-locked diode laser array," *Appl. Phys. Lett.*, vol. 45, pp. 217-219, 1 August 1984.
3. D. R. Scifres, W. Streifer, R. D. Burnham, T. L. Paoli, and C. Lindstrom, "Near-field and far-field patterns of phase-locked semiconductor laser arrays," *Appl. Phys. Lett.*, vol. 42, pp. 495-497, 15 March 1983.
4. D. R. Scifres, R. D. Burnham, and W. Streifer, "High power coupled multiple stripe quantum well injection lasers," *Appl. Phys. Lett.*, vol. 41, pp. 118-120, 15 July 1982.
5. D. R. Scifres, R. D. Burnham, C. Lindstrom, W. Streifer, and T. L. Paoli, "Phase-locked (GaAl)As laser emitting 1.5 W CW per mirror," *Appl. Phys. Lett.*, vol. 42, pp. 645-647, 15 April 1983.
6. R. A. Elliott, R. K. DeFreez, T. L. Paoli, R. D. Burnham, and W. Streifer, "Dynamic characteristics of phase-locked array multiple quantum well injection lasers," *J. Quantum Electron.*, vol. QE-21, pp. 598-602, June 1985.
7. R. K. DeFreez, R. A. Elliott, T. L. Paoli, R. D. Burnham, and W. Streifer, "Dynamic properties of phased-array multiple quantum well injection lasers," *Proceedings 19th Int. Quantum Electron. Conf.*, Anaheim, CA, June 18-21, 1984. Paper PD-B3
8. E. Kapon, J. Katz, and A. Yariv, "Supermode analysis of phase-locked arrays of semiconductor lasers," *Opt. Lett.*, vol. 10, pp. 125-127, April 1984.
9. J. K. Butler, D. E. Ackley, and D. Botez, "Couple-mode analysis of phase-locked injection laser arrays," *Appl. Phys. Lett.*, vol. 44, pp. 293-295, 1 February 1984.
10. D. E. Ackley, "Phase-locked injection laser arrays with nonuniform stripe spacing," *Electron. Lett.*, vol. 20(17), pp. 695-697, August 1984.
11. Y. Twu, K. L. Chen, A. Dienes, S. Wang, and J. R. Whinnery, "High performance index-guided phase-locked semiconductor laser arrays," *Electron. Lett.*, vol. 21, pp. 324-325, 11 April 1985.
12. C. P. Lindsey, E. Kapon, J. Katz, S. Margalit, and A. Yariv, "Single contact tailored gain phased array of semiconductor lasers," *Appl. Phys. Lett.*, vol. 45, pp. 722-724, 1 October 1984.
13. E. Kapon, C. P. Lindsey, J. S. Smith, S. Margalit, and A. Yariv, "Inverted-V chirped phased arrays of gain-guided GaAs/GaAlAs diode lasers," *Appl. Phys. Lett.*, vol. 45, pp. 1257-1259, 15 December 1984.
14. J. Ohsawa, S. Hinata, T. Aoyagi, T. Kadowaki, N. Kaneno, K. Ikeda, and W. Sukai, "Triple-stripe phase-locked diode lasers emitting 100 mW CW with single-lobed far-field patterns," *Electron. Lett.*, vol. 21, pp. 779-780, 29 August 1985.
15. J. J. Yang and M. Jansen, "Single-lobed emission from phase-locked arrays lasers," *Electron. Lett.*, vol. 22, pp. 2-4, 2 January 1986.

16. E. Kapon, L. T. Lu, Z. Rav-Noy, M. Yi, S. Margalit, and A. Yariv, "Phased arrays of buried-ridge InP/InGaAsP diode lasers," *Appl. Phys. Lett.*, vol. 46, pp. 136-138, 15 January 1985.
17. N. Kaneno, T. Kadowaki, J. Ohsawa, T. Aoyagi, S. Hinata, K. Ikeda, and W. Susaki, "Phased array of AlGaAs multistriple index-guided lasers," *Electron. Lett.*, vol. 21, pp. 780-781, 29 August 1985.
18. Y. Twu, A. Dienes, S. Wang, and J. R. Whinnery, "High power coupled ridge waveguide semiconductor laser arrays," *Appl. Phys. Lett.*, vol. 45, pp. 709-711, 1 October 1984.
19. S. Mukai, C. Lindsey, J. Katz, E. Kapon, Z. Rav-Noy, S. Margalit, and A. Yariv, "Fundamental mode oscillation of a buried ridge waveguide laser array," *Appl. Phys. Lett.*, vol. 45, pp. 834-835, 15 October 1984.
20. D. F. Welch, P. S. Cross, D. R. Scifres, and W. Streifer, "Inphase emission from an index-guided laser array to 400 mW," *Technical Digest of CLEO '86*, p. 66, San Francisco, 9-13 June 1986. Paper TUB5
21. R. K. DeFreez, T. L. Paoli, M. Bernstein, and R. D. Burnham, "CW operation of a cleaved-coupled-cavity array of phased-locked GaAlAs lasers," *Electron. Lett.*, vol. 21, pp. 241-242, 14 March 1985.
22. D. Botez and D. E. Ackley, "Phase-locked arrays of semiconductor diode lasers," *IEEE Circuits and Devices*, vol. 2, pp. 8-17, January 1986.
23. R. K. DeFreez, R. A. Elliott, K. Hartnett, and D. F. Welch, "Quasi-instantaneous (< 20 picosecond) phase-locking in single lobe Y coupled laser diode arrays," *Electron. Lett.*, vol. 23, pp. 589-590, 21 May 1987.
24. K. A. Forrest and J. B. Abshire, "Time evolution of pulsed far-field patterns of a GaAlAs phase-locked laser-diode array," *Technical Digest of CLEO '86*, p. 80, San Francisco, June 9-13, 1986. Paper TUG4
25. R. A. Elliott, D. X. Huang, R. K. DeFreez, J. M. Hunt, and P. G. Rickman, "Picosecond optical pulse generation by impulse train current modulation of a semiconductor laser," *Appl. Phys. Lett.*, vol. 42, pp. 1012-1014, 15 June 1983.
26. D. Botez, "Laser diodes are power packed," *IEEE Spectrum*, pp. 43-53, June 1985.
27. S. Takahashi, T. Kobayashi, H. Saito, and Y. Furukawa, "GaAs-AlGaAs DH lasers with buried facet," *Jpn. J. Appl. Phys.*, vol. 17(5), pp. 865-870, May 1978.
28. H. Yonezu, I. Sakuma, T. Kamejima, M. Ueno, K. Iwamoto, I. Hino, and I. Hayashi, "High optical power density emission from a "window-stripe" AlGaAs double-heterostructure laser," *Appl. Phys. Lett.*, vol. 34(10), pp. 637-639, 15 May 1979.
29. H. Kumabe, S. Nita, Y. Seiwa, T. Tanaka, T. Sogo, S. Horiuchi, and S. Takamiya, *Tech. Digest of CLEO Conference*, Washington, D. C., June 1981. Paper FA4
30. J. E. Ripper and T. L. Paoli, "Optical coupling of adjacent stripe geometry junction lasers," *Appl. Phys. Lett.*, vol. 17, pp. 371-373, 1970.
31. M. B. Spencer and W. E. Lamb, Jr., "Theory of two coupled lasers," *Phys. Rev. A*, vol. 5, pp. 893-898, February 1972.

32. D. R. Scifres, R. D. Burnham, and W. Streifer, "Phase locked semiconductor laser array," *Appl. Phys. Lett.*, vol. 33, pp. 1015-1017, December 1978.
33. D. E. Ackley and R. W. H. Englemann, "High power leaky mode multiple stripe laser," *Appl. Phys. Lett.*, vol. 39, pp. 27-29, July 1981.
34. V. I. Malakhova, Y. A. Tambiev, and S. D. Yakubovich, "Regular integrated arrays of stripe injection lasers," *Sov. J. Quantum Electron.*, vol. 11, pp. 1351-1352, October 1981.
35. D. E. Ackley, "Single longitudinal mode operation of high power multiple-stripe injection lasers," *Appl. Phys. Lett.*, vol. 42, pp. 152-154, 15 January 1983.
36. D. Botez, "High power phase-locked arrays of index guided diode lasers," *Appl. Phys. Lett.*, vol. 43, pp. 1096-1098, 15 December 1983.
37. J. Ohsawa, K. Ikeda, K. Takahashi, and W. Susaki, "Phase-locked oscillation of dual SBH lasers," *Tech. Digest of the Fourth IOOC Conference*, pp. 172-173, Tokyo, Japan, June 27-30, 1983. Paper 28B3-1
38. I. Suemune, T. Terashige, and M. Yamanishi, "Phase-locked, index guided multiple-stripe lasers with large refractive index differences," *Appl. Phys. Lett.*, vol. 45, pp. 1011-1013, 15 November 1984.
39. H. Temkin, R. A. Logan, J. P. van der Ziel, C. L. Reynolds, Jr., and S. M. Tharaldsen, "Index-guided arrays of Schottky barrier confined lasers," *Appl. Phys. Lett.*, vol. 46, pp. 465-467, 1 March 1985.
40. C. B. Morrison, L. M. Zinkiewicz, A. Burghard, and L. Figueroa, "Improved high-power twin-channel laser with blocking layer," *Electron. Lett.*, vol. 21, pp. 337-338, April 1985.
41. N. K. Dutta, L. A. Koszi, S. G. Napholtz, B. P. Segner, and T. Cella, "InGaAsP ($\lambda = 1.3\mu\text{m}$) laser array," *Tech. Digest of CLEO Conference*, Baltimore, MD, May 21-24, 1985. Paper TuF5
42. M. Taneya, M. Matsumoto, S. Matsui, S. Yano, and T. Hijikata, "0° Phase mode operation in phased-array laser diode with symmetrically branching waveguide," *Appl. Phys. Lett.*, vol. 47(4), pp. 341-343, August 15, 1985.
43. D. E. Ackley, "Single longitudinal mode operation of high power multiple stripe injection lasers," *Eighth IEEE International Semiconductor Laser Conference*, Ottawa-Hull, Canada, September 13-15, 1982. Postdeadline paper PD5
44. D. R. Scifres, R. D. Burnham, and W. Streifer, "Lateral grating array high power cw visible semiconductor laser," *Electron. Lett.*, vol. 18, pp. 549-550, June 1982.
45. J. J. Yang, R. D. Dupuis, and P. D. Dapkus, "Theoretical analysis of single-mode AlGaAs-GaAs double heterostructure lasers with channel-guide structure," *J. Appl. Phys.*, vol. 53, pp. 7218-7223, November 1982.
46. K. Meehan, P. Gavrilovic, J. E. Epler, K. C. Hsieh, N. Holonyak, Jr., R. D. Burnham, R. L. Thornton, and W. Streifer, "Donor-induced disorder-defined buried-heterostructure $\text{Al}_x\text{Ga}_{1-x}\text{As}$ -GaAs Quantum-well lasers," *J. Appl. Phys.*, vol. 57(12), pp. 5345-5348, June 15, 1982.
47. D. R. Scifres, W. Streifer, and R. D. Burnham, "Experimental and analytic studies of coupled multiple stripe diode lasers," *IEEE J. Quantum Electron.*, vol. QE-15, pp. 917-922, September 1979.

48. T. Kobayashi, H. Kawaguchi, and Y. Furakawa, "Lasing characteristics of very narrow planar stripe lasers," *Japan. J. Appl. Phys.*, vol. 16, pp. 601-607, 1977.
49. P. M. Asbeck, D. A. Cammack, and J. J. Daniele, "Non-Gaussian fundamental mode patterns in narrow-stripe geometry lasers," *Appl. Phys. Lett.*, vol. 33, pp. 504-506, 1978.
50. W. Streifer, R. D. Burnham, and D. R. Scifres, "Symmetrical and asymmetrical waveguiding in very narrow conducting stripe lasers," *IEEE J. Quantum Electron.*, vol. QE-15, pp. 136-141, March 1979.
51. W. T. Tsang, "The effects of lateral current spreading, carrier outdiffusion, and optical mode losses on the threshold current density of GaAs-Al_xGa_{1-x}As stripe geometry DH lasers," *J. Appl. Phys.*, vol. 49, pp. 1031-1044, 1978.
52. T. L. Paoli, "Waveguiding in a stripe-geometry junction laser," *IEEE J. Quantum Electron.*, vol. QE-13, pp. 662-668, August 1977.
53. J. P. van der Ziel, R. M. Mikulyak, H. Temkin, R. A. Logan, and R. D. Dupuis, "Optical beam characteristics of Schottky barrier confined arrays of phase-coupled multiquantum well GaAs lasers," *IEEE J. Quantum Electron.*, vol. QE-20, pp. 1259-1266, November 1984.
54. K. Otsuka, "Coupled-wave theory regarding phase-locked-array lasers," *Electron. Lett.*, vol. 19, pp. 723-725, September 1983.
55. D. Botez, "Array-mode far-field patterns for phase-locked diode-laser arrays: Coupled-mode theory versus simple diffraction theory," *IEEE J. Quantum Electron.*, vol. QE-21, pp. 1752-1755, November 1985.
56. S. R. Chinn and R. J. Spiers, "Modal gain in coupled-stripe lasers," *IEEE J. Quantum Electron.*, vol. QE-20(4), pp. 358-363, April 1984.
57. J. E. Epler, N. Holonyak, Jr., R. D. Burnham, T. L. Paoli, and W. Streifer, "Far-field supermode patterns of a multiple-stripe quantum well heterostructure laser operated (7330Å, 300 K) in an external grating cavity," *Appl. Phys. Lett.*, vol. 45, pp. 406-408, August 1984.
58. J. K. Butler and D. Botez, "Mode characteristics of nonplanar double-heterostructure and large-optical-cavity laser structures," *IEEE J. Quantum Electron.*, vol. QE-18, pp. 952-961, July 1982.
59. D. R. Scifres, R. A. Sprague, W. Streifer, and R. D. Burnham, "Focusing of a 7700-A high power phased array semiconductor laser," *Appl. Phys. Lett.*, vol. 41, pp. 1121-1123, 15 December 1982.
60. G. H. B. Thompson, *Physics of Semiconductor Laser Devices*, John Wiley & Sons, New York, N.Y., 1980.

APPENDIX A

This appendix is a source listing of the Basic language program "transfer1". This program will transfer and process an entire data set. The use of the program is discussed in Chapter 5.

```
1000 REM TRANSFER1
1100 REM SENDS 1 DIMENSIONAL DATA SET
1200 REM TO MicroVAX
1300 A$ = CHR$(1); REM CONTROL A
1400 C$ = CHR$(13); REM CARRIAGE RETURN
1500 D$ = CHR$(4); REM CONTROL D
1550 Q$ = CHR$(8); REM SHIFT Q
1560 P$ = CHR$(46); REM .
1600 TEXT ; HOME ; UTAB 5
1650 INPUT "# OF WINDOWS PER FRAME?";F
1700 INPUT "# OF DATA POINTS TO BE READ?";M
1800 DIM X$(M)
1900 TEXT ; HOME ; UTAB 10
1950 INPUT "TYPE IN THE INITIAL CHARACTER OF FILE PREFIX";L$
1955 INPUT "TYPE IN THE 3 CHARACTER OUTPUT FILE PREFIX";LL$
1960 FOR L = 1 TO 20
1961 IF (L = 6) THEN GOSUB 6050
1962 IF (L = 11) THEN GOSUB 6050
1963 IF (L = 16) THEN GOSUB 6050
1970 IF (L < 10) THEN GOTO 2000
1980 N$ = L$ + STR$(L)
1985 FR$ = STR$(L)
1990 GOTO 2005
2000 N$ = L$ + STR$(0) + STR$(L)
2002 FR$ = STR$(0) + STR$(L)
2005 REM NOW DETERMINE THE 'F' FILENAMES
2006 REM FOR THE FRAME-GRABBED IMAGE
2010 FOR K = 1 TO F
2020 IF (K < > 10) THEN GOTO 2050
2030 NNS = N$ + P$ + STR$(K)
2040 GOTO 2100
2050 NNS = N$ + P$ + STR$(0) + STR$(K)
2100 PRINT D$;"OPEN ";NNS;"D2"
2200 PRINT D$;"READ";NNS
2300 FOR I = 1 TO M
2400 INPUT X$(I)
2500 NEXT I
2600 PRINT D$;"CLOSE";NNS
3200 GOSUB 4900
3210 REM OPEN FILE USING ed ON MicroVAX
3220 PRINT D$;"PR#4"
3230 PRINT "ed ";NNS
3232 FOR J3 = 1 TO 500
3233 W = 666
3234 NEXT J3
3240 PRINT CHR$(97); REM a
3400 FOR I = 1 TO M
3500 PRINT X$(I)
3600 FOR J1 = 1 TO 2
3700 U = 666
3800 NEXT J1
3900 NEXT I
4000 PRINT CHR$(46); REM .
4005 PRINT C$
4010 PRINT CHR$(119); REM w
4015 PRINT C$
4020 PRINT CHR$(113); REM q
4025 PRINT C$
4070 PRINT D$;"PR#0"
4600 GOSUB 4900
4650 NEXT K
```

```
4660 PRINT D$;"PR#4"
4670 PRINT "DATIN.SHELL ";N$
4675 PRINT F
4680 PRINT N$
4685 PRINT LL$
4687 PRINT " / ";FR$;"'"
4690 PRINT D$;"PR#0"
4692 FOR J2 = 1 TO 10000
4693 U = 666
4694 NEXT J2
4695 NEXT L
4700 PRINT A$;"RESET"; REM RESET SSC SWITCH SELECTED ITEMS
4800 GOTO 6100
4900 PRINT D$;"PR#4"
5000 PRINT A$;"BB"
5100 PRINT A$;"0D"; REM 8 DATA BITS 1 STOP
5200 PRINT A$;"0P"; REM NO PARITY
5300 PRINT A$;"E E"
5400 PRINT A$;"0 S"
5500 PRINT A$;"M D"
5600 PRINT A$;"L D"
5700 PRINT A$;C$
5900 PRINT D$;"PR#0"
6000 RETURN
6050 PRINT "CHANGE TO NEXT DATA DISK"
6055 PRINT
6060 INPUT "TYPE 'R' WHEN READY TO TRANSFER THE NEXT 5 SETS OF DATA";R$
6070 IF R$ = "R" THEN RETURN
6100 TEXT : HOME : VTAB 5
6200 INPUT "DID YOU LOGOUT? (Y/N)";Z$
6300 IF Z$ = "Y" THEN GOTO 6900
6400 TEXT : HOME : VTAB 10
6500 PRINT "TYPE BYE <CR>"
6600 PRINT "THEN TYPE CONTROL A"
6700 PRINT "THEN TYPE Q <CR>"
6800 BDSUB 4900
6900 END
```

APPENDIX B

This appendix is a source listing of the Fortran program "mkarray.wnd.trg.f". This program forms the array files from the intensity data files of the individual emitters and is run from within the data transfer routine "transfer1" given in Appendix A. The use of the program is discussed in Chapter 5.


```
C-----
C program mkarray.wnd.trg.f...this program opens and reads the trigger-
C      ing data file 'xxx.trg.max'; extracts delay
C      information for each frame and the total length
C      allowed by the maximum delay for the data set.
C      This provides the compensation necessary for the
C      observed triggering instability . The program then
C      opens and reads the individual emitter data files
C      which comprise one frame grabbed image. These
C      files are read into an array, a(j,l) where l ranges
C      from 1-m --the nth column in the array corresponds
C      to the data file for the nth emitter. The array is
C      normalized to 1 and is then written to a file of the
C      form 'xxx.ar.nn' where nn is the frame number and
C      xxx is the output file prefix given as input to this
C      program (note:this prefix xxx is the same as that for
C      the triggering data files xxx.trg and xxx.trg.max).
C
C $Header$
C
C      double precision a(234,10), anorm(234,10), junk(100,10)
C      integer m,i,li,j,ldigit,rdigit,top,length
C      character prefix*3,suffixl*1,suffixr*1,suffix*4,name*6,dot*1
C      character frame*2,outprefix*3, nameout*9
C read the number of emitters
C      print *, 'input number of emitters/windows...'
C      read *, m
C read the data file prefix, output array file prefix and frame number
C      print *, 'input file prefix of data files...'
C      read *, prefix
C      print *, 'input output array file prefix...'
C      read *. outprefix
C      print *, 'input frame number of output array file (01--20)...'
C      print *, '---surround number with single quotes---'
C      read *, frame
C call the triggering data subroutine to handle the compensation for
C triggering instability
C      call trigger(frame,outprefix,length,top)
C for each of the m data files calculate the filename,
C open the file and read the data into array a(j,li),
C discarding the first points upto ('top'-2) by reading them into
C array junk(j,ii) and the last points by not reading them
C      do 10 il=1,m
C          ldigit = il/10
C          rdigit = il -10*ldigit
C          suffixl = char(ldigit + 48)
C          suffixr = char(rdigit + 48)
C          dot = '.'
C          name= prefix//dot//suffixl//suffixr
C          open(1,file=name)
```

```

        do 20 j=1,top-2
            read(1,800) junk(j,ii)
20      continue
        do 30 j=1,length + 2
            read(1,800) a(j,ii)
30      continue
        close(1)
10    continue
C normalize the array
    call norm(a,length,m,anorm)
C calculate the filename for the array file
    suffix = '.ar.'
    nameout = outprefix//suffix//frame
C open the array file and write the normalized
C array to it
    open(1,file=nameout)
    do 40 i=1,m
        do 50 j=1,length
            write(1,800) anorm(j,i)
50      continue
40    continue
    close(1)
800  format(f8.4)
    stop
    end
C-----
C Subroutine normalize...this subroutine normalizes an array of
C      dimension up to (234,234). A search through
C      the array determines the largest element,rmax,
C      and then each element of the array is divided
C      by this value, rmax. If rmax is 0 no division
C      is performed and a warning is written to the
C      screen that the array to be normalized is a
C      zero array.

    subroutine norm(rarray,n,m,rnorm)
    double precision rarray(234,234), rmax, rnorm(234,234)
    integer i,j
C set rmax to be the first element
    rmax = rarray(1,1)
C search through the array comparing rmax to rarray(j,i)
C if rarray is bigger then it becomes rmax...
    do 100 i=1,m
        do 200 j=1,n
            if(rarray(j,i) .gt. rmax) then
                rmax = rarray(j,i)
            end if
200      continue
100    continue
C if the array is a zero array then bypass the normalization and
```

```

C return
  if(rmax .eq. 0) then
    print *, 'rmax is 0'
    return
  end if
C now divide rarray(j,i) by rmax to normalize
  do 300 i=1,m
    do 400 j=1,n
      rnorm(j,i) = rarray(j,i)/rmax
400    continue
300  continue
  return
  end
C-----
C Subroutine trigger...this subroutine opens the triggering data file
C       and reads the first line which contains the maximum
C       value and then the line corresponding to the current
C       frame being analyzed. This information is sent back
C       to the main program so that an array can be formed
C       which compensates for the triggering instability.
  subroutine trigger(frame,outprefix,length,top)
  integer i,itop,itopp1,itopt,itopo,t(50),top,tmax,length
  character frame*2,outprefix*3,suffixt*8,namet*11

C calculate the index 'itop' in 2 parts--the 10's digit 'itopt' and then
C the 1's digit 'itopo'
C the value of 'itop' corresponds to the number of the frame in the set
C knowing this, the triggering information for this frame can then be
C read from the appropriate row in the triggering data file
  itopt = ichar(frame(1:1))-(48-(ichar(frame(1:1))-48)*9)
  itopo = ichar(frame(2:2))-48
  itop = itopt + itopo
C calculate the triggering data filename--the one that has the maximum
C value of the triggering delay written as the first line in the file
  suffixt = '.trg.max'
  namet = outprefix//suffixt
C open the file and read all of the data up to 'itop'+1 --this includes
C the max value and the delay value for this frame
  open(1,file=namet)
  itopp1 = itop + 1
  do 10 i=1,itopp1
    read(1,900) t(i)
10  continue
  close(1)
C 'top' contains the delay information for this frame
C 'tmax' contains the maximum delay for the data set--all frames
  top = t(itopp1)
  tmax = t(1)
C calculate the maximum length of the arrays for this data set
C note: there are 14 zeros written to the end of all frame-grabbed

```

```
C data files...these zeros are of no value and will be removed
  length = 256 - 14 - tmax
900 format(i3)
  return
end
```

APPENDIX C

This appendix is a source listing of the Fortran program "statc.crl.trg.F". "statc.crl.trg.F" is the program developed to do the statistical analysis on the intensity profiles in the form of array files. The use of the program is discussed in Chapter 5.

```
C-----
C Program statc.crl.trg.F
C     ...this program opens and reads the 'nfile' array files
C     of a given run (specified by the common 3 character
C     file prefix). The array files are of the form:
C     ixx.ar.## --where xx is the drive current
C     without the decimal point and ## is the frame # of the
C     array file ). For each of the 'nfile' intensity data
C     files DFTs and correlations are calculated. These
C     results are then averaged, as is the intensity data.
C     The result files are of the form: ixx.ar.00.aft ,
C     ixx.ar.00.acr ,and ixx.ar.00 respectively.
C     The DFT and correlation of the average intensity data
C     are calculated and written to files of the form :
C     ixx.ar.00.dft and ixx.ar.00.crl . The DFT and
C     correlation results are written to files for only the
C     four array file frame numbers: 05,10,15,20. These
C     files are of the form: ixx.ar.05.dft ; ixx.ar.05.crl
C     for example. These files are all compatible with the
C     graphics routine 'gr'. The intensity data files
C     are not in a form in which all 10 emitters can be
C     displayed simultaneously. The program 'prepare.plot'
C     will put them in this form. The scripts 'splitplt2'
C     and 'splitplt2.stat' with their associated awk scripts
C     command files and parameter files will control the
C     graphic display of both the intensity data and the
C     result files. See the README file in ~/bin for more
C     details.
C
C $Header: statc.crl.trg.F,v 1.7 87/03/03 12:42:27 kathh Exp $
C
C #define MAXROWS 234 /* max nr. of pixels per emitter */
C #define MAXROWS_2 117 /* MAXROWS/2 (for dft routine) */
C #define MAXCOLS 10 /* max nr. of emitters */

double precision a(MAXROWS,MAXCOLS),aa(MAXROWS,MAXCOLS)
double precision ar(MAXROWS,MAXCOLS),sumar(MAXROWS,MAXCOLS)
double precision sumft(MAXROWS,MAXCOLS),sumcrl(MAXROWS,MAXCOLS)
double precision aravg(MAXROWS,MAXCOLS),aaravg(MAXROWS,MAXCOLS)
double precision ftavg(MAXROWS,MAXCOLS),crlavg(MAXROWS,MAXCOLS)
double precision ftres(MAXROWS,MAXCOLS),ftavout(MAXROWS,MAXCOLS)
double precision crlres(MAXROWS,MAXCOLS),crlavout(MAXROWS,MAXCOLS)
double precision sumone(MAXCOLS),oneavg(MAXCOLS)
double precision sumfr(MAXROWS),avgfr(MAXROWS)
integer n,n2,m,l,li,lli,index,ij,jjj,jm1,nfile,ldigit,rdigit
character prefix*3,suffixl*1,suffixr*1,suffix*2,name*9,dot*4
character suffixft*4,suffixcr*4,nameaft*13,nameacr*13,prefixft*7
character dotav*4,nameav*9,dotfr*4,namefr*9
logical debug
debug = .false.
```

```

C define the dimensions of the array--m denotes the number of emitters
  print *, 'input number of emitters/windows...'
  read *, m
C read the length of the file--of an individual emitter
  print *, 'input length of a column in array data file ..'
  read *, n
  n2=(n+1)/2
C read the number of frames in the data set
  print *, 'input number of frames in the data set...'
  read *, nfile
C initially set the sum arrays to 0
  do 10 i=1,m
    do 20 j=1,n
      sumar(j,i)=0.0d0
20    continue
    do 30 jj=1,n2
      sumft(jj,i)=0.0d0
30    continue
    do 40 jjj=1,n
      sumcrl(jjj,i)=0.0d0
40    continue
10  continue
C the number of files to be averaged is nfile
C read the filename prefix of the array files to be averaged
  print *, 'input file prefix--first 3 characters of filename...'
  read *, prefix
C calculate the filenames of each of the array files
  do 100 ii=1,nfile
    ldigit = ii/10
    rdigit = ii-10*ldigit
    suffixl= char(ldigit + 48)
    suffixr= char(rdigit + 48)
    dot = '.ar.'
    name = prefix//dot//suffixl//suffixr
C open each of these array files and read the data into ar(j,i)
C make two copies of ar(j,i) to be used for DFT and correlation analysis
    open(4,file= name)
    do 110 i=1,m
      do 120 j=1,n
        read(4,850) ar(j,i)
        a(j,i) = ar(j,i)
        aa(j,i) = ar(j,i)
120      continue
110    continue
    close(4)
C calculate the average intensity for a frame
C first zero the sum array 'sumfr'
    do 125 j=1,n
      sumfr(j) = 0.0d0
125    continue

```

```
C form the sum
      do 150 j=1,n
          do 175 i=1,m
              sumfr(j) = sumfr(j) + ar(j,i)
175      continue
          avgfr(j) = sumfr(j)/m
150      continue
C calculate the filename for the average intensity for a frame
      dotfr = '.fr.'
      namefr = prefix//dotfr//suffixl//suffixr
      open(1,file=namefr)
      do 200 j=1,n
          jm1 = j-1
          write(1,900) jm1, avgfr(j)
200      continue
      close(1)
C calculate the average intensity for each emitter
      do 325 i=1,m
          sumone(i) = 0.0d0
325      continue
      do 350 i=1,m
          do 375 j=1,n
              sumone(i) = sumone(i) + ar(j,i)
375      continue
          oneavg(i) = sumone(i)/n
350      continue
C calculate the filename for the average intensity of each emitter
      dotav = '.av.'
      nameav = prefix//dotav//suffixl//suffixr
      open(1,file=nameav)
      do 385 i=1,m
          write(1,910) i, oneavg(i)
385      continue
      close(1)
C calculate the DFT and correlation of each array file
      call dft(a,n,m,name,ii,ftres)
      call corrftr(aa,n,m,name,ii,crres)
C determine the sum arrays of the intensity,DFT and correlation
C results of the nfile array files
      do 400 i=1,m
          do 500 j=1,n
              sumar(j,i)=sumar(j,i) + ar(j,i)
500      continue
          do 525 jj=1,n2
              sumfr(jj,i)=sumfr(jj,i) + ftres(jj,i)
525      continue
          do 550 jjj=1,n
              sumcrl(jjj,i)=sumcrl(jjj,i) + crres(jjj,i)
550      continue
400      continue
```



```
C next file...
100 continue
C normalize the sum arrays
  call norm(sumar,n,m,aravg)
  call norm(sumft,n2,m,ftavg)
  call normcrl(sumcrl,n,m,crlavg)
C duplicate aravg(j,i) to be used in determining the correlation
C of the average array file
C note: the DFT routine(NAG/c06eaf) returns the results in aravg(j,i)
C making it necessary to use another copy of aravg(j,i) for the
C correlation analysis
  do 575 i=1,m
    do 600 j=1,n
      aaravg(j,i) = aravg(j,i)
600   continue
575   continue
C define the value of ii and the average array filename
  ii=0
  suffix= '00'
  prefixf=name(1:7)
  name=prefixf//suffix
C calculate the name of the average array file
  name= prefix//dot//suffix
C open this file and write the normalized array to it
  open(4, file=name)
  do 650 i=1,m
    do 700 j=1,n
      write(4,850) aravg(j,i)
700   continue
650   continue
  close(4)
C determine the DFT and correlation of the average array file
  call dft(aravg,n,m,name,ii,ftavout)
  call corrltn(aaravg,n,m,name,ii,crlavout)
C calculate the name of the average correlation file
  suffixcr = '.acr'
  nameacr = name//suffixcr
C open this file and write the results to it, incrementing
C the values in the nth column by (n-1)
  open (3, file = nameacr)
  do 710 i=1,m
    do 720 j=1,n
      im1 = i-1
      crlavg(j,i) = crlavg(j,i) + im1
720   continue
710   continue
  do 730 i=1,m
    do 740 j=1,(n/2 + 1)
      jm1 = j-1
      lli = (n/2 + jm1)
```

```

        index = (-n/2 + jm1) - 1
        write(3,900) index, crlavg(iii,i)
740    continue
        do 750 j=(n/2 + 2),n
            jm1 = j-1
            jj = (jm1 - n/2)
            index = jj - 1
            write(3,900) index, crlavg(jj,i)
750    continue
730    continue
        close (3)
C calculate the name of the average DFT file
        suffixft = '.aft'
        nameaft = name//suffixft
C open this file and write the average DFT array to it
        open(4, file=nameaft)
        do 800 i=1,m
            do 815 j=1,2
                jm1 = j-1
                im1 = i-1
                write(4,900) jm1, 0.0 + im1
815    continue
            do 825 j=3,n2
                jm1 = j-1
                im1 = i-1
                ftavg(j,i) = ftavg(j,i) + im1
                write(4,900) jm1, ftavg(j,i)
825    continue
800    continue
        close(4)
850    format(f8.4)
900    format(i4,f8.4)
910    format(i2,f8.4)
        stop
        end
C.....
C Subroutine dft...this subroutine calculates the discrete fourier
C transform of each column in the array. This corresponds
C to a DFT in the time domain since the columns contain
C intensity information as a function of time for a single
C emitter. The data in the 2D array is read a column at
C a time into a real 1D array required by the NAG routine
C c06eaf. The original sequence is a real sequence and
C consequently the DFT is a particular type of complex
C sequence, a Hermitian sequence with the following
C properties:  $a(N-k)=a(k)$ 
C  $b(N-k)=-b(k)$  ,  $b(0)=0$  ,  $b(N/2)=0$  for N even
C where  $DFT\{z(k)\} = a(k) + ib(k)$  when  $z(k)=x(k)$  (z real).
C A Hermitian sequence of N complex values can then be
C uniquely specified by N independent real values. The NAG

```

```

C      routine c06eaf writes the real parts a(k) for 0<k<N/2 in
C      the first (N/2 + 1) components of array x. The non-zero
C      imaginary components b(k) are written in reverse order
C      to the remaining (N/2 - 1) components of array x.
C      The results are normalized to one and read back
C      into an array file.
C
      subroutine dft(f,n,m,name,ii,ftout)
      double precision f(MAXROWS,MAXCOLS), rnorm(MAXROWS,MAXCOLS)
      integer i,im1, ifail, j, jm1, n2, nj, kk, n,m
      logical debug
      double precision x(MAXROWS)
      double precision r(MAXROWS_2), im(MAXROWS_2),c(MAXROWS_2)
      double precision arft(MAXROWS,MAXCOLS),ftout(MAXROWS,MAXCOLS)
      character name*9,suffix*4,namedft*13
C read the elements of each column of the array
C into x, one at a time
      do 500 kk = 1, m
         do 40 j = 1, n
            x(j) = f(j,kk)
40        continue
         ifail = 0
C call the NAG routine that calculates the DFT
C of a real array x of length n
         call c06eaf(x,n,ifail)
C real and imaginary components are returned to
C x(j) see the above program description for the
C specific locations of the components r(j), im(j)
C the first components are given by
            r(1) = x(1)
            im(1) = 0.0d0
            c(1)=r(1)*r(1)
C now determine the remaining DFT components
            n2 = (n+1)/2
            do 60 j=2,n2
               nj = n - j + 2
               r(j) = x(j)
               im(j) = x(nj)
C find the modulus of the complex value of the DFT
               c(j) = r(j)*r(j) + im(j)*im(j)
60          continue
C determine the last value if n is even
            if (mod(n,2) .ne. 0) go to 80
            r(n2 + 1) = x(n2 + 1)
            im(n2 + 1) = 0.0d0
            c(n2 + 1) = r(n2 + 1)*r(n2 + 1) + im(n2 + 1)*im(n2 + 1)
C write the square of the DFT results to array, arft(j,kk)
C as each column is operated on
            if (debug) print *, 'arft'
80          do 100 j=3,n2

```

```

                arft(j,kk) = c(j)
                if (debug) print *, kk, j, arft(j,kk)
100      continue
C now repeat the process for the next column
500      continue
C normalize the DFT results stored in arft to one
C and return the normalized results in rnorm
      call norm(arft,n2,m,ftout)
      if ((ii .eq. 5) .or.
+ (ii .eq. 10) .or.
+ (ii .eq. 15) .or.
+ (ii .eq. 20) .or.
+ (ii .eq. 0)) then
        go to 550
      end if
      return
550      continue
C compute the filename for the results file
      suffix = '.dft'
      namedft = name//suffix
C open this file and write the normalized result array to it,
C incrementing the values of the mth column by (m-1)
      open (2, file = namedft)
      do 600 l = 1, m
        do 650 j=1,2
          jm1 = j-1
          im1 = l-1
          write(2,900) jm1, 0.0 + im1
650      continue
        do 700 j = 3,n2
          jm1 = j - 1
          im1 = l - 1
          rnorm(j,i) = ftout(j,i) + im1
          write(2,900) jm1, rnorm(j,i)
700      continue
600      continue
      close (2)
900      format (i4,f8.4)
      return
      end

```

```

C.....
C Subroutine corr1tn...this subroutine determines the correlation of
C      the first column of the array with each of the
C      columns. Before this is calculated, the mean of
C      each of the columns is determined and is sub-
C      tracted off from the values. A copy of the first
C      column vector is needed since the NAG routine
C      c06ekf writes the result array back into the

```

```
C          first column vector and the correlation of this
C          column with all other columns is still to be
C          determined.
C
      subroutine corrltn(cr,n,m,name,li,crkout)
      double precision cr(MAXROWS,MAXCOLS), mean(MAXCOLS), sum(MAXCOLS)
      integer i,ii,ifail,j,jj,jm1,n,kk,index
      double precision xa(MAXROWS),xxa(MAXROWS)
      double precision ya(MAXROWS),yya(MAXROWS)
      double precision cri(MAXROWS,MAXCOLS),crlout(MAXROWS,MAXCOLS)
      double precision crkout(MAXROWS,MAXCOLS)
      double precision denoml,denomr
      character name*9,suffix*4,namecrl*13

C initialize the sum array to zero
C and then sum the column of the array
      do 100 kk=1,m
          sum(kk) = 0
          do 150 j=1,n
              sum(kk) = sum(kk) + cr(j,kk)
150          continue
C determine the mean
          mean(kk) = sum(kk)/MAXROWS
100  continue
C subtract off the mean from the values of the array
C copy this array, xa, into xxa since c06ekf writes
C the correlation results back into xa
          do 200 j=1,n
              xa(j) = cr(j,5) - mean(5)
              xxa(j) = xa(j)
200  continue
          do 250 kk=1,m
              do 300 j=1,n
                  xa(j) = xxa(j)
                  ya(j) = cr(j,kk) - mean(kk)
                  yya(j) = ya(j)
300  continue
          ifail = 0
C call the NAG program that does correlations by
C giving the first argument of the call as 2 and
C then giving the two vectors to be compared and their length
C (the argument '2' directs the NAG routine c06ekf to do a
C correlation of the two vectors--a first argument of '1'
C would result in a fourier transform of the correlation)
          call c06ekf(2,xa,ya,n,ifail)
C normalize this by dividing by the product of the sum of the squared
C intensities of each of the two emitters to the 1/2 power.
          do 350 j=1,n
              denoml = xxa(j)*xxa(j) + denoml
              denomr = yya(j)*yya(j) + denomr
```

```
350 continue
    do 375 j=1,n
        crl(j,kk) = xa(j)/dsqrt((denoml*denomr))
375 continue
    denoml = 0
    denomr = 0
250 continue

C normalize the results to one
    call normcrl(crl,n,m,crlout)
    if ((ii .eq. 5) .or.
+ (ii .eq. 10) .or.
+ (ii .eq. 15) .or.
+ (ii .eq. 20) .or.
+ (ii .eq. 0)) then
        go to 275
    end if
    return
275 continue
C compute the new filename for the result file
    suffix = '.crl'
    namecrl = name//suffix
C open this file and write the results to it, incrementing
C the values in the nth column by (n-1)
    open (unit = 3, file = namecrl, status = 'new')
    do 400 i=1,m
        do 450 j=1,n
            im1 = i-1
            crlout(j,i) = crlout(j,i) + im1
450         continue
400 continue
    do 500 i=1,m
        do 600 j=1,(n/2 + 1)
            jm1 = j-1
            ii = (n/2 + jm1)
            index = (-n/2 + jm1) - 1
            write(3,900) index, crlout(ii,i)
600         continue
        do 700 j=(n/2 + 2),n
            jm1 = j-1
            jj = (jm1 - n/2)
            index = jj - 1
            write(3,900) index, crlout(jj,i)
700         continue
500 continue
    close (3)
C increase to f8.4 since the correlation is often 1 and for
C the 10th column this means that jm1 and crlout(j,i) run together
C plot interprets this as a huge number...
900 format (i4,f8.4)
```

```
return  
end
```

```
C-----  
C Subroutine norm...this subroutine normalizes an array of  
C dimension (n,m). A search through  
C the array determines the largest element,rmax,  
C and then each element of the array is divided  
C by this value, rmax. If rmax is 0 no division  
C is performed and a warning is written to the  
C screen that the array to be normalized is a  
C zero array.  
C  
subroutine norm(rarray,n,m,rnorm)  
double precision rarray(MAXROWS,MAXCOLS), rmax  
double precision rnorm(MAXROWS,MAXCOLS)  
integer i,j,m,n  
logical debug  
C set rmax to be the first element  
rmax = rarray(1,1)  
C search through the array comparing rmax to rarray(j,i)  
C If rarray is bigger then it becomes rmax...  
do 100 i=1,m  
if (debug) print *, 'rarray'  
do 200 j=1,n  
if (debug) print *, i, j, rarray(j,i)  
if (rarray(j,i) .GT. rmax) then  
rmax = rarray(j,i)  
end if  
200 continue  
100 continue  
C If the array is a zero array then bypass the normalization and  
C return  
if(rmax .eq. 0) then  
print *, 'rmax is 0--check .dft,.aft,files.'  
print *, '(one of these arrays is a zero array)'  
return  
end if  
C now divide rarray(j,i) by rmax to normalize the array  
do 300 i=1,m  
do 400 j=1,n  
rnorm(j,i) = rarray(j,i)/rmax  
400 continue  
300 continue  
return  
end  
C-----  
C Subroutine normcrl...this subroutine normalizes an array of  
C dimension (n,m). A search through  
C the array determines the largest element,rmax,
```

```
C          and then each element of the array is divided
C          by this value, rmax.  If rmax is 0 no division
C          is performed and a warning is written to the
C          screen that the array to be normalized is a
C          zero array.
C          Note: this is a modification of 'norm' designed
C          to deal with correlation results which cover a
C          range of -1 to 1.  First the results are normalized
C          to one.  One is added to the array to shift the
C          range to 0 to 2.  The array is then renormalized to
C          one by dividing by 2.0d0 and thus making the range
C          0 to 1 which allows the entire array to be plotted
C          on the same graph.
subroutine normcr1(rarray,n,m,rnorm)
double precision rarray(MAXROWS,MAXCOLS), rmax
double precision rnorm(MAXROWS,MAXCOLS)
integer i,j,n,m
C set rmax to be the first element
  rmax = dabs(rarray(1,1))
C search through the array comparing rmax to |rarray(j,i)|
C if |rarray| is bigger then it becomes rmax...
  do 100 i=1,m
    do 200 j=1,n
      if (dabs(rarray(j,i)) .GT. rmax) then
        rmax = dabs(rarray(j,i))
      end if
200    continue
100  continue
C if the array is a zero array then bypass the normalization and
C return
  if(rmax .eq. 0) then
    print *, 'rmax is 0--check .cr1 file,'
    print *, '(the array is a zero array)'
    return
  end if
C now divide rarray(j,i) by rmax to normalize the array
C and add 1.0d0 to shift the range to 0 to 2
  do 300 i=1,m
    do 400 j=1,n
      rnorm(j,i) = rarray(j,i)/rmax + 1.0d0
400    continue
C divide by 2.0d0 to renormalize to 1
  do 500 j=1,n
    rnorm(j,i) = rnorm(j,i)/2.0d0
500  continue
300  continue
  return
end
```


APPENDIX D

This appendix contains a source listing for a representative sample of the programs written to control the graphic display of the discrete Fourier transform and correlation results. The main script is "splitplt2.stat" which controls all of the required processes for both DFT and correlation plots. Supporting scripts and programs for the DFT plots are given here-- "splitplt2.dft.awk" and "cfile.dft.f". Similar scripts and programs exist for the correlation plots. The use of these programs is discussed in Chapter 5.

Mar 5 13:13 1988 splitplt2.stat Page 1

```
#!/bin/csh -fx
@ suffixl = 0
@ suffixr = 0
set suffix = "$suffixl$suffixr"
set prefix = $1
@ n = $2
@ m = $3
@ rfile = $4
@ rhalf = $n / 2
@ anhalf = 0 - $nhalf
while ($suffix <= "$nfile")
  if ($suffix == "00") then
    set dftfile = "$prefix.$suffix.aft"
    (echo "$nhalf $dftfile" ; cat $dftfile) |\
    awk -f splitplt2.dft.awk
    (echo "$dftfile" ; echo "$nhalf" ; echo "$m") |\
    cfile.dft | gr $dftfile.* -p prms.dft
    rm $dftfile.*
    set crlfile = "$prefix.$suffix.acr"
    (echo "$nhalf $crlfile" ; cat $crlfile) |\
    awk -f splitplt2.crl.awk
    (echo "$crlfile" ; echo "$nhalf" ; echo "$mnhalf" ; echo "$m") |\
    cfile.crl | gr $crlfile.* -p prms.crl
    rm $crlfile.*
  endif
  set dftfile = "$prefix.$suffix.dft"
  (echo "$nhalf $dftfile" ; cat $dftfile) |\
  awk -f splitplt2.dft.awk
  (echo "$dftfile" ; echo "$nhalf" ; echo "$m") |\
  cfile.dft | gr $dftfile.* -p prms.dft
  rm $dftfile.*
  set crlfile = "$prefix.$suffix.crl"
  (echo "$nhalf $crlfile" ; cat $crlfile) |\
  awk -f splitplt2.crl.awk
  (echo "$crlfile" ; echo "$nhalf" ; echo "$mnhalf" ;\
  echo "$m") | cfile.crl | gr $crlfile.* -p prms.crl
  rm $crlfile.*
  if ($suffixr == 0) then
    @ suffixr = 5
  else
    @ suffixr = 0
    @ suffixl = $suffixl + 1
  endif
  set suffix = "$suffixl$suffixr"
endwhile
eri
```

Mar 5 13:43 1988 cfile.dft.f Page 1

```
C program cfile.dft.f
character frame*13, framenum*2, zero*2, type*3
read *, frame
read *, n2
read *, m
framenum = frame(8:9)
zero = char(48)//char(48)
type = frame(11:13)
print *, 'dw0'
print *, n2
print *, '0'
print *, m
if ( framenum .eq. zero ) then
  if ( type .eq. "dft" ) then
    print*, 'qdlhdiscrete fourier transform(**2) of avg.intensit
Cy-', frame
  else
    print*, 'qdlhaverage discrete fourier transform(squared)--',
C frame
  endif
else
  print*, 'qdlhdiscrete fourier transform(squared) --', frame
endif
print*, 'mhQ'
end
```

Mar 5 13:43 1988 splitplt2.dft.awk Page 1

```
BEGIN { fcount = 1}
{
  if (NR == 1) { sentinel = $1 - 1 ; outfile = $2; next}
  if ($1 != sentinel) {
    a[$1] = $2
  } else {
    a[$1] = $2
    for (i = 0; i <= sentinel; i++) {
      print i, a[i] > outfile "." fcount
    }
    fcount++
  }
}
```

BIOGRAPHICAL NOTE

The author was born in Plattsburgh, New York on 12 September 1961. She attended Bowdoin College in Brunswick, Maine, and received a Bachelor of Arts degree with magna cum laude in Physics in May 1983. She received a Surdna Foundation Undergraduate Research Fellowship for her thesis work at Bowdoin.

The author was an American Physical Society Graduate Industrial Intern with DuPont at their research facility, the Experimental Station in 1983. She began her graduate studies in Physics at Boston University in 1983. She returned to DuPont's Experimental Station for a summer internship in 1984.

In September 1985, the author began her studies at the Oregon Graduate Center. She completed the requirements for the degree Master of Science in Applied Physics in March 1988. In April 1988 she accepted a position with DuPont as Development Representative with the Instrument Systems Group.